Targeting ion sensors to synaptic vesicles using a Nanobody against luminal Synaptotagmin 1

Dissertation

for the award of the degree

"Doctor rerum naturalium"

of the Georg-August-Universität Göttingen

within the doctoral program

International Max Planck Research School for Molecular Biology

of the Georg-August University School of Science (GAUSS)

submitted by

Rashi Goel

from New Delhi, India

Göttingen, 2021

Thesis Committee

Prof. Dr. Reinhard Jahn

Department of Neurobiology, Max Planck Institute for Biophysical Chemistry, Göttingen

Prof. Dr. Silvio O. Rizzoli

Dept. of Neuro- and Sensory Physiology, University Medical Center Göttingen

Prof. Dr. Claudia Steinem

Institute for Organic and Biomolecular Chemistry, Georg-August-Universität Göttingen

Members of the Examination Board

1st Referee

Prof. Dr. Reinhard Jahn

Department of Neurobiology, Max Planck Institute for Biophysical Chemistry, Göttingen

2nd Referee

Prof. Dr. Silvio O. Rizzoli

Dept. of Neuro- and Sensory Physiology, University Medical Center Göttingen

Further members of the Examination Board

Prof. Dr. Ulf Diederichsen

Institute for Organic and Biomolecular Chemistry, Georg-August-Universität Göttingen

Dr. Dieter Klopfenstein

Third Institute of Physics, Dept. of Biophysics, Göttingen

Prof. Dr. Tiago Fleming Outeiro

Experimental Neurodegeneration, University Medical Center Göttingen

Date of oral examination: 2nd November, 2021

Declaration

Herewith I declare that I prepared the dissertation titled **"Targeting ion sensors to synaptic vesicles using Nanobody against luminal Synaptotagmin1"** in my capacities with no other sources and aids than quoted.

Rashi Goel

Göttingen, September 2021

I dedicate this thesis to two men in my life who have helped me discover my inner strength. My brother, Arpit Goel, without whom, I wouldn't be who I am. My dearest friend, Dr. Aditya Singh, who reminded me that I am a glorious female warrior.

Table of Contents

Acknowledgments

I thank Reinhard, he allowed me to work in his lab, to experience the process of doing research. While there were many emotional rollercoasters along this journey, I am very glad that he believed in me. I remember from Richard Feynman's, 'Oh, Surely, you are joking Mr. Feynman' last chapter, where he describes the process of doing research, he says that research is getting highly institutionalized and while it is hard, I hope that you get to experience the real flavor one day. I think I managed to do that. I loved the amount of freedom he gave me to try new ideas and his support and discussions were invaluable. It gave me the guts to do what was unthinkable. Thank You, Reinhard, for everything!

I owe my Ph.D. to my friends, family, and most importantly, to the interns and students who allowed me to work with them. I would first like to thank the students who helped me with different parts of my projects: Lars did his Bachelor thesis with me and he taught me how to teach. I learned from him where and how I can improve myself and he helped me to come up with my system of teaching, to take teaching courses, and improve during the process. My second student Margarita did a lab rotation with me. She helped me wrap up the Stem Cell project by characterizing it. Her passion for science was invigorating and gave me jolts of energy. I thank Fredi who worked with me for a few months quite meticulously and efficiently. Next, I thank Benjamin, who is a chemist. I learned from this experience how to teach biology to a chemist. What I loved about him and found inspiring was his lab journal maintaining abilities. Ben would write when he would start the experiment and finish it to the minute's precision. He told me that this was the best experience that he had ever had working in a laboratory. Next, I thank Jenni! She is an angel in my story. '*in vitro* reconstitution of Cl sensor' project was a difficult one for me. I had spent a lot of time with at least 4 different ideas. And then, during Vedran's mock defense presentation, I had a eureka moment. Then I performed a preliminary experiment and shaped that idea. Every piece in that puzzle made sense theoretically, I just did not have time to do it all by myself and manage it together with other experiments. Having Jenni was perfect, it taught me how just some guidance and supervision can make an experience rich and exciting, especially if the student is already great to start with. It was an honor to work with her. Lastly, Margarita came back as a fellow and stayed for eight months. I can write about our experience for pages as I learned a lot from her. It was the first time that I was supervising someone who I also knew personally. After her time of rotation in our lab, we had become friends. She made me come up with ways to have honest and difficult conversations.

I thank my friends for being my family away from home. Because of them, I have grown a lot in the last four years. From the first day of my Ph.D. until right now, I have been blessed with friends that are just beyond the scope of this document. In the beginning, it was a treat to discuss scientific problems along with personal problems with people like Valentina (aka Vale), Salma, Ina, and Sonja. From the first year, my interactions with Vale, Laura, and Salma have been very enriching and fulfilling. Later, I became closer

with 3 people – Aditya, Tarana, and Vale; Aditya, perhaps, I can write an entire book about our experience together, helped me realize my inner strength and helped me realize that I want more from life and that I am fully capable of that. Tarana has been a constant support on whom I can practically rely upon. Our time in Malta equipped me with better mental health. I must thank her and our Malta trip, even right now when I feel anxious, I go to our Malta images, which magically work on me to uplift my mood. Her excitement for science also encouraged me and reminded me of things that I love to do. Vale is another angel in my life. Talking to her makes me realize how similar we both are in terms of managing our emotional and logical sides. Being from different continents, we both share such similarities. She has been a very valuable part of my journey. Next, I thank Abhishek, who helped me sail through some difficult periods during the Ph.D., like the animal experiments. It was a big deal for me and he made me realize many things that helped me conquer my fears. My partner, Shyam, I can again talk about him for ages, but briefly, I think that he has seen the worst side of me, and he brings a lot of life and stability in my dead times. I would like to extend my gratitude towards very special friends and colleagues: Linda and Sonja. Right from day one of my Ph.D., they have been my pillars during all the good and bad times in the lab. I also want to thank Bekir, who supervised me during my master thesis. Without his teaching and support, I would have felt hollow in my professional life. More towards the end of my Ph.D., I also thank Vova, for his support, many trips, and great conversations. Thank You, guys! For helping me throughout and making me who I am.

I got professional support from a lot of people. It is amazing how many people have been involved in this story. From Dr. Sven Truckenbrodt's help, after I just randomly reached out to him, to a full-blown collaboration with Dr. Eugenio Fornasiero, Prof. Silvio Rizzoli's lab has been an umbrella figure for me. Working with them has been an honor and a privilege. I would like to thank Dr. Steffen Frey from Nanotag, for his quick and very valuable input, when I got stuck with any nanobody-related question. Additionally, my collaboration with Dr. Patrick Menzel from the Chemistry department has been a rich experience, and I would like to thank him for synthesizing many compounds. It was quite cool to brainstorm ideas, and simply synthesize compounds and try them. Next, the collaboration that I started completely by myself, with Dr. Miso Mitkowski from MPI-EM was extremely profitable. I thank him for lots of technical support, stimulating discussions, and for giving me his valuable time. This Ph.D. would have been incomplete without the support of my lab mates, Marcelo (for all the interesting discussions and proofreading my thesis), Angel (for discussions, teaching me many techniques and, for ordering pizza when we were staying until late in the lab), Sasha (for teaching me how to culture neurons), Brigitte (for lots of assistance from getting an apartment to ordering chemicals in the lab), Dieter (for administrative support), Dr. Alexander Stein's lab (for giving me TEV protease and antibodies) and the entire Neurobiology department who made an excellent atmosphere and helped me in all highs and lows. I would especially like to thank Sigrid Schmidt, for her emotional and lots of technical support, exactly when I needed it the most. I also want to thank Tina from the Rizzoli lab, for providing me with excellent quality of cultured neurons in the last phase of my Ph.D. I would like to thank Dr. Vladimir Belov from the Chemical Facility, MPI-BPC. He conjugated many fluorophores with Halo ligands. It was fantastic to discuss the scientific possibilities with him.

I want to thank my brother, I can again write a book about our relationship, but I couldn't have been me if he wasn't in my life. I thank my parents for always trusting, believing, and supporting me, no matter what. I would also like to extend my gratitude towards my teachers from college and school for being truly the mentors. Thanks to Dr. Ravi Muddashetty, from NCBS, Bangalore, for giving me an exciting internship opportunity and instilling a passion for research.

Very special gratitude to Dr. Steffen Burkhardt and Kerstin Grueniger, coordinators of the IMPRS Molecular Biology Program. Their constant support, both administrative and personal, has been an extremely rich resource for me. They have set perfect examples of how a graduate program should be. A very special thanks to my therapist. She has helped me deal with the Ph.D. stresses in unimaginable ways.

Special thanks to a few podcasts like 'Self Improvement Daily', 'Simon's, A bit of Optimism', Amit Varma's 'The Seen and the Unseen', and many more to give me a piece of thought daily and have something to chew on every day. Special and a huge thanks to 'the trips' that I had with my friends, for making me realize my true inner strength and connecting me to myself. Indeed, I have a lot of stories to tell to my adopted children!

Abbreviations

aa	amino acid
Ab	antibody
AF	AcidiFluor Orange
AP	action potential
APS	ammonium persulfate
BAC	10,10'-bis[3-carboxypropyl]- 9,9'-biacridinium dinitrate
bp	basepair
Ca^{2+}	calcium
Cl^-	chloride
Cy5	cyanine-5
DIV	days in vitro
DNA	deoxyribonucleic acid
DTT	dithiothreitol
E. coli	*Escherichia coli*
EDTA	ethylenediaminetetraacetic acid
Em.	Emission
Exc.	Excitation
FRET	forster resonance energy transfer
GABA	gamma-aminobutyric acid
HEPES	4-(2-hydroxyethyl)-1-piperazineethanesulfonic acid
IPTG	isopropyl-β-D-1-thiogalactopyranoside
IR	infrared
*K*app	K apparent
kDa	kilodalton
K_{SV}	stern-volmer constant
MA, USA	Massachusetts, United States of America
MACA	N-methylacridinium-9-carboxamide
MEQ	6-methoxy-N-ethylquinolinium
KO	knock out
MQAE	N-(ethoxycarbonylmethyl)-6-methoxyquinolinium
MWCO	molecular weight cut-off
Nb	nanobody
NT	neurotransmitter transporter
OD	optical density
PI	protease inhibitor

P_i	inorganic phosphate
PM	plasma membrane
PNA	peptide nucleic acid
psi	pounds per square inch
ROI	Region of interest
RRP	readily releasable pool
rpm	rotations per minute
SDS-PAGE	sodium dodecyl sulfate-polyacrylamide gel electrophoresis
SLC	solute carrier
αSNAP	Alpha-soluble NSF attachment protein
SNARE	soluble N-ethylmaleimide-sensitive factor (NSF) attachment protein receptors)
SNR	signal to noise ratio
SPQ	6-methoxy-N-(3-sulfopropyl) quinolinium
SySy	synaptic systems
Syt1	Synaptotagmin 1
TCEP	tris(2-carboxyethyl)-phosphine hydrochloride
TEMED	tetramethylethylenediamine
TMR	tetramethyl Rhodamine
TEV	tobacco etch virus
TF0F1	*bacillus thermophilus* ATP-Synthase
V-ATPase	vacuolar-type H^+-ATPase
VGLUT	vesicular Glutamate transporter
ΔpH	pH gradient
ΔμH+	electrochemical gradient
VO	Virginia Orange
v/v	volume/volume
WT	wild type
w/v	weight/volume

List of figures

Note: Illustrations are created using BioRender and Adobe Illustrator.

List of Tables

Abstract

The synapse is a specialized nanostructure that connects two neurons where the ionic composition in each of its nano compartments is the driving process for synaptic transmission. Synaptic transmission relies on the repetitive fusion of neurotransmitter-containing synaptic vesicles (SVs) with the plasma membrane (PM) of the presynaptic neuron, to release the neurotransmitter molecules into the synaptic cleft that bind to the receptors present at the postsynaptic neuron. The amount of neurotransmitters stored in an SV directly modulates the strength of the synaptic transmission. SVs are filled with neurotransmitters through the neurotransmitter transporters (NTs) at the expense of the energy derived from the electrochemical gradient across the SV membrane. The electrochemical gradient comprises a pH gradient ΔpH and an electrical gradient $\Delta\psi$, both of which are regulated by different ion fluxes across the vesicle membrane. The ionic composition inside the SV constantly changes during the recycling of SVs. SVs are recycled in the exo-endocytosis cycle, where an SV fuses with the PM, and its lumen gets exposed to the extracellular fluid followed by its retrieval through endocytosis. During endocytosis, the SV encapsulates the ionic content from the extracellular fluid. An SV then exchanges its ionic content with the neurotransmitter molecules and stores the neurotransmitters inside its lumen until the further round of release. The type and quantity of ions residing in an SV are critical in regulating the activity of NTs by either allosteric binding of the ion with the NT or by a coupled exchange of ions with the neurotransmitter molecules via the NTs. This makes it especially critical for an SV to maintain the appropriate ionic stoichiometry to allow an efficient filling with the neurotransmitters. How do the neurotransmitter transporters remain operational when the solute composition inside the SV changes dramatically? To study this, there is a need to have ion sensors targeted to the SV lumen to understand how the neurotransmitter transporters operate to fill the SV with thousands of neurotransmitter molecules within seconds. The project aims to develop a method to target fluorescence-based ion-sensitive probes and measure the concentration of various ions present inside the SVs. To this aim, we have generated a nanobody (Nb) against the luminal domain of an SV protein, Synaptotagmin 1 (Syt1). By fusing the Nb with a HaloTag protein (Nb-Halo), we have developed a flexible system, where the Nb-Halo can bind with an ion probe conjugated to a Halo ligand. In this method, the ion probe serves as a sensing module that can be delivered into the lumen of the SV using the Nb as a targeting module. Thus, the Nb probes can be used to target the sensor to the lumen of SVs during the endocytosis process. As there are Syt1 molecules stranded at the PM from the rounds of Exo and endocytosis, the Nb-Halo fluorescent probe binds with them and makes it difficult to distinguish the fluorophore signal of SV from that of the PM. To remove nonspecific fluorescence generated from probes at the PM, a TEV protease cleavage site has been engineered in the Nb. Thus, it enables the removal of the sensors from the Nb at the PM and helps us to obtain a clean vesicular signal. Using the above method, we have targeted novel pH and Cl^- sensors and measured the luminal resting pH of Glutamatergic and GABAergic SVs in cultured hippocampal neurons. We have measured a resting pH of ~5.1 in both Glutamatergic and GABAergic SVs, which is much lower than what has been reported earlier. I hope that our method of targeting specific

sensors into SVs will open new avenues to measure various others ion concentrations and will allow mapping out the ionic composition of an SV.

1 Introduction

1.1 Synaptic transmission

The human brain contains ~ 86 billion neurons (Azevedo et al., 2009), connected via specialized, anatomically identifiable junctions called synapses. Considering the vast number of neurons, highly efficient communication systems are needed at the synapse for sustaining this neuronal network. There are mainly two types of synapses: electrical and chemical which interact with one another to ensure normal brain development. At the electrical synapse, ionic current and small molecules (ATP, cAMP, and metabolites) diffuse from one cell (presynaptic neuron) to the other (postsynaptic neuron) through specialized membrane channels called gap junctions. Current flow at the electrical synapse is rapid and, in most cells, bidirectional. The bidirectional property of electrical synapses enables them to work together and synchronize electrical activity among a population of interconnected neurons (Bennett and Zukin, 2004). In contrast, at the chemical synapse, communication from one cell to the other happens by the secretion of small molecules called neurotransmitters, from the presynaptic neuron. The release of neurotransmitters generates a secondary current flow by activating specific receptors present at the postsynaptic neuron. Neurotransmitters are synthesized and packaged in lipid bilayered organelles called synaptic vesicles (SVs) and released by the presynaptic cell in response to an action potential. Action potential caused is by the rise and fall of membrane potential by the opening of voltage-gated Na^+ and K^+ channels present at the plasma membrane (PM) and it induces depolarization at the presynaptic terminal. The action potential induced depolarization leads to the opening of voltage-gated Ca^{2+} channels resulting in a rapid influx of Ca^{2+}. An increase in cytoplasmic Ca^{2+} concentration allows SVs to undergo a complex priming and fusion process with the PM to release their neurotransmitter content into the synaptic cleft (Purves, 2006).

1.2 Synaptic Vesicle Cycle

The chemical transmission depends on the fusion of a high number of SVs with the PM. The high number of SVs can range from ~200 in a synapse of a rat cultured hippocampal neuron (Schikorski and Stevens, 1997) to nearly a million in the rat Calyx of Held, a giant nerve terminal in the auditory brainstem (de Lange et al., 2003; Sätzler et al., 2002). The pool of neurotransmitter-filled SVs is replenished by the recycling of SVs. The process of exocytosis, (Jahn and Fasshauer, 2012; Rizo and Xu, 2015) compensatory endocytosis, (Haucke et al., 2011; Saheki and De Camilli, 2012), and filling of SVs with neurotransmitters represents the synaptic vesicle cycle (Rizzoli, 2014)(Figure 1.1). We will briefly discuss each one of them in the following

sections to finally focus on the filling of SVs with neurotransmitters, which is the central theme of the work presented in this thesis.

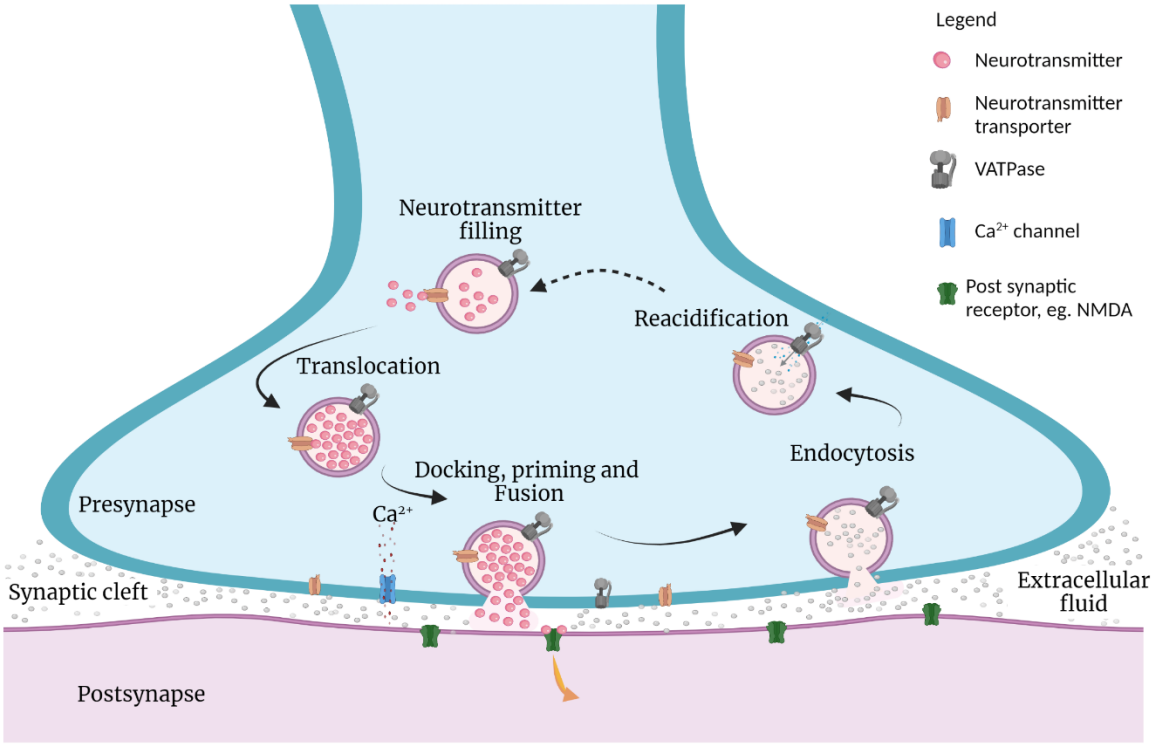

Figure 1. 1 Synaptic Vesicle (SV) recycling

Schematic showing the various steps of SV recycling. SVs (purple round double layered circles) are filled with neurotransmitters (pink circles), via an NT protein (yellow), powered by the energy across the SV membrane maintained due to the proton electrochemical gradient built up by V-ATPase (in grey). SVs are then docked and fuse with the PM, in response to Ca^{2+} (blue dots from a blue Ca channel), SVs. Neurotransmitters are released into the synaptic cleft and then bind to the postsynaptic receptors (in green), to start a signaling cascade into the postsynaptic cell. SVs are then retrieved back by endocytosis and undergo the reacidification process. During endocytosis, vesicles bulk endocytose the extracellular fluid (shown in green circles), which they exchange with the neurotransmitter molecules while filling again. Adapted from (Jahn and Fasshauer, 2012).

1.2.1 Exocytosis

Exocytosis of SVs to release their neurotransmitter content occurs in a chain of events; docking and priming of SVs at the active zone on the PM are followed by their fusion with the PM in response to Ca^{2+}. Active zones are specialized regions of unique multi-domain proteins that provide a scaffold for SVs to dock and prime at the PM. Docking may be initiated by the interaction of the SV with scaffolding proteins like Bassoon (Hallermann et al., 2010) and Piccolo present at the active zone (Parthier et al., 2018). Priming prepares the SVs for release by undergoing reactions that make the SVs competent for fusion with the PM (Südhof, 2012). The processes of docking, priming, and fusion are mediated by a multitude of proteins such as SNARE proteins (soluble N-ethylmaleimide-sensitive factor (NSF) attachment protein receptors) (Südhof and Rizo, 2011). SNAREs undergo a regulated assembly and disassembly process at the expense of ATP by an AAA-ATPase NSF together with its cofactor alpha-soluble NSF attachment protein (αSNAP). The SNARE protein family members contain the following proteins; Synaptobrevin (also called

vesicle-associated membrane protein 2 or VAMP 2) which is present at the SV membrane, and Syntaxin 1 and SNAP 25 which are present at the PM. These three proteins associate in trans configuration (SNARE's residing on two opposite membranes) to form a bundle of four parallel α helices, thus zippering and pulling the two membranes tightly together (Jahn and Fasshauer, 2012). This assembly of proteins is associated with a release of a large amount of energy required to initiate the membrane fusion. Besides SNAREs, other proteins have emerged as key regulators of the fusion machinery; Munc 18 and Munc 13 initiate the trans SNARE assembly by binding to Syntaxin 1 with moderate affinity (Burkhardt et al., 2008) and provide a template to bring the three SNARE proteins together to favor SNARE complex formation (Ma et al., 2013). Synaptotagmin 1 (Syt1) is a crucial protein that governs the Ca^{2+}dependent triggering: Synaptotagmin 1 (Syt1) binds Ca^{2+} upon an increase of the presynaptic Ca^{2+} concentration in response to neuronal activity. Ca^{2+} bound Syt1 simultaneously interacts with SNAREs and with the acidic phospholipids on the PM, thus stabilizing and driving the fusion process (Chapman, 2008). However, how these proteins orchestrate the assembly pathway and the precise sequence of their action remains enigmatic. Following fusion, the ternary SNARE complex resides in the PM in a cis configuration and is disassembled by NSF, and Synaptobrevin 1 is endocytosed to take part in another round of exocytosis (Jahn and Fasshauer, 2012).

1.2.1.1 SV Pools

In cultured hippocampal neuron preparations, each synaptic bouton comprises ~200 SVs (Schikorski and Stevens, 1997). Based on the number of action potentials (in the form of external electrical stimuli) required and the ability of SVs for exocytosis, SV pools can be distinguished into three categories: readily releasable pool, reserve pool, and recycling pool (Figure 1.2). A readily releasable pool (RRP) comprising 1-2 % of total SVs is docked at the active zone and primed to be released within 5-15 bursts of high-frequency stimulation. The recycling pool is about 5-20 % of all SVs and is released on moderate stimulation. The reserve pool comprises 80-90 % of all SVs and requires intense neuronal stimulation for release (Rizzoli and Betz, 2005). The reserve pool acts as a storehouse of SVs and is recruited upon requirement. This concept was better understood by experiments by Kuromi and Kidokoro: the authors used a Drosophila temperature-sensitive mutant called *shibire*. These flies function normally at RT (RT) but cannot recycle vesicles at 34°C. They found that stimulation at RT caused the mobilization of only the recycling pool, however, at high temperatures, vesicle release continued from the reserve pool. Furthermore, reserve pool mobilization is seen in *shibire* (recycling pool loss), high-frequency stimulation, and drug treatments (Kuromi and Kidokoro, 1998, 1999, 2000). While understanding the three pools seems to be straightforward, the mechanistic details are still obscure and require further validation. Interestingly, it was shown that the different pools of the SVs may reflect a mechanism where old vesicles from the actively recycling pathway are moved to the reserve pool, so that the neurons promote the release of younger vesicles, if available (Truckenbrodt et al., 2018).

While neurotransmitter release is mostly triggered by an increase in cytosolic [Ca^{2+}] (evoked release), it can also happen at resting intracellular [Ca^{2+}] termed as the spontaneous release (Vyleta and Smith, 2011). The spontaneous release of neurotransmitters is a common feature of all kinds of synapses and has been known

for almost seven decades (Del Castillo and Katz, 1954). It occurs independently of an action potential, giving rise to miniature postsynaptic potentials (minis). However, it is not known if spontaneous release originates from recycling or reserve pool, or both. In a very interesting study, it was shown that the SVs released by evoked or spontaneous fusion originated from the common recycling pool and the spontaneous release is just a consequence of the machinery that drives fusion (Hua et al., 2010; Lou et al., 2005). Additionally, Hua et al had found that more than 80% of SVs responsible for minis were from the recycling pool and not from the reserve pool. Thus, SV fusion either by evoked or spontaneous exocytosis continuously reuses the SVs by cycles of Exo and endocytosis to ensure that the transmission at the synapse proceeds uninterrupted

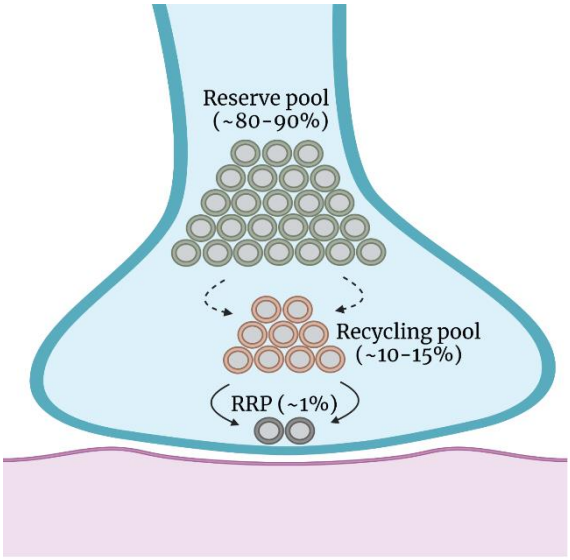

Figure 1. 2: Synaptic vesicle pools.

The classic three pool model of SVs: Reserve pool with ~80-90 % of total SVs, Recycling pool with ~10-15 % of total SVs, and readily releasable pool (RRP) with ~1 % of total SVs that are to be primed for release. Adapted from (Rizzoli and Betz, 2005).

1.2.2 Endocytosis

The property of neurons to sustain synaptic transmission, without exhausting their SV pools, relies on the ability to endocytose and reuse the excess membranes delivered by exocytosis. Although the mechanistic details of endocytosis have been debated and difficult to put together in a model, it is believed that clathrin-mediated endocytosis plays a central role in the retrieval of SVs (Jung and Haucke, 2007). Clathrin was discovered nearly 45 years ago by Pearse when she biochemically analyzed coated vesicles from the brain, adrenal medulla, and non-secreting lymphoma cell line (Pearse, 1976). She named it clathrin in reference to the cage-like structure that it forms. Clathrin is a trimer of three heavy chain proteins bound with three light

chains and organizes itself to form striking lattices (Jung and Haucke, 2007; Kirchhausen, 2000). These lattices function as a scaffold for the clustering of a multitude of adaptor proteins that are needed for the internalization of the membrane cargo. Retrieved clathrin-coated vesicles are then uncoated (in an ATP-dependent manner) and merged with sorting endosomes and with themselves to give rise to SVs (Heuser and Reese, 1973). The physical separation of clathrin-coated bud into a free vesicle requires a protein called Dynamin. Dynamin oligomerizes and organizes into stacks of interconnected rings at the newly budded neck of the endocytosed membrane and mediates fission at the expense of GTP hydrolysis (Hinshaw and Schmid, 1995; Takei et al., 1996). However, there is also evidence for endocytosis requiring a low amount of clathrin, for example, bulk endocytosis (Heuser and Reese, 1973). Bulk endocytosis happens under intense stimulatory conditions when many SVs are released within a short period (Gaffield et al., 2009), perhaps to avoid damage to the membranes with excessive stimulatory exocytosis. Excess membranes are immediately recaptured as endocytic vacuoles (Takei et al., 1996) via membrane infoldings which then undergo fission to give rise to SVs. The mechanism behind the production of SVs from endocytic vacuoles and protein sorting is still not clear, although there are two hypotheses: first, endosomes derived from vacuoles fuse with synaptic organelles containing the SV proteins to give rise to SVs, second, adaptor complex AP3 may coat the endosome to recruit SV molecules like Synaptobrevin 1 (Salem et al., 1998; Voglmaier et al., 2006). The other endocytic processes that occur at time scales faster than Clathrin dependent endocytosis (~20 s) are endocytosis via 'the kiss and run' mechanism (Alabi and Tsien, 2013; Fesce et al., 1994) and 'ultrafast endocytosis' that occurs within ~50-100 ms (Watanabe et al., 2013). 'Kiss and run' involves only a transient interaction and takes place without a full collapse of the SV with the PM. Thus, 'kiss and run' results in an incomplete fusion of the bilayers and rapid closure of the fusion pore, just enough to release the neurotransmitter content (Wu et al., 2014). Ultrafast recycling is believed to occur to rapidly restore the surface area of the membranes. It seems different from kiss and run as it involves the uptake of flattened and large pieces of membranes (Rizzoli, 2014). The functioning of these pathways has been a matter of debate for over 30 years and the evidence supporting either of the models keeps growing, only to be contested later. See the review by Rizzoli and Jahn that summarizes the debate quite well (Rizzoli and Jahn, 2007). Ultimately, the newly endocytosed vesicle seems to propel within the cell by actin polymerization (Merrifield et al., 1999). The area that surrounds the active zone which is specialized for endocytosis is called the periactive zone and is marked by the presence of actin, thus forming a strong link between actin and endocytosis (Bloom et al., 2003).

An important point of discussion in the process of endocytosis is what triggers it. There have been several hypotheses and assumptions in this regard: 1) trigger by the insertion of new membranes after exocytosis (Ceccarelli and Hurlbut, 1980; Heuser and Reese, 1981), 2) a contradictory view is that SVs are endocytosed in response to stimulation rather than being released (Gandhi and Stevens, 2003), and 3) extracellular Ca^{2+} leading to a Ca^{2+} influx causing dephosphorylation of several endocytosis factors have been shown to trigger endocytosis (Clayton et al., 2007; Cousin and Robinson, 2001; Evans and Cousin, 2007). Another speculative and simple possibility is that the Ca^{2+} entry modulates the interaction of soluble cofactor

proteins from vesicles, and these newly freed cofactors (Denker et al., 2011) diffuse to SV patches and complete the endocytosis process (Rizzoli, 2014).

However, among the chain of SV recycling steps, the most critical and rate-limiting one is the filling of SVs with thousands of neurotransmitter molecules (Burger et al., 1989; Riveros et al., 1986) and this will be the central theme of this dissertation.

1.3 Filling of SVs with neurotransmitters

SVs are packages of neurotransmitters that are ejected every time that SV fuses with the PM in response to neuronal firing. The neurotransmitters are packaged and concentrated into the SV via the NTs (specific for each neurotransmitter) present on the vesicular membrane (Takamori, 2016; Takamori et al., 2006). Vesicular NTs are classified into three solute carrier (SLC) families: SLC 17 is responsible for the uptake of anionic neurotransmitters like Glutamate and ATP (Reimer, 2013; Reimer and Edwards, 2004), SLC 18 for cationic neurotransmitters like acetylcholine and monoamines (Erickson et al., 1996; Parsons, 2000) and SLC32 for electroneutral transmitters like GABA and Glycine (Gasnier, 2004). To transport the neurotransmitter molecules, the transporters utilize the energy from the proton electrochemical gradient generated by the activity of vacuolar-type ATPase (V-ATPase) (Farsi et al., 2017). V-ATPase is the largest molecular complex on SVs which transports protons (H^+) into the vesicular lumen at the expense of ATP hydrolysis by its V0 subunit. By transferring H^+ into the lumen, it generates a pH gradient (ΔpH) and an inside positive membrane potential ($\Delta\psi$) across the vesicular membrane. The NT then uses the energy from the electrochemical gradient to transport neurotransmitters against their concentration gradient. The transport mechanism depends on $\Delta\psi$ and ΔpH to a different extent based on the charge of the neurotransmitter and its stoichiometry of coupling to H^+. The negatively charged transmitter such as Glutamate and ATP mostly depend on $\Delta\psi$, the positively charged neurotransmitters such as acetylcholine and monoamines largely depend on ΔpH. The neutral neurotransmitters such as GABA and Glycine depends both on ΔpH and $\Delta\psi$ (Ahnert-Hilger et al., 2003; Blakely and Edwards, 2012; Edwards, 2007; Eiden et al., 2004; Farsi et al., 2016; Gasnier, 2004; Maycox et al., 1988; Omote et al., 2011; Reimer, 2013).

Typically, in an acidified vesicle, the $\Delta\psi$ and ΔpH are ~ 80mV (Farsi et al., 2016; Johnson et al., 1981) and ~ 1.8 pH units (Egashira et al., 2015; Miesenböck et al., 1998) respectively. In 1971, Bernard Katz said that it is uncertain how many molecules of acetylcholine make up each quantal unit of discharge. He had said that at least 1000 molecules are present or maybe more (Katz, 1971). Now we know that the electrochemical gradient can result in a ~ 10^5-fold enrichment and accumulation of ~ 1 molar monoamine concentration in the lumen of chromaffin granules. Chromaffin granules are the subcellular organelles in chromaffin cells of the adrenal gland. They store large quantities of catecholamines; epinephrine and norepinephrine that are released to enter the systemic circulation where they play a myriad of metabolic effects on target organs (Johnson, 1988). Indeed, we have come a long way since then and have learned a great deal about quantal size and vesicle filling with neurotransmitters.

1.4 Quantal Size

The amount of neurotransmitters in a single SV is called a quantum and the amplitude of the postsynaptic current elicited by a quantum is generally referred to as the quantal size. Initially, it was thought that the magnitude of neurotransmitter release depends on presynaptic factors: 1) the number of SVs docked for release (pool of releasable SVs) or on the probability of the SV release (Renger et al., 2001), and postsynaptic factors: 2) on the number and sensitivity of the postsynaptic receptors (Sheng, 2002). These factors can be modulated to produce a long-lasting synaptic strength known as long-term potentiation (LTP). However, later studies demonstrated that quantal size depends on many presynaptic factors including the number of neurotransmitters stored in SVs (Takamori, 2016). This hypothesis is supported by the following reasoning. If one quantum is enough to saturate the postsynaptic receptors, then an increase in the neurotransmitter content in one quantum has no more effect on synaptic efficacy. Indeed, it was directly shown that an exceeding number of postsynaptic receptors present at the post synapse that is not saturated by contents of single SVs indicating that the vesicular neurotransmitter content is an important determinant of synaptic efficacy (Ishikawa et al., 2002; Liu, 2003; Yamashita et al., 2003). The authors had shown this by infusing L-Glutamate via the whole-cell recording pipettes into the giant Glutamatergic synapse, calyx of Held in brainstem slices in immature synapses (Ishikawa et al., 2002) and mature synapses (Yamashita et al., 2003), and measured the amplitude of miniature excitatory postsynaptic currents (mEPSCs). mEPSCs represent the events arising from transmitters released by single SVs. They had found that indeed the amplitude of mEPSCs had markedly increased at physiological temperature suggesting that an increased amount of neurotransmitter increased the occupancy of postsynaptic receptors. Thus, the variability in the number of neurotransmitters in an SV can influence the extent and duration of activating the postsynaptic receptors (Van der Kloot, 1991). Moreover, the quantal size can be regulated by multiple presynaptic factors: expression level of NTs, neurotransmitter concentration in the cytoplasm, regulation of the electrochemical gradient by the number of ions present inside and outside the vesicle, proton exchangers on the vesicular membrane, luminal buffers and many more (Edwards, 2007; Takamori, 2016).

1.5 The electrochemical gradient

Electrochemical gradient $\Delta\mu_{H+}$ describes the proton gradient across the vesicular membrane. The total free energy provided by the V-ATPase to drive neurotransmitter transport is the sum of electrical ΔG_{ψ} and chemical energy ΔG_{pH}.

$$\Delta G_{total} = \Delta G_{\psi} + \Delta G_{pH} \quad (1)$$

These components can be described as follows (Farsi et al., 2017):

$$\Delta G_{\psi} = z_{H^+} \cdot F \cdot \Delta\psi \quad (2)$$

$$\Delta G_{pH} = R \cdot T \cdot \ln\left(\frac{H^+ luminal}{H^+ cytoplasmic}\right) \quad (3)$$

Where z_{H+} is the valence of a proton, *F* is Faraday's constant, $\Delta\psi$ is the membrane potential, *R* is the gas constant and *T* is the absolute temperature. Combining the above equations, the electrochemical proton gradient $\Delta\mu_{H^+}$ can be calculated as:

$$\Delta\mu_{H^+} = \Delta\psi + 2.303\,\frac{RT}{F}\,\Delta pH \quad (4)$$

While the chemical component is mainly driven by $[H^+]_{luminal}$ and $[H^+]_{cytosol}$, the electrical component $\Delta\psi$ is difficult to calculate. $\Delta\psi$ not only depends on the concentration of free H^+ but also on the net accumulation of charged ions in the lumen of the vesicle. The net charge can depend on factors like ion flux, variations in vesicle volume, proton buffering capacity of the vesicular matrix, and protein composition.

1.6 Factors that regulate the electrochemical gradient

The following text will highlight the main factors that influence the ion composition across the membrane and how that influences the electrochemical gradient and thus, the neurotransmitter filling process in an SV. For more details, refer to a comprehensive review that summarizes the biophysical parameters involved in this process (Farsi et al., 2017).

1.6.1 Donnan potential

The potential that appears across semi-permeable membranes where ion species are unequally distributed is called Donnan potential. Because of the unequal distribution of impermeable ion species, the distribution of permeable ions is different across the membrane (Fievet, 2015). For example, the ions having an opposite charge compared to impermeant ions will be concentrated more on the side of the impermeant ions (Teorell, 1935). The fixed charged species inside the vesicular lumen provide a charge that gets balanced by the movement of counter ions. These fixed charges come from the anionic side chains of luminal domains of transmembrane proteins, the presence of charged lipid head groups on the vesicular membrane, and proteins forming the luminal matrix. This movement of counter ions generates the Donnan potential. The overall membrane potential across the vesicle depends on the ion gradients after endocytosis and the ionic status quo of the vesicle at a given time. This influences whether the ion will be more concentrated or diluted at a particular side of the membrane.

The Donnan potential across the vesicular membrane can be derived from (modified from (Fievet, 2015)):

$$\Delta\psi_D = \psi^v - \psi^c = \frac{RT}{z_i F} ln \frac{a_i^c}{a_i^v} \quad (5)$$

$\Delta\Psi_D$ is the Donnan potential, ψ is the electric potential, R is the gas constant, T is absolute temperature, F is Faraday's constant, z_i is the charge number of ion i, a_i is its activity: as ions in solution interact with each other and with water, their effective concentration is less than their true concentration. This effective concentration is the activity of the individual ion a_i. v refers to the vesicle containing the impermeant ion and c refers to the cytoplasm containing the permeant ion. The parameters v and c can change based on which side the permeant and impermeant ions are on.

The membrane potential is defined as the difference in electric potential arising due to the difference in concentration of an ion species between the interior and exterior of the vesicle. The membrane potential is affected by Donnan potential as follows:

$$\Delta\psi_m = \Delta\psi_D^{\Delta X} - \Delta\psi_D^0 + \Delta\psi_{diffusion} \quad (6)$$

Here, $\Delta\psi_m$ is the membrane potential, $\Delta\psi_D$ is the Donnan potential at the interface of the membrane and most diluted solution ($\Delta\psi_D^{\Delta X}$) and interface of the membrane and most concentrated solution ($\Delta\psi_D^0$), the diffusion potential $\Delta\psi_{diffusion}$ is the diffusion in the transport of ions through the pores in the membrane.

1.6.2 Buffering capacity

Buffering capacity β (mol/pH) is the extent to which the amino acid side chains of the luminal matrix proteins can buffer H^+ present in the solution. Additionally, bicarbonate, which is present in the extracellular fluid and is taken up during endocytosis, might contribute to the buffering capacity. Essentially, buffering capacity is the change in the free H^+ concentration of lumen and the change in pH (Grabe and Oster, 2001) as described by the following equation.

$$\Delta[H^+] = \beta \cdot \Delta pH \quad (7)$$

Here, Δ[H+] is the change in the proton concentration of the lumen, β the buffering capacity, and ΔpH is the change in pH.

Moreover, the difference in ion concentration can give rise to water movement across the membrane that leads to osmotic pressure. This can regulate the vesicular volume and may alter the luminal pH. Considering the minuscule volume of ~20 zeptoliters of a vesicle (Takamori et al., 2006), one free H^+ would result in a pH of ~4. It is known that SVs can acidify up to a pH of 5.7 which corresponds to more than 1000 H^+

pumped inside the vesicle implying that SVs must have a high buffering capacity and simulations suggest that an SV contains less than one free H^+ (Singh et al., 2019)! Previously, it has been reported that the buffering capacity is not constant and it increases with decreasing pH in SVs (Farsi et al., 2016) and endosomes (Van Dyke and Belcher, 1994).

1.6.3 Proton efflux

Net proton movement is a trade-off between pumping by the V-ATPase and H^+ leak from the SV. Acidification stops when these two forces are at equilibrium. Simulations predict that at steady-state levels, there might be H^+ pumping from V-ATPase but there is no further decrease in the pH. This suggests that there must be some H^+ efflux pathways that balance the incoming H^+ from the pump, as has been shown in various organelles (Farinas and Verkman, 1999; Schapiro and Grinstein, 2000; Wu et al., 2000). This passive flow of H^+ could be due to several reasons: due to leakage from the membrane (Wan et al., 2002) due to ion exchangers whose activity to transport a molecule is coupled to the transport of H^+, or via NT directly. Additionally, the proton efflux can be regulated by the surface area of the vesicle, by its volume as well as by the lipid fluidity (Wan et al., 2002; Zhang et al., 2000), Thus, there exists a complex interplay of ionic composition that is regulated by ion channels, pumps, physical properties of the matrix and the organelle geometry. Moreover, water molecules move across the membrane depending upon the dynamic ion composition, adding further complexity.

Other than H^+ coupled transport by specific neurotransmitter transporters, two main ion-proton exchangers on SVs are known to contribute to the regulation of ion gradients across the membrane: Na^+/H^+ exchangers (NHE) and Cl^-/H^+ exchangers (CLCs).

1.6.4 NHE exchangers

NHE 6 and NHE 9 are proposed to transport cytosolic Na^+ and K^+ in exchange for luminal H^+ with a stoichiometry of 1:1 (Bianchini and Pousségur, 1994). Another study on NHE 7 has shown that these NHEs can transport Na^+ and Li^+ but not K^+ (Milosavljevic et al., 2014). In either case, both Na^+/H^+ and K^+/H^+ exchange results in a decrease in ΔpH while $\Delta\psi$ remains the same (as the exchange is electroneutral). This results in a decrease in the total proton motive force that further allows V-ATPase to pump H^+ and acidify the lumen. The net effect of these two forces is a decrease in ΔpH and an increase in $\Delta\psi$. This is beneficial for the anionic neurotransmitter like Glutamate transport in two ways: cation/H^+ exchange provides a counter-ion other than proton for VGLUT to function, and it provides an H^+ efflux pathway that can prevent over-acidification of the lumen and continue to transport Glutamate. Manipulating the presynaptic K^+ modulated the minis even when the Glutamate amount was kept unchanged indicating that K^+/H^+ exchange regulates Glutamate release (Goh et al., 2011). Similarly, changing the intracellular resting Na^+ concentrations affected the quantal size (Huang and Trussell, 2014). Additionally, NHEs have been

shown to act bidirectionally (Milosavljevic et al., 2014). This means that even ahead of V-ATPase activity, they can use the large Na^+ gradient (directed from lumen to cytoplasm) to pump protons in and acidify the vesicle lumen. However, it was shown that K^+/H^+ exchange in SVs was not blocked by NHE inhibitor, suggesting that VGLUT itself (and not NHEs) might be responsible for K^+ transport (Farsi et al., 2016; Preobraschenski et al., 2014).

1.6.5 CLC exchangers

Vesicular CLCs are voltage-dependent and exchange two Cl^- ions for one H^+ (Accardi and Miller, 2004). CLC-3 is present on early and late endosomes and SVs (Stobrawa et al., 2001) However, a significant presence of CLC on SVs has been questioned and it was shown that instead of ClC, VGLUT1 exhibit the Cl^- permeation pathway (Schenck et al., 2009). Thus, the role of CLCs in influencing the electrochemical gradient is not fully clear, but might be important. For example, it is possible that when the $[Cl^-]_{lumen}$ is low, Cl^- is transported in via CLC once the proton pump starts pumping in protons (Jentsch and Pusch, 2018; Jentsch et al., 2005). This reduces the membrane potential and provides a counter ion for the proton pump to keep running. Alternatively, when the SV is endocytosed with high $[Cl^-]_{lumen}$, CLCs may operate in a reverse direction by using the Cl^- gradient from lumen to the cytoplasm to pump the protons in and acidify the lumen as has been shown in CLC-5 (Scheel et al., 2005; Smith and Lippiat, 2010) and as the V-ATPase powers up, CLCs may switch direction. Further investigation is needed to clarify the possible contribution of CLCs in regulating the ion fluxes in SVs.

1.6.6 A complex interplay of ions that regulate the electrochemical gradient

When vesicles are endocytosed, they engulf the extracellular fluid containing a high Na^+ concentration (145 mM extracellular versus 5-15 mM intracellular), a high Cl^- (110 mM extracellular versus 4-30 mM intracellular), and a low K^+ concentration (5 mM extracellular versus 140 mM intracellular) inside them. This generates steep Na^+ and Cl^- gradients from the vesicular lumen to the cytoplasm and a steep K^+ gradient from the cytoplasm to the lumen of the vesicle. To cope with the highly changing ionic environment inside the vesicular lumen, NTs such as VGLUTs exhibit complex interactions with H^+ and Cl^- ions. For example, the allosteric regulation of VGLUTs by H^+ provides a mechanism to prevent extracellular efflux of Glutamate when VGLUTs are translocated to the PM during exocytosis (Eriksen et al., 2016; Li et al., 2020; Mackenzie et al., 2008). This is because the pH inside the vesicle is lower (~pH 5.5) than that of the extracellular fluid (pH 7.4), and the H^+ ions bind and activate the VGLUT to allow the Glutamate uptake. Moreover, the inhibition of non-vesicular efflux of Glutamate prevents the possibility of excitotoxicity (Lau and Tymianski, 2010). It has been proposed that VGLUTs have an associated Cl^- conductance that they use to remove the endocytosed Cl^- to make space for Glutamate (Chang et al., 2018; Eriksen et al., 2016; Martineau et al., 2017; Preobraschenski et al., 2014; Schenck et al., 2009) The Cl^- conductance of VGLUTs was shown directly by electrophysiological measurements and very recently

directly identified in the structure of VGLUT 2 (Eriksen et al., 2016; Li et al., 2020). The structure indicated that the Cl^- channel was found to be intersecting with the Glutamate binding site. This likely allows the Cl^- ions to balance the osmotic forces after endocytosis and fine-tune the Glutamate filling process by acting as a sensor of Glutamate over or underfilling. VGLUTs show a peculiar biphasic dependence on Cl^- concentration. It has been shown in numerous studies that VGLUTs need 4 mM of $[Cl^-]_{cytosol}$ for their optimal function, perhaps due to allosteric activation of the transporter. In the absence of Cl^- or at high Cl^- concentration (Bellocchio et al., 2000; Hartinger and Jahn, 1993; Juge et al., 2010; Preobraschenski et al., 2014; Schäfer et al., 2002; Schenck et al., 2009; Wolosker et al., 1996). Glutamate transport is substantially reduced. It is possible that at high Cl^- concentration, the membrane potential is dissipated and thus, the driving force required for Glutamate uptake is compromised. Additionally, at high Cl^- concentration, Cl^- can compete with Glutamate and thus directly interact with the transporter to inhibit its function (Bellocchio et al., 2000; Li et al., 2020; Preobraschenski et al., 2014; Schenck et al., 2009) although, this idea is debated sometimes (Juge et al., 2006, 2010). To complicate the matter more, it was also shown that VGLUTs can operate as K+/H+ exchanger and use the K^+ gradient to build a higher membrane potential at the expense of pH thereby avoiding over-acidification (Farsi et al., 2016; Preobraschenski et al., 2014). Furthermore, it was also shown that changes in presynaptic Na^+ above or below the resting Na^+ concentration of 13 mM regulated vesicular Glutamate uptake (Huang and Trussell, 2014). While VGLUTs predominantly utilize $\Delta\psi$ for its apparent affinity for Glutamate, it has been argued that ΔpH is necessary for retaining Glutamate inside the vesicles by antagonizing the effect of high Cl^- , it was shown that selective dissipation of ΔpH in the presence of Cl^- leads to a substantial Glutamate efflux (Wolosker et al., 1996). Compared to VGLUTs, there is much less known about the GABA transporter VGAT. VGAT has been shown to depend both on $\Delta\psi$ and ΔpH, and presumably exchanges luminal protons for its substrates (Burger et al., 1991; Egashira et al., 2016; Farsi et al., 2016; Hell et al., 1991). Alternatively, VGAT has been proposed to act as GABA/Cl^- cotransporter using a purified reconstituted VGAT in artificial lipid systems (Juge et al., 2009). Thus, the functioning of neurotransmitter transporters involves a complex interplay of many different ions to ensure an optimal filling with the respective neurotransmitter while maintaining an osmotic balance across the SV membrane.

1.7 There is a need for tools and ion-sensitive probes to study the acidification and neurotransmitter filling of SVs.

Despite intensive research, we know little about the molecular mechanisms that regulate the activity of NTs in a constantly changing ionic environment of SVs. There are still several open questions regarding the rate-limiting steps and interrelated effects that require further investigation. Particularly, how the neurotransmitter transporters are linked to Cl^-, H^+ and other ions and how the transmitters are stored inside the lumen without getting leaked out has remained enigmatic. Three major problems slow the progress in this field: 1) A lack of high-resolution structures of the transporters - The dynamic ionic changes that allosterically regulate the transporters in the highly changing environment of SVs, makes it difficult to

determine the transporter's structure, especially in different conformations or in a substrate-bound form. Only recently, the structure of VGLUT 2 was determined and helped the scientific community to contextualize the mechanistic insights behind the functioning of VGLUTs, especially to understand the interdependency of pH and Cl^-. 2) Lack of techniques to quantitatively monitor the ions that control the electrochemical gradient across SVs in a functional synapse. Recent technical developments such as a light-driven proton pump, pHoenix (Rost et al., 2015), new pH probes like mOrange2 (Egashira et al., 2015) have already advanced the field, although there is still a long way to go. 3) It is difficult to access the intracellular transporters especially in small organelles like SVs and endosomes. Their lack of accessibility makes it harder to probe them. Attempts to adapt the methods of electrophysiology and measure the Cl^- currents through VGLUTs have been made in the past (Eriksen et al., 2016). Eriksen et al achieved this by expressing a version of vesicular transporter VGLUT 2 with an increased expression on the PM and defective internalization, later the method was applied in other studies too (Eriksen et al., 2016; Martineau et al., 2017). Additionally, Cl^- selective microelectrodes have been used to measure the $[Cl]_i$ in snails (Neild and Thomas, 1974), mice (Ozawa et al., 1988), and fish retina (Djamgoz and Laming, 1987). However, Cl^- current measurement and Cl^- sensitive microelectrodes can only be reliably applied in large cells and offer limited selectivity (Thomas, 1978). Other than current measurement, radioactive tracers (Harris and Allan, 1985; Schwartz et al., 1985; White and Miller, 1981) provide an alternative tool. However, they are not very sensitive, have limited time resolution, and typically report Cl^- fluxes rather than Cl^- concentrations. Both electrophysiological methods and radioactivity tracers are slow and time-consuming, can be invasive and the recordings can be distorted by the interference of the electrode. Thus, there is an explicit need to move from electrophysiology and radioactivity to newer, faster, and more reliable fluorescence-based sensors that can offer the ability to spatially resolve ion concentrations.

1.8 Fluorescence-based ion sensors

Given the importance of ions in shaping the electrochemical gradient, this dissertation aims to develop a fast and flexible system of targeting new fluorescence-based ion sensors to SVs. Fluorescence-based sensors can be broadly classified into two categories: protein-based fluorophores and small molecule organic dyes. Each of these has its advantages and disadvantages. While proteins can be genetically expressed in a cell, organic dyes need to be delivered with some targeting system like microinjection, which is often disruptive. Additionally, organic dyes can be toxic and poorly retained in the cell. However, organic dyes can offer advantages that protein-based sensors do not, for example, organic dyes are much smaller in size and protein-based sensors are usually more pH-sensitive (which can be a problem in measuring concentration other than H^+). In the following section, we will delve into the existing library of sensors, their limitations, and targetability. For the scope of this thesis, we will limit the text to pH and chloride sensors.

1.8.1 pH sensors and resting pH

Organelle proton concentration plays a fundamental role in many cellular processes. For example, osteoclasts secrete H+ into an extracellular area to start bone resorption (Chatterjee et al., 1992), endosomes need low pH for proper sorting of receptors from their ligands (an excellent review by (Futai et al., 2000)), while SVs accumulate H^+ that forms the electrochemical gradient to drive the secondary transport of neurotransmitters (Moriyama and Futai, 1990).

The resting pH of an SV is its pH at equilibrium. It is the balance of the proton gradient forces, such as proton pumping by the V-ATPase, proton efflux, Donnan potential, buffering capacity, proton transport through NTs, and so on. The SV acidification is required for neurotransmitter uptake, in exchange for H^+. This also helps to prevent a non-vesicular efflux of neurotransmitters from the PM, as there is no ΔpH at the PM (Edwards, 2007).

The pH sensors are characterized by their pKa value. pKa of a sensor defines the pH range in which the sensor is most operational (highly sensitive). It is the value at which 50% of the probe molecules are protonated (Bal et al., 2012; Egashira et al., 2015; Frankær et al., 2019). Generally, it can be assumed that the sensor is most sensitive in the range of ± 1 of the pKa. For example, if a pH sensor has a pKa of 7.1, it means that it is most sensitive from pH 6.1 to pH 8.1. There have been numerous attempts in the past to estimate the luminal pH of the vesicle. Most of these studies have used pH-sensitive GFP; pHlourin (Miesenböck et al., 1998). A study from our lab using pHlourin containing isolated SVs found that the GABA vesicular pH is higher than that of Glutamate and that VGAT functions as a GABA/H^+ antiporter (Farsi et al., 2016). However, studies on isolated vesicles or reconstituted liposomes do not particularly reflect the luminal H^+ state of SVs, as the ionic composition of SVs is altered during the isolation procedure. Therefore, studies in functional synapses in living neurons are important to get more accurate measurements of resting pH. pH-sensitive proteins like pHlourin and pH-sensitive dyes like CypHer have been targeted to SV lumen to understand the exo- and endocytic events in neuronal cultures (Hua et al., 2011). However, these pH sensors have a pKa > 7; this has raised questions about the accuracy of pH determination in the late acidification phase of the SV, where the pH is < 6. Recently, pH-sensitive protein, mOrange2 with a pKa of 6.5 was fused to the luminal region of Synaptophysin 1 and used to measure the pH of Glutamate and GABA SVs (Egashira et al., 2015, 2016). The response range of mOrange 2 is more in the range of acidic lumen (~ 5.7) of SVs compared to pHlourin. Measurement using mOrange2 also showed a relatively long reacidification time of 15 s (Egashira et al., 2016) compared to that of 3-5 s measured in single vesicle events or newly endocytosed reacidifying SVs after stimulation, using pHlourin (Atluri and Ryan, 2006; Balaji and Ryan, 2007; Granseth and Lagnado, 2008; Kwon and Chapman, 2011). However, a major pitfall of all these sensors (pHlourin, CypHer, and mOrange2) is that they are all dark at a low pH, and they lack the pH sensitivity below the pH of 5.5. An optimal pH sensor would have a pKa

around the resting pH and will be brighter in the low pH range. It is possible that the resting pH of SVs is much lower than 5.7 and the established pH sensors are unable to determine that.

1.8.2 Chloride sensors

Chloride (Cl^-) is the most abundant anion in extra and intracellular space and plays diverse physiological roles, such as regulation of cell volume, pH, and stabilization of resting membrane potential in all kinds of cells. Dysfunctional Cl^- transport affects processes from neuron excitability to water secretion. Disorders like epilepsy (Ben-Ari et al., 2012) and Cystic Fibrosis (Saint-Criq and Gray, 2017) are linked with impaired Cl^- homeostasis. Cl^- channels have been involved in pH regulation (Mindell, 2012; Novarino et al., 2010) where they provide a counter-ion for the electrogenic V-ATPase that drives the acidification of SVs (Maycox et al., 1988), lysosomal degradation (Chakraborty et al., 2017; Weinert et al., 2010), and ER (Jia et al., 2015) and mitochondrial function (Ponnalagu et al., 2016).

$[Cl^-]_{cytosol}$ can range from 6-80 mM in neurons and has been shown to play a key role in the regulation of $\Delta\mu_{H+}$. In mature neurons of the CNS, the intracellular concentration of Cl^- determines the neuron's excitability. Presynaptic release of GABA and Glycine activates their postsynaptic receptors by opening the associated Cl^- channel and releasing Cl^- down its concentration gradient, thus hyperpolarizing the postsynaptic neuron. The intracellular Cl^- concentration is maintained at low levels in mature neurons by the K^+/Cl^- co-transporter KCC2 that couples Cl^- and K^+ movement to drive Cl^- against its gradient (Doyon et al., 2016); where K^+ gradient is maintained by Na^+ K^+ ATPase.

Developing effective Cl^- reporters is crucial for characterizing the existing Cl^- transporters and discovering the new ones. However, each reporter has an appropriate sensing characteristic that should match the demand of the transporter in its specific functional context. For example, pH sensitivity, Cl^- sensing range, and the extent of quantification are important parameters in employing a Cl^- probe. Therefore, dyes conjugated to macromolecules and protein reporters have been used in the past to unravel Cl^- biology. The details about Cl^- sensors and their importance have been very elegantly summarized in a review of the demand for Cl^- sensors in biology (Zajac et al., 2020).

1.8.2.1 History of Chloride sensors

The study of Cl^- homeostasis using fluorescent reporters began with the identification of Cl^- sensitive dyes and the discovery that YFP is halide sensitive. The first of the Cl^- sensitive dyes were quinoline-based: SPQ, MQAE, and MEQ, and these dyes have been used in a variety of cell types (Biwersi and Verkman, 1991; Matthew et al., 1981). They function by a process called dynamic collisional quenching; whereas these fluorophores get excited, they collide with Cl^- ions and return to the ground state through a non-radiative decay (Lakowicz, 2013). Thus, their fluorescence decreases with increasing Cl^- concentration. They have a very fast response rate (in the microsecond range) and are insensitive to pH and bicarbonate. However, they are not ratiometric, thus the fluorescence readout depends on the distribution of the probe. They are also sensitive to photobleaching (Geddes, 2001), excite at a low wavelength, and can gradually leak from

the labeled cells (Krapf et al., 1988). Additionally, these dyes self-quench at high concentrations (Kaneko et al., 2004) and they need to be imaged by a short interval exposure or long acquisition times (Schwartz and Yu, 1995). The low wavelength excitation problem of these dyes has been resolved by long-wavelength excitation acridinium-based dyes such as Lucigenin and MACA (Biwersi et al., 1994). Soon after this study, YFP was discovered to be halide sensitive (Wachter and Remington, 1999). Then, the protein was developed with a higher affinity for Cl^- and used as intracellular Cl^- reporter (Wachter et al., 2000). The halides act as ligands that affect the fluorophore's charged state. However, it has been suggested that the halide sensitivity of YFP comes from its pH-dependent ground state binding of the chromophore with the halide (Jayaraman et al., 2000).

A major limitation of all the above sensors including the pH-sensitive dyes is the lack of an emission peak that is Cl^- insensitive; this is extremely important for accurate quantitative measurements since it could be used to internally normalize the probe distribution. An elegant solution to overcome this was to link both the Cl^- sensitive and Cl^- insensitive fluorophores to a macromolecule scaffold. For example, Cl^- sensitive fluorophore BAC was conjugated to dextran, together with a Cl^- insensitive fluorophore TMR. However, this also suffers from a limitation, as the degree of labeling cannot be precisely controlled, thus it has a batch-to-batch variability. To overcome this, a double-stranded DNA-based sensor called Clensor was developed. It has a Cl^- sensitive BAC on one strand and Cl^- insensitive Alexa647 on the other strand in a precise 1:1 stoichiometry (Prakash et al., 2016a; Saha, 2015). Clensor has been used to show that high luminal Cl^- is necessary for lysosomal degradation, mediated with the activity of ClC-7 (Chakraborty et al., 2017; Weinert et al., 2010).

Additionally, there has also been an effort in making ratiometric protein-based halide sensors to overcome the above problems. One such sensor was Clomeleon which has a yellow fluorescent protein (YFP) and a Cyan fluorescent protein (CFP) connected by a flexible peptide linker, such that the two chromophores act as a Foerster resonance energy transfer (FRET) pair (Kuner and Augustine, 2000). However, its Cl^- sensitivity is from 87-167 mM which is far from the physiological cytosolic concentration of 3-60 mM, and it has a slow response rate too. Clomeleon was further improved by replacing the YFP with its triple mutant that can span the physiological range of sensing (Markova et al., 2008). However, YFP in general has a lag time as it requires 100 ms to bind with Cl^-. Also, YFP and CFP bleaching rates are different which can distort the calibration of the sensor; in fact, it can cause overestimation of Cl^- while reducing the emission ratio. The sensor was further improved by random mutagenesis using cell-free protein engineering to come up with SuperClomeleon. SuperClomeleon also used brighter donor Cerulean instead of CFP and has a shorter linker for an improved signal-to-noise ratio (Grimley et al., 2013). Nevertheless, both the protein-based sensors mentioned above are highly sensitive to pH, especially in the physiological range as their Cl^- binding affinity depends on the ionization of the chromophore. Intracellular and intra-organellar Cl^- affects pH, making pH and Cl^- changes depending on each other. In the cytoplasm, pH variations are not so drastic, and thus the error in estimating Cl^- concentration lies in 3-10 mM (Markova et al., 2008). Thus, to

determine the pH-independent modulation of Cl^- changes such as in an SV or a lysosome environment, one needs a pH-independent Cl^- sensor. One way to bypass this problem is to simultaneously measure the pH changes and correct for changes in K_d. ClopHsensor (Arosio et al., 2010) achieved this by having a self ratiometric pH sensor (pKa – 6.8) fused to a Cl^- sensitive EGFP and a DsRed monomer to normalize the EGFP emission intensity and produce accurate Cl^- readings. The Cl^- measurement can be corrected using the K_d value at the observed pH. Additionally, there have been more Cl^- sensors, however several of them are toxic in cells while others work only at low pH (below pH 2.3). There are also naturally occurring, self ratiometric, Cl^- sensitive proteins, although it is either impractical to use them at the physiological pH or it needs to be carboxylated and cannot function above pH 5.5 (Zajac et al., 2020). Because of the complicated pH sensitivity, it is extremely difficult to detect small changes in Cl^- and obtain quantitative information. Thus, ratiometric and pH-insensitive reporters are needed to obtain quantitative information. Table 1.1 below summarizes the pros and cons of the available small molecule, organic, Cl^- sensitive fluorophores.

Table 1. 1 Pros and cons of the available small molecule, organic, Cl- sensitive fluorophores.

Probe	**Exc/Em (nm)**	**Ksv (M-1)**	**Molar extinction coefficient ($cm^{-1}M^{-1}$)**	**Pros and Cons**
SPQ	350/450	118	3700	✓ fast response rate ✓ pH insensitive × photobleaching × non-ratiometric ×self-quench at high concentration × requirement of UV excitation
MQAE	350/460	200	2800	✓ fast response rate ✓ pH insensitive × photobleaching × non-ratiometric ×self-quench at high concentration × requirement of UV excitation
MEQ	344/442	145	3900	✓ fast response rate ✓ pH insensitive × photobleaching × non-ratiometric × Cell-impermeable ×self-quench at high concentration × requirement of UV excitation
MACA	424/500	225	3500	✓ fast response rate ✓ pH insensitive ✓ Long-wavelength excitation × photobleaching × non-ratiometric × self quench at high concentration
Lucigenin (BAC)	455/505	390	7500	✓ fast response rate ✓ pH insensitive ✓ Long-wavelength excitation × photobleaching × non-ratiometric

×self-quench at high concentration

1.8.2.2 Clensor

In this study, we have used Clensor, as it is fast (<1 millisecond response rate), pH-insensitive, and has been used in living cells (Chakraborty et al., 2017; Osei-Owusu et al., 2021; Saha et al., 2015); moreover, the Cl^- sensitive fluorophore BAC has an excitation wavelength in the visible spectrum, it has the highest molar extinction coefficient (a measure of absorbance) and the highest Cl^- sensitivity (Stern Volmer constant K_{sv}) compared to all the other available dyes.

The Cl^- sensitive fluorophore, BAC, is attached to a peptide nucleic acid (PNA) strand which is duplexed with a DNA strand containing a Cl^- insensitive fluorophore Alexa647, is spectrally well separated from BAC (Figure 1.3A). The Alexa647 dye acts as an internal normalization control to accurately report Cl^- concentration by taking the Alexa 647 (R) by BAC (G) ratios. PNAs are a hybrid of DNA and protein: they have a neutral, achiral, pseudo peptide backbone onto which the naturally occurring DNA nucleobases are attached (Figure 1.3B). PNAs are capable of hybridizing with complementary single-stranded DNA, RNA or other PNA strands in stable duplexes. PNA-PNA strands are thermally more stable than PNA-DNA strands, which in turn are more stable than DNA-DNA strands, mainly due to the lack of electrostatic repulsions in uncharged PNA strands (Egholm et al., 1993). Prakash et al. showed recently that, when BAC was conjugated directly with single or double-stranded DNA, it lost its Cl^- sensitivity. However, conjugating it with a PNA strand preserved its Cl^- sensing properties (Prakash et al., 2016). BAC and other small molecule sensors mentioned in Table 1.1 work by collisional quenching; we will discuss the mechanistic details of collisional quenching in the upcoming section.

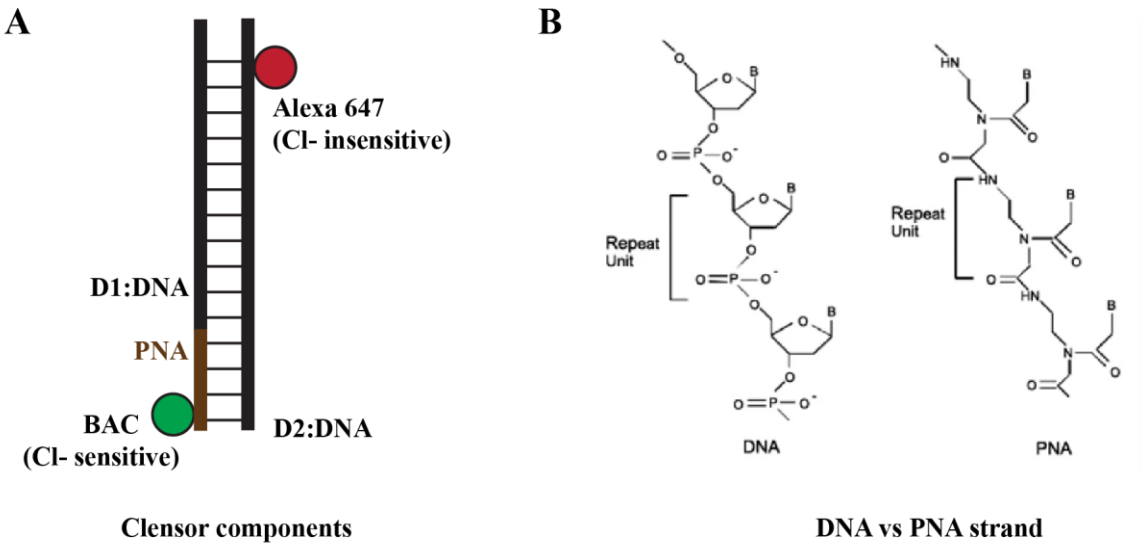

Figure 1. 3 Clensor components and structure of Peptide Nucleic Acid (PNA) strand.

(A) Clensor components: sensing module PNA (in brown) is conjugated to BAC fluorophore (Green ball), targeting module DNA oligo D1 (in black) and normalizing module D2 conjugated with Alexa 647 (red ball). (B) Comparison

of structures of PNA and DNA. Note that the DNA strand has a sugar-phosphate backbone as the repeating unit while the PNA has a pseudo peptide (N-(2 aminoethyl) glycine) repeating unit (Wang and Xu, 2004).

1.8.2.3 Collisional Quenching and Stern Volmer Equation

When a fluorophore encounters a quencher during its excited state by diffusion, the fluorophore returns to its ground state without the emission of a photon. This is called collisional quenching (or dynamic quenching) and the molecules remain unaltered in this process. Another process of quenching is called static quenching where the fluorophore forms a non-fluorescent complex with a quencher.

G.G. Stokes had first described collisional quenching in 1869 when he observed that the fluorescence of quinine was reduced when he added Cl^- ions in the form of hydrochloric acid (Stokes, 1869). In this process, both the fluorescence and the lifetime of the fluorophore (the time that a fluorophore spends in its excited state) are reduced in the presence of the quencher Q. It is described by Stern-Volmer kinetics:

$$\frac{I_0}{I} = 1 + k_q \tau_0 [Q] \quad (8)$$

$$K_{SV} = k_q \tau_0 \quad (9)$$

In equation 8, I_0 and I are the fluorescence intensities in the absence and the presence of quencher Q, respectively. K_q is a constant describing the collisional electronic energy, it is a useful parameter that reflects the accessibility of the fluorophore to the quencher. τ_0 is the fluorescence lifetime in the absence of a quencher. K_{sv} is the Stern-Volmer constant (units M^{-1}) which can be obtained by plotting I_0/I as a function of [Q]. When we will look at the results using the BAC fluorophore, we will focus on some of these parameters.

1.9 How do we target and visualize the sensors inside the SVs?

1.9.1 Approach to target sensors into SVs

There has been a wide variety of genetically engineered fluorescent proteins sensitive for pH or Cl^- covering a broad spectrum of sensitivity. There have been only a few suitable sensors (mostly organic dyes) for measuring pH and Cl^- changes independently in the acidic lumen of the vesicle (for example in lysosomes). The advantage of genetically encoded biosensors is that they can be targeted and spatially directed genetically, under the control of a promoter to measure the changes in an SV. In contrast, the organic dyes must be microinjected in the cell but then, they distribute in the cell through diffusion. Additionally, there are organic dyes that work well but are toxic to the cells, thus cannot be easily applied in biological applications. Ideally, there should be a way to target the reporters to the organelle using a peptide or a chemical tag. Prakash et al found an elegant solution to solve this in lysosomes: the authors used the

transferrin RNA aptamer (RNA oligonucleotide that can bind a specific target) that can bind and target Clensor to the trafficking pathway (Prakash et al., 2016; Saha et al., 2015). However, there have been no reported RNA aptamers for SVs so far.

In this study, we have used the following strategy for labeling the SVs with the required probe. Cultured neurons are incubated in a solution containing the Antibody (Ab) or a nanobody (Nb) (see the section below) against the luminal domain of Synaptotagmin 1 (Syt1). During a spontaneous release, the SVs open to the extracellular solution where they encounter the Ab/Nb labeled sensor. The sensor binds to the inner membrane leaflet and gets encapsulated into the vesicle during endocytosis. Neurons are washed to remove the unbound dye and the freshly labeled vesicles can be imaged. An example of an Ab labeled with a pH-sensitive fluorophore has been shown in Figure 1.4.

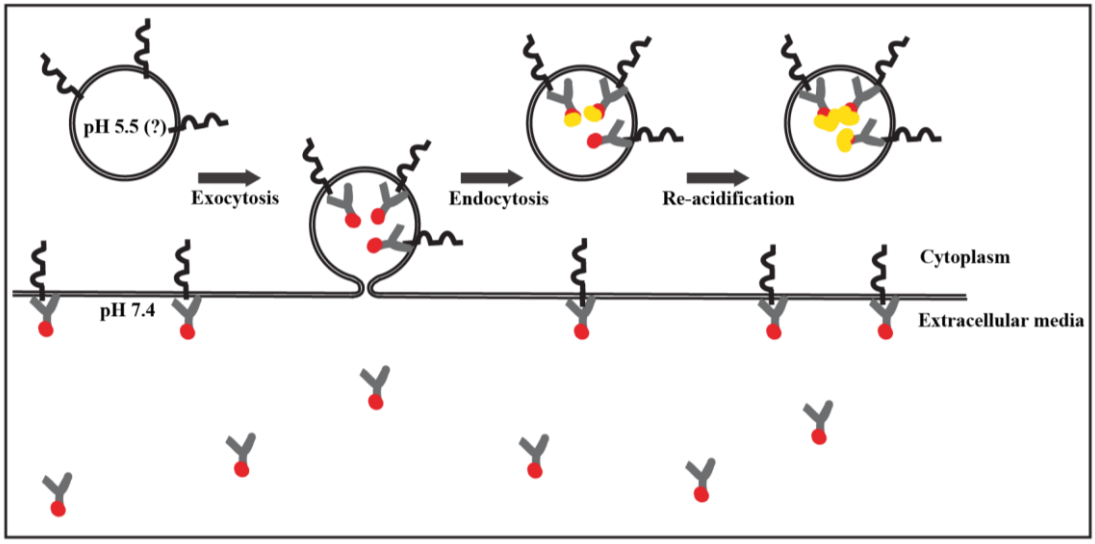

Figure 1. 4 Labeling of SVs with Antibody (Ab) bound with a fluorophore using exo-endocytosis.

Neurons were incubated in their media containing the Abs (in grey) against the luminal domain of Synaptotagmin1 (the black protein on the vesicle membrane) conjugated to a pH-sensitive fluorophore (in red). Labeled Abs would get encapsulated inside the lumen of the SV when the luminal domain of Syt1 would get exposed to the outside medium after exocytosis. When the vesicle gets endocytosed and gets acidified, the pH sensor would get brighter (indicated by yellow).

1.9.2 Nanobodies

Discovered by Casterman and colleagues, nanobodies (Nbs) are single-domain Abs derived from camelids such as Alpacas, llamas, and relatives (Hamer-Casterman, Atarchouch, T et al., 1993) (Figure 1.5). Figure 1.5). They are much smaller than Abs (~12-15 kDa, 2-3 nm compared to ~150 kDa, 15 nm of Abs) (Fornasiero and Opazo, 2015), and are monovalent as opposed to the divalent nature of Abs. Their smaller size enables them to penetrate more easily in samples and detect a greater number of epitopes. Almost a decade ago, it was shown that Nbs against GFP can precisely be used for molecular localization in cell

biology, using super-resolution microscopy (Ries et al., 2012). Additionally, monoclonal recombinant Nbs can be easily produced in large quantities and they can be engineered with a sequence of choice to customize their usage (Hamer-Casterman, Atarchouch, T et al., 1993; Muyldermans, 2013).

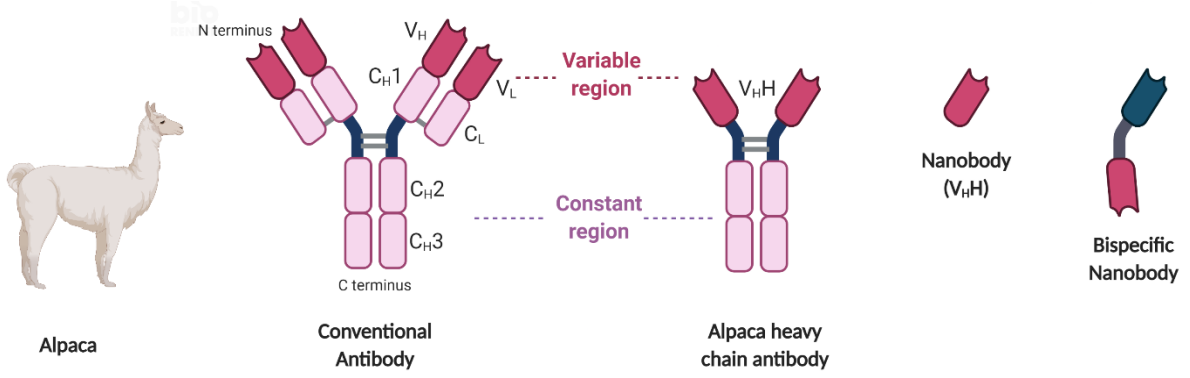

Figure 1. 5 Antibody (Ab) vs Nanobody (Nb)

Comparison of conventional Abs with Nbs derived from Camelids such as Alpaca/Llamas and relatives. Two Nbs each having its target can be fused to generate a bispecific Nb.

1.9.3 Fluorescence Lifetime Imaging (FLIM)

The fluorophores targeted to the SV using the Ab or Nb targeting approach (Section 1.9.1) can be visualized and spatially identified using microscopy. In this study, we have performed conventional epifluorescent microscopy and fluorescence lifetime imaging (FLIM), to visualize the targeted ion sensors. The fluorescence lifetime of a fluorophore is the time that it spends in the excited state (S1) before it emits fluorescence and returns to the ground state (S0). Fluorescence lifetime (FL) is an intrinsic property of a fluorophore and its environment (temperature, pH, ion concentrations), and does not depend upon the fluorescence intensity and the number of fluorophore molecules. Additionally, it does not depend on the laser intensity and the detector gain. Quenching of the excited state by the external factors decreases the FL and the resulting reduction in the FL can be quantified to get an idea about the environment of the fluorophore. For example, the FL of BAC can be used to quantitatively monitor the reduction in its FL in the presence of Cl^- ions.

Typically, to measure the FL, a fluorophore is excited with a sequence of photon pulses generated by femtosecond - picosecond pulsed lasers of a defined pulse frequency (MHz), desired wavelength, and pulse duration. The time duration between the excitation pulse and the first emission detected photon is measured, and it is known as time-correlated single-photon counting (TCSPC). TCSPC requires a defined start signal provided by the laser, and a defined stop signal detected by the single-photon sensitive detectors. The measurement of this time delay is repeated 1000-100,000 times and the time values are sorted in a

histogram. The TCSPC histogram is finally fitted to a monoexponential or a multi-exponential function and an average FL τ_{mean} is reported (Figure 1.6).

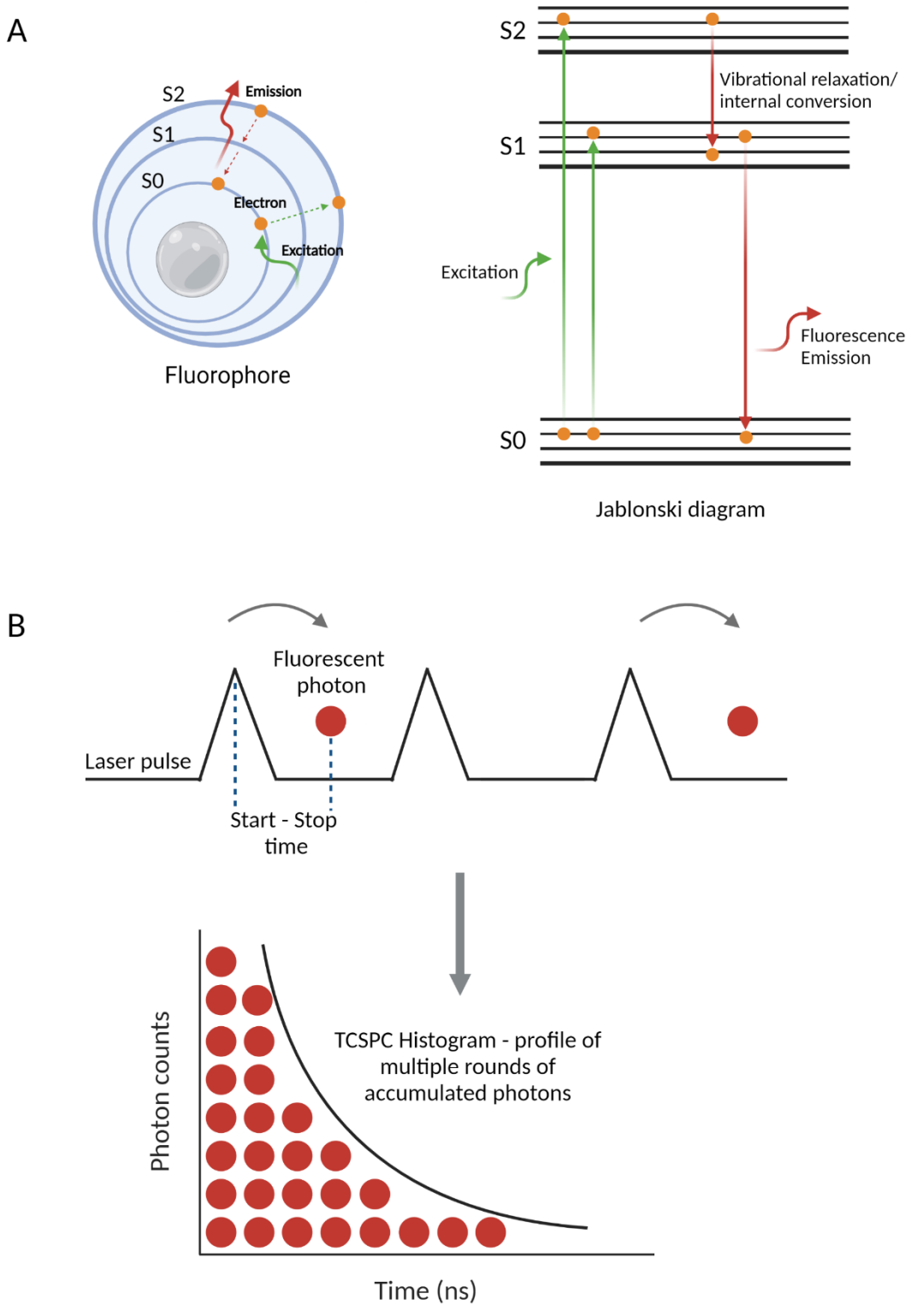

Figure 1. 6 Illustration of FLIM and TCSPC

(A) Scheme showing a fluorophore atom and electron excitation and emission of the photon, in the form of a Jablonski diagram. (B) The time duration from 'the start' of the laser pulse to 'the stop' signal from the detector when it receives

the first emitted photon is measured in TCSPC. The process is repeated multiple times to plot a histogram and calculate the average lifetime. Adapted from (Orthaus-Müller et al., 2016).

FLIM in live cells is quite intuitive, it offers an advantage of separating the cell compartments or fluorophore populations based on their lifetime. For example, the autofluorescence lifetime of the tissue can be separated from the lifetime of the fluorophore if the two lifetimes are different. With the improvement of microscopes and analysis workflows, FL of multiple fluorophores can be measured simultaneously, thus, it offers an additional possibility of multiplexing. Intensity-based imaging combined with ratiometric sensors used for FRET are great for the quantitative determination of concentrations but at the cost of greater spectral bandwidth. In contrast, FLIM offers the possibility to use single wavelength indicators for quantitative estimation and can be combined with other single wavelength probes, thus decreasing the load on the spectral bandwidth. Previously, many sensors, especially FRET-based sensors have been used to measure the ion concentration (for example Ca^{2+}) in synapses, and the cytoplasm of the neuron. Cl^- in the dendrites has also been measured using FLIM (Weilinger and LeDue, 2020) by microinjecting the Cl^- sensitive fluorophore MQAE through a micropipette. However, to our knowledge, there have been no FLIM measurements performed directly inside the SVs. This is most likely due to the lack of sensors and means to target them to SVs. The only study that has attempted to perform FLIM in SVs is one with a pH-sensitive protein called Cerulean expressed in the lumen of SVs to measure the resting pH of vesicles (Ph.D. thesis, Ralf Felix Beinlich, Munich, Germany, 2018,(Beinlich, 2018))

1.10 Objectives of this study

Despite intensive research, it has been difficult to study the mechanistic details of how the NTs operate to pump thousands of neurotransmitter molecules inside the SVs. The dissertation aims to develop a flexible targeting system that enables the delivery of any fluorophore (or ion sensor) to the lumen of an SV. To this aim, we have generated a new Nb against the luminal domain of Synaptotagmin 1 (Syt1) and have fused it with a HaloTag (Nb-Halo), separated by a sequence that can be recognized by a Tobacco Etch Virus (TEV) protease. By coupling the Nb with a Halo ligand labeled with a fluorescence-based ion sensor of interest, we have targeted the sensors to SVs using the exo-endocytic cycling. Furthermore, the SV proteins also appear at the PM after exocytosis, a stable cell surface pool facilitates rapid endocytosis and recycling. We have cleaved the PM pool of the sensor molecules that bind with the stranded Syt1 molecules using the TEV protease. This helps us to obtain a clean vesicular signal, and image the probe readout exclusively from the SV lumen. We have then characterized the neurons after the TEV cleavage and looked at their activity by electrically stimulating them with different action potentials. The further objective of this dissertation is to show that the Nb-Halo system of targeting can be used to target the required pH and Cl^- sensors to SVs and measure the ionic composition to resolve the ionic composition of an SV. To visualize the fluorophores together with the conventional epifluorescent microscopy, we have performed FLIM to

measure the FL changes in the BAC fluorophore with increasing Cl^- concentrations. Finally, we will discuss the results and accompanying challenges and how to potentially overcome them.

2 Materials and Methods

2.1 Chemicals and Materials

The standard chemicals (analysis grade purity) were purchased from Merck (Darmstadt, Germany) and Sigma-Aldrich (Steinheim, Germany). Other chemicals are listed in Table 2-1. All buffers were prepared in MilliQ water (Millipore, MH Aqua-Tech GmbH, Germany). Final volumes were measured using volumetric flasks (Fortuna GmbH, Germany) instead of measuring cylinders (VWR International, Pennsylvania, USA) for better accuracy. Buffers in all fluorescence-related experiments were filtered using 0.22 μm filter pore size (GE Healthcare, Illinois, USA) wherever applicable and the pH was set using a sensitive pH meter (Thermo Fisher Scientific). The pH meter was calibrated with standard pH buffers (Orion™, 910104, 910107, 910110) each time before use. The composition of all the buffers used in this study is mentioned in Table 2.2.

Table 2. 1 List of chemicals and cell culture reagents used in this study

Chemical	Company	Catalog Number
APV	Santa Cruz	A8054
Bicine	AppliChem	A1024.0250
Bis Acrylamide 19:1 (40 % w/v)	Serva	10679.01
Bovine Serum Albumin	AppliChem	A1391
Coomassie Brilliant Blue G250	AppliChem	A3480
CNQX	Santa Cruz	115066 14-3
D-glucose	AppliChem	A0883
DMSO	Sigma	D-2650
DNAse I	Sigma	D5025
Dulbecco's Modified Eagles Medium (DMEM)	Lonza	BE12-733F
Dulbecco's Modified Eagles Medium (DMEM)-F12 Medium	Sigma	D6421
Dithiothreitol (DTT)	Thermo Fisher Scientific	20290
Eagle's Minimum Essential Medium	Sigma	M2414
Fetal Bovine Serum (FBS)	Pan Biotech	P30-8500

5-Fluoro-2'-deoxyuridine (FUDR)	Sigma	F0503
2-[4-(2-hydroxyethyl)piperazin-1-yl]ethanesulfonic acid (HEPES)	Gerbu Biotechnik	1009.1000
L-cystein	Sigma	30129
L-glutamine	Invitrogen	25030123
MEM-Vitamine	Sigma	K0373
Mito+Serum extender	Corning	355006
Opti-Mem I Reduced-serum Medium	Invitrogen	11058021
Papain suspension	Cell Systems	LS003126
Paraformaldehyde	Sigma	P6148
Poly-D-lysine	Sigma	P-6407
Protease Inhibitor Cocktail	Merck	K42092903
Sodium dodecyl sulfate (SDS)	Serva	20765.03
Trybutyltin-Cl (TBT-Cl) (Cl/OH antiporter)	Sigma-Aldrich	T50202
Trypsin-EDTA	Lonza	17-161E
2-Amino-2-hydroxymethyl-propane-1,3-diol (Tris)	VWR International	103156X

Table 2. 2 Composition of buffers, reagents, media, and gels used in this study

Buffer	**Composition**
ÄKTA buffer A (for ion exchange chromatography of Bispecific Nb)	20 mM HEPES, 1 mM EDTA, 0.2 mM TCEP, 200 mM Sucrose
ÄKTA buffer B (for ion exchange chromatography of Bispecific Nb)	1 M NaCl, 20 mM HEPES, 1 mM EDTA, 0.2 mM TCEP, 200 mM Sucrose
Brain Lysis Buffer	400 µl of 1 M Tris HCl pH 8 (final 20 mM Tris HCl pH 8), 500 µl of 5 M NaCl (final 137 mM NaCl), 200 µl Triton (final 1 % Triton X-100), 80 µl 0.5M EDTA (final 2 mM EDTA),1 pill Protease inhibitor cocktail, total 20 mL
1X (+) ve Chloride buffer	120 mM KCl, 20 mM NaCl, 1 mM $CaCl_2$, 1 mM $MgCl_2$, 20 mM HEPES, pH, 7.4
1X (-) ve Chloride buffer	120 mM KNO_3, 20 mM $NaNO_3$, 1 mM Ca $(NO_3)_2$, 1 mM Mg $(NO_3)_2$, 20 mM HEPES, pH 7.4
Cleavage Buffer for Bispecific Nb purification	20 mM Tris-HCl, 200 mM NaCl, 10 mM Imidazole, 200 mM Sucrose, pH8.0
Coomassie stain solution	0.2 % (*w*/*v*) Coomassie Brilliant Blue R-250, 50 % (*v*/*v*) methanol, 10 % (*v*/*v*) acetic acid

Destain 1	20 % (*v*/*v*) isopropanol, 10 % (*v*/*v*) acetic acid
Destain 2	10 % (*v*/*v*) isopropanol, 5 % (*v*/*v*) acetic acid
Dialysis Buffer for protein purification	20 mM Tris, 150 mM NaCl, 0.1 mM TCEP, pH 7.5
GBSS	1.5 mM $CaCl_2 \cdot 2H_2O$, 4.9 mM KCl, 0.2 mM $NaH_2PO_4 \cdot H_2O$, 11 mM $MgCl_2 \cdot 6H_2O$, 0.3 mM $MgSO_4 \cdot 7H_2O$, 130 mM NaCl, 2.7 mM $NaHCO_3$, 0.8 mM Na_2HPO_4, 5 mM D-glucose, 22 mM HEPES, pH 7.4 in Milli-Q water
High Salt PBS	411 mM NaCl, 8.1 mM KCl, 30 mM Na_2HPO_4, 5.2 mM KH_2PO_4, pH 7.4
Inactivation solution	Neuronal serum medium, 0.25 % BSA, 0.1 mg/mL DNAse I
Native polyacrylamide gel (10 %)	1.25 ml 40 % acrylamide/bis-acrylamide (19:1), 0.5 ml 10X TBE buffer, 3.25 ml ddH_2O, 6.25 µl TEMED, 62.5 µl 10 % (*w*/*v*) APS
Neuron Plating media	DMEM/F12, 1X B-27, 2 mM L-Alanyl-L-Glutamine
Neuron Serum Media	Eagle's MEM, 5 % FBS, 2 mM L-Alanyl-L-Glutamine, 1X MEMVitamine, Mito+Serum extender, 3.8 g/L D-glucose
Papain Enzymatic Solution	GBSS, 11.39 mM L-cysteine, 0.5 mM Na EDTA, pH 8. 1 mM $CaCl_2$, 3 mM NaOH, 0.1 mg/mL DNAse I, 1 % Papain suspension
PBS	137 mM NaCl, 2.7 mM KCl, 10 mM Na_2HPO_4, 2 mM KH_2PO_4, pH 7.4
pH calibration High K^+ Buffer	122.4 mM KCl, 20 mM NaCl, 10 mM HEPES or MES, 10 mM glucose, 2 mM $CaCl_2$, and 1 mM $MgCl_2$
Poly-D-Lysine solution	0.01 g/L poly-D-lysine, 25 mM H3BO3, 6.3 mM Na2B4O7·10H2Oin Milli-Q water
Resuspension/Wash Buffer for Bispecific Nb purification	50 mM Tris-HCl, 300 mM NaCl, 20 mM Imidazole, pH8.0
SDS-PAGE anode buffer	0.2 M Tris, pH 8.9
SDS-PAGE cathode buffer	0.1 M Tris, 0.1 M tricine, 0.1 % (*w*/*v*) SDS
SDS-PAGE gel buffer	3 M Tris, 0.3 % (*w*/*v*) SDS, pH 8.45
SDS-PAGE loading dye (5X)	200 mM Tris, 5 % (*w*/*v*) SDS, 3.85 % (*w*/*v*) DTT, 37.5 % (*v*/*v*) glycerol, 0.015 % (*w*/*v*) bromophenol blue, pH 6.8
SDS-PAGE resolving gel (10 %)	1.75 ml 30 % acrylamide, 1.7 ml gel buffer, 0.5 ml ddH_2O, 1.05 ml 50 % (*v*/*v*) glycerol, 3.5 µl TEMED, 25 µl 10 % (*w*/*v*) APS

SDS-PAGE stacking gel	200 µl 30 % acrylamide, 400 µl gel buffer, 915 µl ddH_2O, 2 µl TEMED, 10 µl 10 % (*w/v*) APS
Size Exclusion Chromatography Buffer	20 mM HEPES, 150 mM NaCl, 1mM EDTA, 0.2 mM TCEP, 200 mM Sucrose, pH 7.5
Stimulation Buffer	Tyrode's Buffer, 10 µM CNQX, 50 µM APV
TBE	100 mM Tris-base, 89 mM boric acid, 2 mM EDTA, pH 8.3
TBS	15 mM Tris-HCl, 150 mM NaCl, pH 7.4
TBST	15 mM Tris-HCl, 150 mM NaCl, 0.05 % (*v/v*) tween 20, pH 7.4
Terrific broth (TB) medium	12 g/l tryptone, 24 g/l yeast extract, 0.4 % (v/v) glycerol, 2.31 g/l KH_2PO_4, 12.54 g/l K_2HPO_4
Tyrode's Buffer	130 mM NaCl, 4 mM KCl, 1 mM $MgCl_2$, 5 mM $CaCl_2$, 48 mM Glucose and 10 mM HEPES, pH set to 7.4
Wash buffer for IP from whole brains	100 µl 1M Tris HCl pH 8, 100 µl 1M Tris HCl pH 7 (final 10 mM Tris, pH to ~7.4),40 µl 0.5M EDTA (final 1 mM EDTA), 40 µl 0.5 M EGTA (final 1 mM EGTA), 600 µl of 5M NaCl (final 150 mM NaCl), 200 µl Triton (final 1 % Triton X-100), Protease inhibitor cocktail, total 20 mL
Western Blot transfer buffer	20 % (*v/v*) 5X Trans-Blot Turbo Transfer Buffer (Bio-Rad), 20 % (*v/v*) ethanol

Table 2. 3 List of primary antibodies used in this study

WB- Western Blotting (1:1000), ICC – Immunocytochemistry (1:500), SySy- Synaptic Systems GP – Guinea Pig, AF – AcidiFluor Orange CpH – CypHer

Primary Ab	Species, Clonality	Application	Source	Catalog No.
Bassoon	Mouse Monoclonal	ICC	Enzo	SAP7F407
GAPDH	Mouse Monoclonal	WB	Thermo Scientific	MA5-15738
FLAG tag	Mouse monoclonal	WB	Sigma-Aldrich	F3165
MAP-2	Mouse monoclonal	ICC	SySy	188011
PSD-95	Polyclonal serum	ICC	SySy	124002
Synaptophysin 1	Rabbit polyclonal serum	ICC	SySy	101002
Syt1 lumen	Mouse monoclonal 604.2	ICC, WB	SySy	105311
Syt1 lumen CpH	Mouse monoclonal	ICC	SySy	105311 CpH
Syt1 lumen AF	Mouse monoclonal	ICC	SySy	105311AF

Syt1/2 Cyt	Rabbit polyclonal purified	ICC	SySy	105003
Syt1 Cyt	Rabbit monoclonal 41.1	ICC	SySy	105008
VAMP2	GP polyclonal serum	ICC	SySy	104204
VGAT lumen Cy3	Rabbit polyclonal purified	ICC	SySy	131103 C3
VGAT lumen Cy5	Rabbit polyclonal purified	ICC	SySy	131103 C5
VGAT lumen CpH	Rabbit polyclonal purified	ICC	SySy	131103 CpH
VGAT lumen AF	Rabbit polyclonal purified	ICC	SySy	131103 AF
VGAT Cyt	Mouse monoclonal	ICC	SySy	131011
VGAT Cyt C2	Mouse monoclonal	ICC	SySy	131011 C2
VGAT Cyt C3	Mouse monoclonal	ICC	SySy	131011 C3
VGLUT 1	Rabbit polyclonal serum	ICC, WB	SySy	135302
VGLUT1 Cy3	Mouse monoclonal	ICC	SySy	135011 C3
VGLUT1 Cy5	Mouse monoclonal	ICC	SySy	135011 C5
VGLUT Nb C5	Nanobody FluoTagX2	ICC	Nanotag	N1602

Table 2. 4 List of secondary antibodies used in this study.

WB- Western Blotting (1:15000), ICC – Immunocytochemistry (1:400)

Secondary Ab	Species	Application	Source	Catalog Number
IRDye 800CW anti-Rabbit	Goat polyclonal	WB	Licor	926-32211
IRDye 680CW anti Mouse	Goat polyclonal	WB	Licor	926-68070
Anti-Rabbit Alexa488	Goat Polyclonal	ICC	Dianova	111-035-144
Anti-Rabbit Cy3	Goat polyclonal	ICC	Dianova	111-165-008
Anti-Rabbit Cy5	Donkey polyclonal	ICC	Dianova	711-175-152
Anti-Mouse Alexa488	Goat Polyclonal	ICC	Dianova	115-165-205
Anti-Mouse Cy3	Goat Polyclonal	ICC	Dianova	115-165-020
Anti-Mouse Cy5	Goat Polyclonal	ICC	Dianova	115-175-071
Anti-GP Cy5	Donkey Polyclonal	ICC	Dianova	706-175-148

2.2 General Methods for Protein Analyses

2.2.1 BCA Protein Estimation

Pierce™ BCA Protein Assay Kit (#23225, Thermo Fisher Scientific, MA, USA) was used to estimate the concentration of proteins according to manufacturer's instructions in a 96 well flat-bottomed plate (Greiner GmbH, Germany). Protein standard buffers (#23208, Thermo Fisher Scientific, MA, USA) were used to plot a BSA standard curve. Absorbance at 650 nm was measured in a plate reader (Tecan Genios Pro,

Männedorf, Switzerland) according to the manufacturer's manual ((BCA Protein Assay, 2020) modified from (Smith et al., 1985)).

2.2.2 SDS Schägger Gels

Protein samples were analyzed using SDS-PAGE on Schägger gels (Schägger, 2006). 10 µg of protein samples were mixed with the loading buffer and run on a 10 % resolving gel and 4 % stacking gel. Gels were run at 60 V until the samples entered the resolving gel and then it was run at 120 V (Bio-rad Laboratories, Hercules, CA). The PageRuler™ prestained protein ladder 10-180 kDa (#26617, Thermo Fisher Scientific, MA, USA) was used as a molecular marker. Gels were stained by bathing the gels in Coomassie stain and boiling in a microwave for a minute followed by shaking for 10 minutes at RT (RT). They were then incubated in destaining buffer 1 and again boiled for a minute followed by shaking for 30 minutes. Finally, they were destained in the destaining buffer 2 overnight and then scanned on a scanner (HP, California, US).

2.2.3 Western Blotting and Dot Blot Assay

Gels were transferred on a nitrocellulose membrane after running on Schägger gels according to (Yang and Mahmood, 2012) with the following modifications. A TransBlot Turbo Transfer machine (Bio-Rad Laboratories, Hercules, CA) was used to perform the transfer in 7 minutes according to the manufacturer's instructions. The membrane was blocked in 5 % milk in TBST/PBST. Further, the membranes were incubated in the required primary antibody prepared in 5 % milk in TBS/TBST/PBST (depending on the Ab stability, TBS or PBS (with or without Tween) was used) at 4°C overnight or 1-2 hours at RT. Membranes were then washed with TBST/PBST and then incubated in secondary infrared (IR) dye-labeled antibodies prepared in TBS/PBS for an hour at RT. For a list of primary and secondary Abs used in this study, refer to tables 2.3 and 2.4 respectively. After three washing steps of 15 minutes each, fluorescent protein bands were visualized using Odyssey CLx IR Imaging System (Li-Cor Biosciences, GmbH, Germany). To perform the dot blot assay, a pre spotted array on a membrane was ordered with a crude purity synthesis quality of specific short sequence peptides of Syt1 luminal domain to identify the sequence to which the Nb binds (GenScript Biotech, Netherlands). The dot blot assay was performed by Dr. Eugenio Fornasiero, University Medical Center, Göttingen.

2.3 Immunoprecipitation of Syt1 from WT and KO Syt1 mice brains using Nanobody against the luminal domain of Syt1

Syt1 WT and KO Mice brains were provided by the lab of Prof. Volker Hauke, Berlin, Germany. The protocol for Syt1 immunoprecipitation (IP) was adapted from Abcam (Cambridge, UK) (Abcam, 2010) and modified as follows for optimization by Dr. Eugenio Fornasiero. WT and KO IP were performed in duplicates.

Pre-loading GFP tagged Nanobody (Nb) on the beads- 20 µL of bead slurry (GFP Selector, # N0130, Nanotag, Germany)/sample was pre-incubated with 5µL of GFP Nb (100 µM) in 75 µL of lysis buffer. 'No

Nb' control was also prepared in the same way. Bead slurry with Nb was constantly agitated for 30 minutes at 4°C on an orbital shaker in the cold room. It was then centrifuged for a minute at 1000 g (ThermoScientific™ Heraeus™) and the supernatant was carefully removed. 1 mL of lysis buffer was added and rotated for 5 minutes at 4°C. Beads were ready to use after centrifuging once more for a minute at 1000 g.

Lysate from tissue - Frozen brains were thawed and 300 µL of Lysis Buffer (composition, Table 2.2) per brain was added in an Eppendorf tube (Sarstedt AG & Co.KG, Germany). Brains were homogenized using a small Teflon homogenizer 3-4 strokes up and down manually. Debris and nuclei were pelleted down by centrifugation at 1000 g (ThermoScientific™ Heraeus™) for 5 minutes and the supernatant was used for protein extraction. The supernatant was constantly agitated for 30 minutes at 4°C on an orbital shaker followed by centrifugation for 10 minutes at 12,000 g in a microcentrifuge (ThermoScientific™ Heraeus™). Tubes were removed and kept on ice and the supernatant was transferred to fresh cold low binding Eppendorf tubes. Protein concentration was estimated using the BCA protein estimation kit as described previously.

Pre-clearing of the lysate – Pre-clearing the lysate helps reduce non-specific binding and reduces the background. 100 µL of lysate was mixed with naked (not the ones with preloaded Nb) bead slurry for 30 minutes on an orbital shaker at 4°C. Beads were sedimented by spinning at 1000 g for a minute and the supernatant was used for the IP.

Each sample (50 µL lysate and 20 µL slurry) was incubated at 4°C for an hour on an orbital shaker. Beads were then sedimented by centrifugation at 1000 g for a minute and resuspended in 1 mL lysis buffer in a fresh Eppendorf tube. It was again centrifuged for a minute at 1000 g and the supernatant was discarded. This washing step was repeated one more time. The beads were finally resuspended in 20 µL of SDS buffer (composition, Table 2.2) and heated at 95°C for 5 minutes. The samples were loaded on an SDS gel and western blotting was performed using Syt1 cytoplasmic and GAPDH antibodies (Table 2.3).

2.4 Clensor formation and its quality check

2.4.1 Binding of DNA oligos

Clensor was formed as previously described (Saha, 2015). DNA oligo D1 carrying a Halo ligand (Biomers, Germany) and DNA oligo D2 labeled with Alexa647 (IBA GmbH, Germany) were already supplied in water (Table 2.5). PNA-BAC, referred to as PNA from here on, was synthesized (laboratory of Prof. Diederichsen by Dr. Patrick Menzel and Elena Cotero, Institute for Organic and Biomolecular Chemistry, Göttingen, refer Ph.D. thesis of Dr. Patrick Menzel) using standard Fmoc chemistry, using analytical grade reagents and purified by reverse-phase HPLC. Lyophilized PNA was resuspended in MilliQ water to make a 1mg/mL stock solution. All the three components (Table 2.5) were aliquoted into small fractions and stored at -20°C until further use. The concentration of each component was measured on a Nanodrop (NanoDrop™ 1000, Thermo Fisher Scientific) using the molar extinction coefficients of Alexa647 as

ε = 270,000 $M^{-1} \cdot cm^{-1}$ and for BAC ε = 65,000 $M^{-1} \cdot cm^{-1}$. The concentration of PNA was titrated each time (to obtain the highest yield) against 1:1 fixed molar ratio of D1:D2 such as Clensor (D1: D2: PNA) was formed at 1:1:1, 1:1:2, 1:1:3 and so on in 10 mM Sodium Phosphate buffer, pH 7.4 (filtered) to a final concentration of Clensor of 20 μM. The mixture was briefly vortexed to mix all the components well. Annealing was done on a PCR machine (T-Personal Combi PCR-Cycler, Biometra, Jena, Germany) by heating the solution at 95°C and cooling it at a rate of 5°C every 15 minutes until the temperature reached to 25°C. All the samples were incubated at 4°C for 48 hours. However, later, we confirmed that 24 hours of incubation was also enough to stabilize the Clensor molecule. Clensor formation was confirmed by running it on a gel (see below).

Table 2. 5 Halo-Clensor DNA oligo sequences and their role.

Oligo	sequence	Role
D1	5'CACCAGACAGCAAGATCCTATATATA 3'	DNA strand: targeting module
D1 Halo	5'Halo-CACCAGACAGCAAGATCCTATATATA **G-Halo ligand3'**	DNA strand: targeting module modified with HaloTag ligand attached to one base overhang
D2	5'TATA**T**ATAGGATCTTGCTGTCTGGT GTGCAGTGTTGAT3'	DNA strand: normalizing module (Alexa 647 modification on the T shown in bold)
PNA	BAC-NHε-Lys-ATCAACACTGCA-Lys-COOH	PNA strand: Chloride sensing module
ALFA-PNA	BAC-NHε-Lys-ATCAACACTGCA-Lys-COOH-ALFA peptide (SRLEEELRRRLTE)	PNA strand: Chloride sensing module modified with ALFA peptide

2.4.2 Gel Shift Assay

Clensor formation was confirmed on a mobility gel shift assay as described previously (Saha, 2015). 10 % Native Polyacrylamide gels were prepared in 10X TBE and pre-run in 1X TBE buffer at 200 V for 30 minutes at 4°C (Bio-Rad Laboratories, Hercules, CA). 1 μL of D2 and 3 μL of Clensor (20 μM stock) samples were enough to visualize a clear band. Samples were mixed with a 6X DNA loading dye (Thermo Fisher Scientific, MA, USA) and loaded in the gel. The dye fronts of Bromophenol Blue and Xylene Cyanol were perfect to monitor the movement of the Clensor which would lie in between the two dye fronts. Gels were run at 200 V at 4°C until the Xylene Cyanol dye front reached the bottom-most of the gel. Gels were then imaged on Fujifilm FLA 7000 scanner (FUJIFILM Life Science, Stamford, CT; at exposure times: Alexa488 (for BAC visualization) PMT:1000 and Cy5, (for Alexa visualization) PMT: 500). Images were further analyzed on FIJI (NIH, USA).

2.5 Cloning and Purification of bispecific NbSyt1-NbALFA and GFP ALFA

All the protocols and reagents for cloning, bacterial transformation and, protein purification were obtained from the website of New England Biolabs (NEB Massachusetts, US). More details are as follows.

2.5.1 Gibson Assembly

Plasmid backbones were obtained from Dr. Steffen Frey, Nanotag Göttingen, Germany (table 2-6).

Table 2. 6 List of plasmids used in this study

Name	Encoded protein	Source
pNT1236	His14-bdSUMO-NbSyt1-TEV-3xFLAG-GFP	Nanotag
pNT-NAM01	NbALFA	Nanotag
pNT1050	His14-bdSUMO-shGFP2-ALFA	(Götzke et al., 2019)

Plasmids encoding NbSyt1-TEV-3XFLAG-GFP and NbALFA were used to exchange GFP with the NbALFA sequence to produce a plasmid that encodes NBSyt1-TEV-3XFLAG-NbALFA. Primers for Gibson Assembly were designed using the Primer design feature of the NEbuilder Assembly tool (NEB Massachusetts, US) and were ordered from Eurofins Genomics. PCR-based amplification was done for each 'Vector' and 'Insert'. Briefly, reactions were performed by mixing the reaction buffer, dNTPs, forward and reverse primers, template DNA, high fidelity DNA Polymerase, 5X Enhancer and, nuclease-free water in appropriate volumes calculated using NEB Gibson Assembly protocol. Melting Temperature was calculated using T_m calculator (NEB Massachusetts, US). All the DNA constructs were run on a 1 % Agarose Gel (100V, 40 minutes) to confirm the amplification. The required bands were excised and the DNA was purified using the Gel purification kit (#A9281/2/5, Wizard® SV Gel and, PCR Clean-up system, Promega Corporation, Madison, USA) DNA concentration was measured using the Nanodrop (NanoDrop™ 1000, Thermo Fisher Scientific). The purified vector and the insert were mixed in appropriate proportions in the presence of the NEB2X Assembly mix. NEB *E.coli* 5 alpha was transformed using the PCR ligation product (standard protocols from NEB). A single colony was grown in LB media (Bertani, 1951) and the DNA was purified and sequenced to confirm that there were no other random mutations.

2.5.2 Protein expression and purification

NEB Shuffle Express T7 *E.coli* (C3029) was transformed and grown overnight. A single colony was picked and grown in a liter of TB medium ((CSH Protocols 2006), Composition Table 2.2) in the presence of 50 µg/mL Kanamycin until the optical density at 600 nm (BioPhotometer 6131 Spectrometer, Eppendorf AG, Hamburg, Germany) reached 0.8. Expression was then induced with 0.3 mM isopropyl-β-D-1-thiogalactopyranoside (IPTG) and the cells were incubated for 14-16 h at 25 °C and 120 g in a shaker (Infors HT, Switzerland).

The protein was purified using Nickel binding affinity chromatography using the protocol adapted from (Götzke et al., 2019). Bacterial cells were centrifuged for 25 minutes at 4,000 g and 4 °C (rotor: H-12000, Thermo Fisher Scientific, MA, USA). The pellet (15 g wet weight) was resuspended in a 50 mL resuspension buffer (Table 2.2) containing protease inhibitors and homogenized with a glass douncer three times manually. Cell resuspension was processed twice with the microfluidizer at 18,000 psi (M110-Microfluidizer, Microfluidics, MA, USA) and centrifuged at 40K g at 4°C for 30 minutes (rotor: Ti45, Beckman, California, USA). Meanwhile, Nickel-NTA resin beads (HisPur™ Ni-NTA Resin, #88222, Thermo Fisher Scientific) were equilibrated with a resuspension buffer by centrifuging for a minute at 800 g on a tabletop centrifuge at 4°C. This was repeated three times to equilibrate the beads well. Cell supernatant was collected after the centrifugation and rotated with equilibrated beads at 4°C for 2-3 hours. The supernatant bead suspension was then run over 50 mL Gravity flow column (Econo-column® Bio-Rad Laboratories, Hercules, CA) and the flowthrough (FT) was collected. Beads were washed three times with 50 mL Wash Buffer (Table 2.2) and once with the Cleavage buffer (Table 2.2). After excessive washing, beads were transferred in a 10 mL cleavage buffer in a 15 mL falcon tube. 1 µM of Ulp1 (The yeast homolog of SUMO protease, purified in Dr. Alex Stein's lab, MPI-BPC) was added and incubated for another hour at 4°C on constant rotation. Beads were poured back into the column and flowthrough was collected. They were washed once again with 10 mL Cleavage Buffer and remaining eluted protein was collected and 5mM DTT was added. Protein was further concentrated up to 5 mL using 3 kDa MWCO VivaSpin concentrator (Sartorius Stedim Biotech, Göttingen, Germany),

Proteins were additionally purified using ion-exchange chromatography on a MonoQ 10/100 GL column (GE Healthcare Life Sciences, Pittsburgh, PA) using an ÄKTA system (GE Healthcare Life Sciences, Pittsburgh, PA). ÄKTA buffers A and B (Table 2.2) were filtered (0.2 µm membrane filter, Sartorius Stedim Biotech, Göttingen, Germany) and degassed. The column was equilibrated with ÄKTA buffer A and a protein sample was injected into the column. The protein was eluted with an increasing salinity gradient by gradually increasing the buffer B/A ratio. Purified proteins were then run on Schägger gel for analysis.

GFP-ALFA protein (from plasmid pNT1050, Table 2-6) was also purified similarly as the Bispecific Nb purification but with slight modifications. NEB BL21 (DE3) competent *E.coli* was used for protein expression. The purified protein was subjected to size exclusion chromatography using the HiLoad Superdex 75 HR 16/60 column (GE Healthcare Life Sciences, Pittsburgh, PA).

2.6 Complex formation of Bispecific Nb ALFA with its substrates

Bispecific Nb and GFP ALFA - Purified Bispecific Nb and GFP ALFA were mixed in an equimolar ratio to form a complex. The complex was furthermore dialyzed against PBS and then purified by running it on a size exclusion chromatography using Superdex 75 HR 10/30 (Pharmacia Biotech, Uppsala, Sweden). Samples were run on Native PAGE for further analyses.

Bispecific Nb and fluorophores labeled ALFA peptide complex formation - Fluorophore labeled ALFA peptide was synthesized by Dr. Patrick Menzel (Prof. Diederichsen lab, Institute for Organic and Biomolecular Chemistry, Göttingen, refer Ph.D. thesis of Dr. Patrick Menzel). Bispecific Nb and fluorophore-labeled ALFA peptides were mixed in equimolar ratios at RT for 15 minutes for the complex to form. Samples were run on Native PAGE for further analyses (Saha, 2015).

2.7 Fusion of Nb with HaloTag and its binding with HaloTag fluorescent ligands

HaloTag fused with NbSyt1 was purified by Dr. Steffen Frey at Nanotag. Nb fused with HaloTag and HaloTag fluorescent ligands (Table 2.7 below) were mixed in equimolar ratio at a final concentration of 10 μM for 15 minutes at RT. The complex formation was confirmed using the gel shift assay described previously.

Table 2. 7 HaloTag ligands used in this study.

HaloTag fluorescent ligands	Company/ Catalog No.	Type of Sensor	Excitation /Emission (nm)
Alexa647	Promega	-	649/666
TMR	Promega	-	555/580
AcidiFluor Orange	Goryo Chemical	pH	552/570
Virginia Orange	Gift from Lavis lab	pH	555/581
BAC	Generon(AF-0406-D005.0-001), conjugated with Halo ligand in Chemical facility, MPI	Chloride	434/505
D1 oligo	Biomers	-	-
pHrodo	Thermo Fischer Scientific (C36600)	pH	560/585

2.8 Fluorometry

Fluorometry was performed on Fluorolog®-3 (Horiba Scientific, Kyōto, Japan) using 250 μL glass cuvettes (Starna GmbH, Germany) to use the minimum volume of precious fluorophores and proteins.

2.8.1 mOrange2/pHlourin pH calibration

In vitro pH calibration of pHlourin/mOrange2 fused proteins was performed as previously described (Egashira et al., 2015) with slight modifications. MES buffer (Table 2.2) was used for pH values 5, 5.6, and 6.2 and HEPES buffer was used for pH values above 6.8. The concentration of 0.8μM of the two proteins was enough to give a substantial number of counts (>100 K counts) on the Fluorolog. The protein was added in 250 μL of each of the pH clamped buffers in Eppendorf tubes and vortexed briefly. The mixture was put in cuvettes and the emission spectra were recorded. Data were analyzed on Graph Pad Prism.

2.8.2 Clensor sensitivity to Cl^- and pH

pH calibration buffers (Table 2.2) were used to confirm the pH insensitivity of Clensor using Fluorometry (Egashira et al., 2015). Cl^- calibration buffers were prepared as previously described (Saha, 2015). Cl^- calibration buffers were prepared by appropriately mixing 1X Cl^- positive and 1X Cl^- negative buffers (Table 2.2) to get a final Chloride concentration of 0, 20.25, 40.5, 81, 101.25, 121.5, 141.25 and, 162 mM. 3 µL (final concentration: 240 nM) of 20 µM Clensor was added to each of these buffers in an Eppendorf tube. This dilution was done to obtain at least 100 K counts for reliable measurements. This was repeated for D2-Alexa alone to reconfirm Alexa fluorophores' Cl^- insensitivity. In the same manner, the emission spectra of BAC were also recorded for free BAC-Halo and Nb bound BAC-Halo.

Table 2. 8 Excitation and Emission wavelengths of BAC and Alexa 647 fluorophores in Clensor

Fluorophore	Excitation spectra range	Emission spectra range	$\lambda_{Excitation}$/ $\lambda_{Emission}$ (nm)	Slit size (nm)
BAC	300-485 nm	455-640 nm	434/505	5
Alexa 647	500-650 nm	660 – 760 nm	650/670	2

R/G ratios were calculated at each Cl^- concentration by dividing the Alexa (R) counts (at 670 nm) with BAC (G) counts (at 505 nm). Fold change was compared between 0 mM and 162 mM Cl^- values. R/G ratio was plotted against the Cl^- concentrations and was fitted with the modified Stern Volmer Equation to obtain the Stern Volmer K_{sv} constant.

$$\frac{R}{G} = 1 + K_{SV} \cdot [Cl^-] \quad (10)$$

2.9 Animals and cell culture

Neurons were cultured as described previously (Yagensky et al., 2019). Briefly, postnatal day zero (P0) Wistar rat pups were brought from the local animal facility of MPI-BPC. Brains were taken out and hippocampi dissected and put in an enzyme solution (Table 2.2) containing Papain for 30 minutes. Hippocampi were then transferred to the inactivation solution. Digested tissue pieces were triturated using fire-polished glass pipettes first with a bigger hole and then with a fresh fire-polished pipette with a smaller hole until there is a smooth homogenous solution. The cells were passed through a 0.22 µm cell strainer after which they were centrifuged at 5000 g for 5 minutes. The supernatant was sucked off carefully and the cell pellet was suspended in serum media. Cells were counted using a hemocytometer (Neubauer, Paul Marienfeld GmbH, Germany) manually. 20,000 cells/cm^3 were added in wells of a 12 well plate containing Poly D Lysine (PDL) coated coverslips already containing neuron culture medium. Cells were grown in a 37°C and 5 % CO_2 incubator and used for imaging between 14-18 DIV. In the second part of the project

involving Nb-Halo protein, neurons were obtained from the lab of Prof. Silvio Rizzoli (Dept. of Neuro- and Sensory Physiology, University Medical Center, Göttingen). They were cultured according to the protocols described before (Truckenbrodt et al., 2018).

2.10 Labeling of cultured neurons with Nb/Ab by spontaneous endocytosis

Labeling of neurons was performed as described before (Truckenbrodt et al., 2018) although with the following modifications. 200 µL of media from 18 mm diameter coverslip (Karl Hecht Assistant, Germany) containing cultured hippocampal neurons was taken in an Eppendorf tube, mixed with the required labeled antibody (Ab) or a nanobody (Nb) (refer to Table 2.9 below). The mixture was centrifuged at 13K g for 10 minutes at 37°C to get rid of the dye aggregates. The coverslip was incubated in the media for 10 minutes and placed in a 37°C/5 % CO_2 incubator to label the recycling pool of SVs. Neurons were then washed fast 3 times with a warm Tyrode buffer (Table 2.2). Experiments were performed on neurons from 14 to 18 DIV. Imaging was done instantly in the warm Tyrode's buffer. For HaloTag fused Nb uptake, Nb Halo fusion protein was premixed with Halo ligand (refer to Table 2.7) for 15 minutes at RT. The above procedure of labeling was then performed.

Table 2. 9 Nb and Ab constructs used for imaging.

Nb/Ab	Ligand/ label (if any)	Company /Catalog No.	Final Concentration during uptake	Type of Sensor	$\lambda_{Excitation}$/ $\lambda_{Emission}$ (nm)
604.2 Syt1 Ab	AF	SySy 105 103AF	100nM	pH	552/570
VGAT Ab	AF	SySy 131 103AF	100nM	pH	552/570
pHlourin/GFP Nb	-	Nanotag	2.5 µM	pH	488/507
mOrange 2 Nb	-	Nanotag	2.5 µM	pH	548/562
Nb-HaloTag	HaloTag ligands (Table 2.7)	Nanotag	2.5 µM		

2.11 Immunostaining

Immunostaining was performed according to the Immunostaining manual by Abcam (Abcam, 1998). Briefly, cells were fixed with 4 % (w/v) paraformaldehyde (PFA) (P6148, Sigma-Aldrich) in 4 % Sucrose (0.12M) in PBS for 20 minutes at RT followed by washing three times with 1X PBS. Excess PFA was quenched with 100 mM NH_4Cl for 20 minutes followed by washing three times with PBS. The unspecific binding was blocked with incubating the coverslip in 2.5 % BSA and 0.1 % Triton X-100 in PBS for 15 minutes. The cells were then incubated in a humidified chamber at RT for 1 hour in primary antibodies

diluted in 2.5 % BSA and 0.1 % Triton in PBS. Cells were then washed twice with 2.5 % BSA and 0.1 % Triton in PBS and then, once with 2.5 % BSA in PBS. Finally, the coverslips were incubated for 1 hour in a humidified chamber at RT in secondary Abs diluted in 2.5 % BSA in PBS. After washing the coverslips thrice with 2.5 % BSA in PBS, they were washed once with PBS containing high salt (400 mM NaCl), again washed with PBS, and finally mounted on slides with a mounting medium. Mounted coverslips were left at RT for a few hours and then kept at 4°C overnight, and were imaged the following day.

2.12 Microscopy

2.12.1 Epi-fluorescent microscopy

Images were acquired on Nikon Ti 2E (Nikon Corporation, Chiyoda, Tokyo, Japan) inverted epi-fluorescent microscope equipped with a 60X oil objective and Photometrics 95B camera. A dark Okolab (Ottaviano, Italy) cage incubator system was used to maintain 37°C and 5 % CO_2 (OKO Air Pump and CO_2 controller). GFP/pHlourin was imaged in Alexa488 channel (EX 472/30, DM 495, BA 520/35) while AcidiFluor Orange was imaged in Cy 3 channel (EX 531/40, DM 562 BA 593/40). Alexa647 was imaged in the Cy5 channel (EX 628/40, DM 660, BA 692/40).

2.12.2 Fluorescence Lifetime Imaging (FLIM)

Data were acquired on an inverted fluorescence microscope (Leica TCS SP8 falcon, Leica Microsystems, Wetzlar, Germany) equipped with 63X objective (11506353, Glycerol immersion, Numerical Aperture 1.3, Working Distance - 300 μM). 8 well glass-bottomed slides (#80807, Ibidi, Gräfelfing, Germany) were used to image samples for calibration profiles. BAC containing samples were excited by a 440 nm pulsed laser (PicoQuant, Berlin, Germany) at a frequency of 80 MHz. For live-cell imaging and the measurement of autofluorescence spectra in living cells, the microscope cage was heated to 37°C and contained a humidified gas mixture (Okolab, Ottaviano, Italy). Additionally, 5 % CO_2 was maintained in a small enclosed chamber (custom-built, MPI-EM, Göttingen) containing the cells mounted in the perfusion type magnetic chamber (EC B18, Live Cell Instrument, Gyeonggi-do, Republic of Korea). Before every experiment, Oregon Green 488 was used as the reference dye whose lifetime was estimated, and the settings were calibrated accordingly. Oregon Green 488 was also excited using the same laser and same settings as the BAC excitation. Data were collected using Time correlated single photon counting (TCSPC) (Becker and Hickl GmbH, Berlin, Germany). At least 60 frame repetitions were made to capture photons in the range of 10^2 if the fluorophore followed a monoexponential decay and up to 10^4 if the fluorophore had a biexponential decay. Photons were detected using a hybrid cooled single-molecule detection (SMD) detector. In each experiment, reflection was adjusted to the coverslip/glass surface thickness to obtain accurate measurements. The intensity time graphs were fitted with monoexponential or biexponential functions integrated with the Leica software. Cl^- calibration of BAC-Halo was performed using buffers clamped at specific Cl^- concentration. 6 μM final concentration of BAC-Halo was used to measure the lifetime at varying Cl^- concentrations. Autofluorescence spectra of unlabeled neurons were also plotted at the same setup. Autofluorescence

lifetimes were estimated at different parts of the cell like the cell body and the neurite using the PicoQuant laser and settings used to measure the lifetime of BAC fluorophore as described before.

2.13 Electrical Stimulation of cultured neurons

A perfusion-type electrical stimulation magnetic chamber (EC B18, Live Cell Instrument, Gyeonggi-do, The Republic of Korea) was used to achieve field stimulation at indicated frequencies and pulses with A310 Accupulser Stimulator (Precision Instruments, Sarasota, FL, USA). Stimulation was performed in the presence of CNQX and APV to reduce recurrent activity from excitatory synapses. 1 image every 2 seconds was captured for a total of 3.5 minutes. After the first 30 seconds, electrical stimulation was applied and 3 minutes later, 50 mM NH_4Cl was applied. For the Bafilomycin A1 control experiment, 250 nM Bafilomycin A1 was included right from the beginning of the image acquisition, in the Tyrode's buffer. Exposure times and light intensity were adjusted to obtain minimum photobleaching. 'Perfect Focus System' feature was used before the start of the experiment, to avoid any focal drift caused due to stimulation or addition of NH_4Cl, or change of pH/Cl^- clamped buffers.

2.14 *in vivo* pH calibration and estimation of resting pH

The *in vivo* pH calibration profile and resting pH were estimated according to (Egashira et al., 2015). with slight modifications. Additionally, under the assumption that the H^+ and Cl^- ions can move freely when the membranes are perfused with blockers and ionophores, the pH/Cl^- concentration inside the probe containing SV should be equal to the outside bath solution. This method has been used in almost all previous studies involving pH and Cl^- calibration (Egashira et al., 2015; Saha, 2015; Sonawane and Verkman, 2003).

Plotting the pH calibration profile - Neurons were subjected to ionophore cocktail containing proton uncoupler FCCP, K^+ ionophore Valinomycin, V-ATPase inhibitor Bafilomycin A1, membrane solubilizer Triton X-100 and K^+/H^+ exchanger Nigericin (Table 2.10) to perfuse the membranes in high K^+ (122.4 mM) buffers clamped at a specific pH (Table 2.2, Buffer compositions). Images acquired at each pH value were analyzed using bouton analysis as described in the next section (Section 2.17, Image analysis). A pH calibration profile was thus plotted to obtain the pKa of each of the pH probes (Table 2.9).

Note that it was shown in a previous study that mild PFA fixation (2.5 % PFA) for a couple of minutes before treating them with the ionophore cocktail can also be used for measuring the calibration profile to keep the cells intact (Saha, 2015). This is because the state of the neurons treated with ionophore cocktail is already not physiological and is thus comparable with those of mildly fixed ones.

TEV Protease treatment - Neurons were treated with TEV protease (purified in Dr. Alexander Stein's lab, MPI-BPC) at a final concentration of 5 μM to remove the PM pool of fluorophores. A time course was plotted at 37°C to identify the time point of maximal cleavage similar to a previous study (Wienisch and Klingauf, 2006).

Estimating the resting pH - Neurons were treated with TEV protease for 3 minutes to get a pure vesicular signal which was categorized as the 'resting' state. They were very briefly incubated in ionophores containing two pH clamped buffers - maximum and minimum pH based on the pH calibration curve. The images were captured immediately and were referred to as 'max' and 'min'. Furthermore, cells in the same region of interest (ROI) were immunostained with primary labeled Abs against VGLUT and VGAT (Table 2.3) to differentiate the synaptic populations into Glutamatergic and GABAergic. The ROI was preserved by performing the experiment on top of the microscope stage and saving the X-Y position for every image that was captured

These images were analyzed and fitted with the following equation.

$$F = F_0 + \frac{F_{max}}{1 + 10^{pKa-pH}} \quad (11)$$

The pKa was calculated from the pH calibration data. F is the fluorescence readout at 'resting' condition, whose pH is unknown. F_0 and F_{max} are the fluorescence values at the minimum and maximum pH respectively whose pH is known, and thus the unknown resting pH is calculated.

Table 2. 10 List of blockers and ionophores used in this study.

Blocker	Working concentration	Stock	Manufacturer/Catalog No.
APV	50 μM	10 mM	Santa Cruz, A8054
Bafilomycin A1	250 nM for stimulation and 2 μM for pH calibration	1mM	CalBiochem, 196000
CNQX	10 μM	10 mM	Santa Cruz, 115066-14-3
FCCP	20 μM	20 mM	Abcam, 21910-1182
Nigericin	10 μM	10 mM	Sigma Aldrich, N7143
Triton X-100	0.02%	10 %	Merck, 108603
Trybutyltin-Cl (TBT-Cl)	10 μM	10 mM	Sigma-Aldrich, T50202
Valinomycin	10 μM	10 mM	Sigma Aldrich, V0627

2.15 *in vivo* Cl^- calibration

The Nb-Halo-Clensor complex was targeted to synapses in cultured neurons by bathing the cells in their media containing the Nb-Clensor complex. The images were captured in both Alexa and BAC channels. Cl^- imaging using Clensor was performed as previously described in (Saha, 2015). Neurons were bathed in K^+/H^+ antiporter Nigericin, K^+ ionophore Valinomycin and Cl^-/OH^- antiporter TBT-Cl (refer Table 2.10 for concentrations) containing buffers clamped at 0 mM and 162 mM chloride to calculate the fold change in Cl^- sensitivity.

2.16 Image Analysis

Images were processed and analyzed with FIJI (NIH, USA). For stimulation data, the plugin 'Time Series Analyser V3' was used to mark the ROI. The average intensity across the time series was calculated by the plugin.

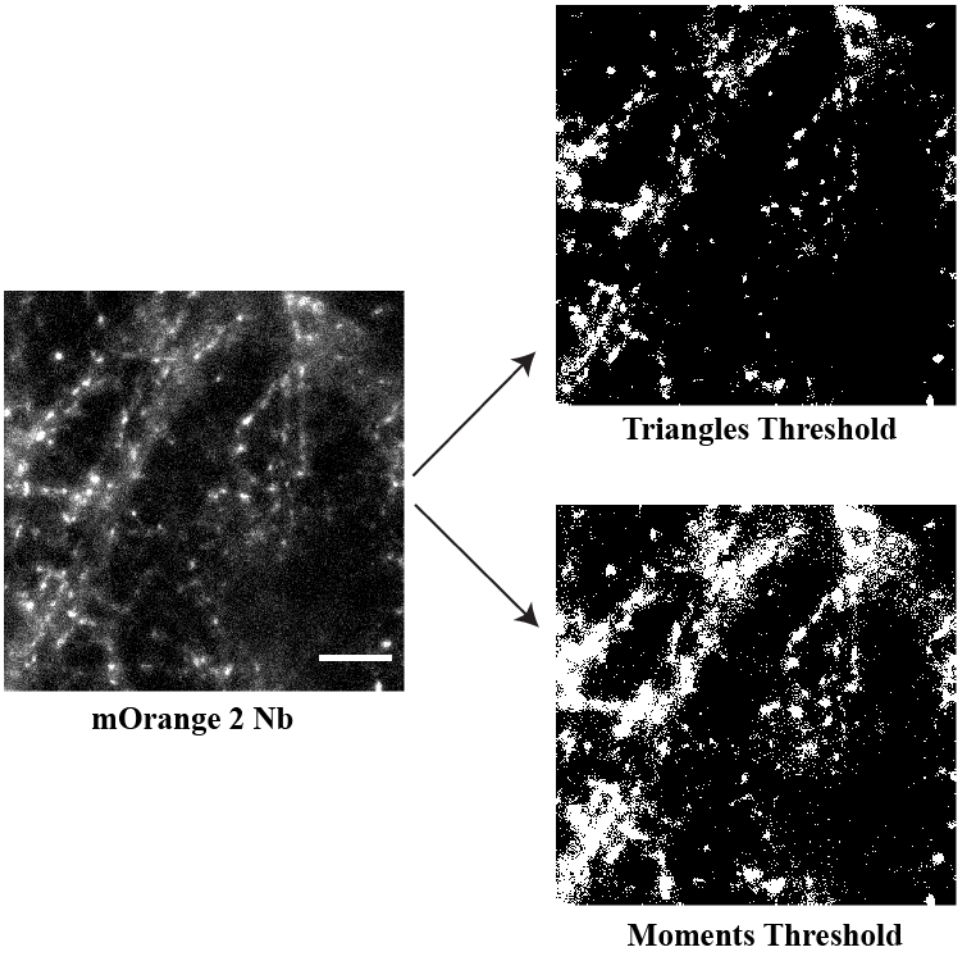

Figure 2. 1 Intensity thresholding of synaptic boutons labeled with Nb-mOrange2 fusion protein.

Bouton selection was performed on a background-subtracted image (after mOrange2-Nb labeling in this case) by using a 'Triangles' (top image) or a 'Moments' (bottom image) intensity threshold algorithm on Image J. Both the algorithms are successful to perform particle analysis which identifies single boutons. Depending upon the image quality, either of the thresholding methods is used. Scale bar: 10 μm.

Images for resting pH or pH/Cl^- calibration were first aligned using the plugin 'Stacks shuffling' and 'Align slices in Stack' to correct for minor x-y movements. These translation movements may happen due to solution exchange during the image acquisition. Images were subjected to background subtraction by either of the three methods: 1) A small ROI was selected where there were no visible cell structures, and the mathematical value of that ROI was subtracted from the entire image. 2) Images were subjected to the 'Background subtraction' plugin preinstalled in ImageJ. 3) At least 10 circular spots were manually selected in the regions where there were no visible cell bodies or neurites using the plug-in 'V3 Time-series analyzer'. The average intensity of these boutons was treated as the background signal in each image and was subtracted from the average signal from the synaptic boutons. All these methods gave comparable results.

To identify boutons, aligned images (16 bit) were intensity thresholded using the 'Triangles' or 'Moments' algorithm built-in Image J (Figure 2.1). 'Triangles' algorithm finds the maximum peak (mode) near one end of the intensity histogram and searches for the threshold within the largest range. 'Moments' algorithm attempts to preserve the moments of the original image (Imagej.net). Post thresholding, particles were selected using the 'Analyse particles' tool at 0.2-10 μm^2 and 0.2-1 circularity. Selected ROIs were automatically added to the ROI manager. The intensity of a single frame or multiple frames across time was then measured for these selected ROIs. Data were analyzed on either Origin Pro 2015 or Graph Pad Prism or Microsoft Excel.

VGLUT and VGAT bouton superimposition was performed by image alignment plugin 'Stacks shuffling' and 'Align slices in Stack'. VGLUT/VGAT image was used to create a threshold mask and identify boutons automatically which were then 'read' from resting/min/max pH images. Furthermore, the automatically selected boutons were manually annotated with the 'max' image, to make sure that the selected bouton from the VGLUT/VGAT image map does contain the requisite probe. Statistical Analysis was done on Graph Pad Prism with major parameters as mentioned in the figure legends.

For FLIM image analysis, data were fit using the inbuilt Leica software. Fitted curves were exported and values were plotted using Graph Pad Prism.

3 Results

3.1 Targeting of fluorophores to SVs using labeled antibodies against luminal domains of Synaptotagmin 1 and VGAT proteins

The objective of this dissertation is to target fluorophores or ion-sensitive probes to SVs in cultured hippocampal neurons. Dyes coupled with antibodies (Abs) against luminal domains of synaptic vesicle proteins can be used to label the recycling pool of vesicles. These Abs detect the protein molecules after exocytosis and get internalized during endocytosis. Three SV proteins: Synaptotagmin 1(Syt1), VGAT, and Synaptophysin 1 have a luminal domain that can be targeted to generate Abs against them. Ab against luminal Synaptotagmin 1(Syt1), a major SV protein (Chapman and Jahn, 1994; Matthew et al., 1981; Perin et al., 1991) has validated the labeling of synapses for over three decades. It has been shown that the Ab (polyclonal rabbit) retain within SVs for days and take part in multiple rounds of exo-endocytosis (Matteoli and Takei, 1992). In another study, the authors demonstrated that Cy3 conjugated Ab Syt1 (polyclonal rabbit) is a vital tool to quantitatively monitor SV exocytosis. They showed that the ability to form synaptic clusters in the axon is independent of the formation of presynaptic specializations (Kraszewski et al., 1995). Monoclonal Mouse Ab (clone 604.2) against the luminal domain of Syt1 (referred to as Syt1 Ab from here on) and VGAT Ab against the luminal domains of VGAT have been used and characterized in many studies (Hoopmann et al., 2010; Hua et al., 2011; Martens et al., 2008; Opazo et al., 2010; Truckenbrodt et al., 2018; Wienisch and Klingauf, 2006; Willig et al., 2006). In contrast, Abs against the luminal domain of Synaptophysin 1 recognized the epitope only after PFA fixation, but they couldn't be used in live cells (Truckenbrodt et al., 2018).

In previous studies, Syt1 Ab and VGAT Ab were labeled with pH-sensitive dye Cypher to reliably monitor exo-endocytosis (Hua et al., 2011). Moreover, the specificity of Syt1 Ab and VGAT Ab were extensively characterized and were used to study whether the newly produced or aged proteins are present in the recycling pool of SVs (Truckenbrodt et al., 2018). The authors had shown that the Abs targeted to SVs using spontaneous labeling remained bound in the fixed neurons for up to 10 days and could be induced to take part in exocytosis upon 1200 action potentials (APs) (Truckenbrodt et al., 2018). Thus, the spontaneous activity of neuronal networks has been a method of choice in this study.

Here, we have used Syt1 and VGAT Abs labeled with a pH-sensitive fluorophore AcidiFluor Orange (AF) (SySy, 105211AF, 131103AF). Primary active rat neurons were tagged with labeled Abs by spontaneous

network activity of the mature cultures (Figure 3.1). Neurons were successfully labeled and synapses appeared as 'beads on a string', resembling phase contrast and concentrated puncta of presynaptic accumulation of proteins (Fletcher et al., 1991). Note that Syt1 AF Ab labels the entire recycling pool of SVs as they all contain Syt1 protein, in contrast, VGAT AF Ab labels GABAergic SVs specifically. Different labeling times such as 10 minutes, 30 minutes, and 1 hour were tested. Within already 10 minutes, substantial labeling is achieved. Therefore, we used 10 minutes of spontaneous labeling with any given probe.

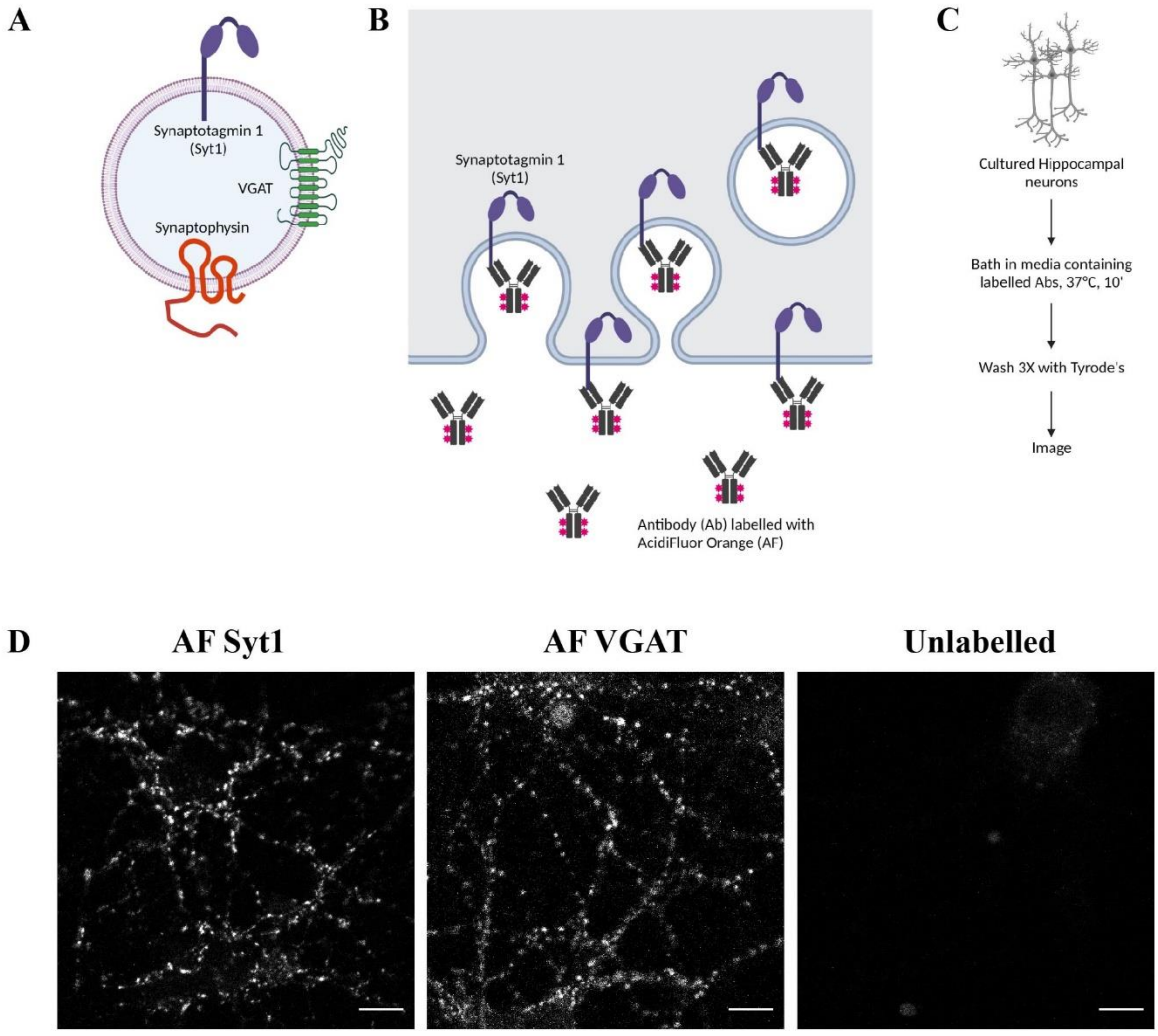

Figure 3. 1 Uptake of AcidiFluor Orange (AF) conjugated antibodies (Abs) against the luminal domain of Synaptotagmin 1(Syt1) or VGAT Abs.

(A) Scheme showing SV proteins that have a luminal domain against which labeled Abs can be used. (B) Scheme showing SV exo-endocytosis to encapsulate the labeled Abs inside the lumen, example here with Syt1. (C) Workflow to label the cultured neurons with sensor/dye conjugated Abs. (D) Hippocampal cultured neurons (14-18 DIV) were incubated in their media containing 5µg/mL AF conjugated Syt1 (left), AF VGAT (middle), or none (right) Abs for 10 minutes at 37°C. The label forms a punctated pattern where the individual puncta represent a bouton. These are representative images after subtracting the background. 'Unlabeled' image shows the autofluorescence in this channel. Scale bar: 10 µM

To check the specificity of AF labeled boutons, neurons were co-stained with an Ab against the cytoplasmic side of VGAT and multiple boutons were found to colocalize (Figure 3.2). AF was further characterized by monitoring the change in fluorescence with respect to change in pH. Neurons labeled with Syt1 AF Ab were bathed in buffers clamped at a specific pH after a brief treatment of ionophore cocktail to perfuse the buffer across the entire cell. Images were subjected to bouton analysis (Methods, Image Analysis section 2.17) and the data was plotted as a function of pH. The resulting curve was fitted with the Boltzmann equation and the pKa of AF was estimated to be 5.503 ± 0.084 (Figure 3.3). This pKa enables us to monitor the pH changes taking place in the acidic lumen of the vesicle.

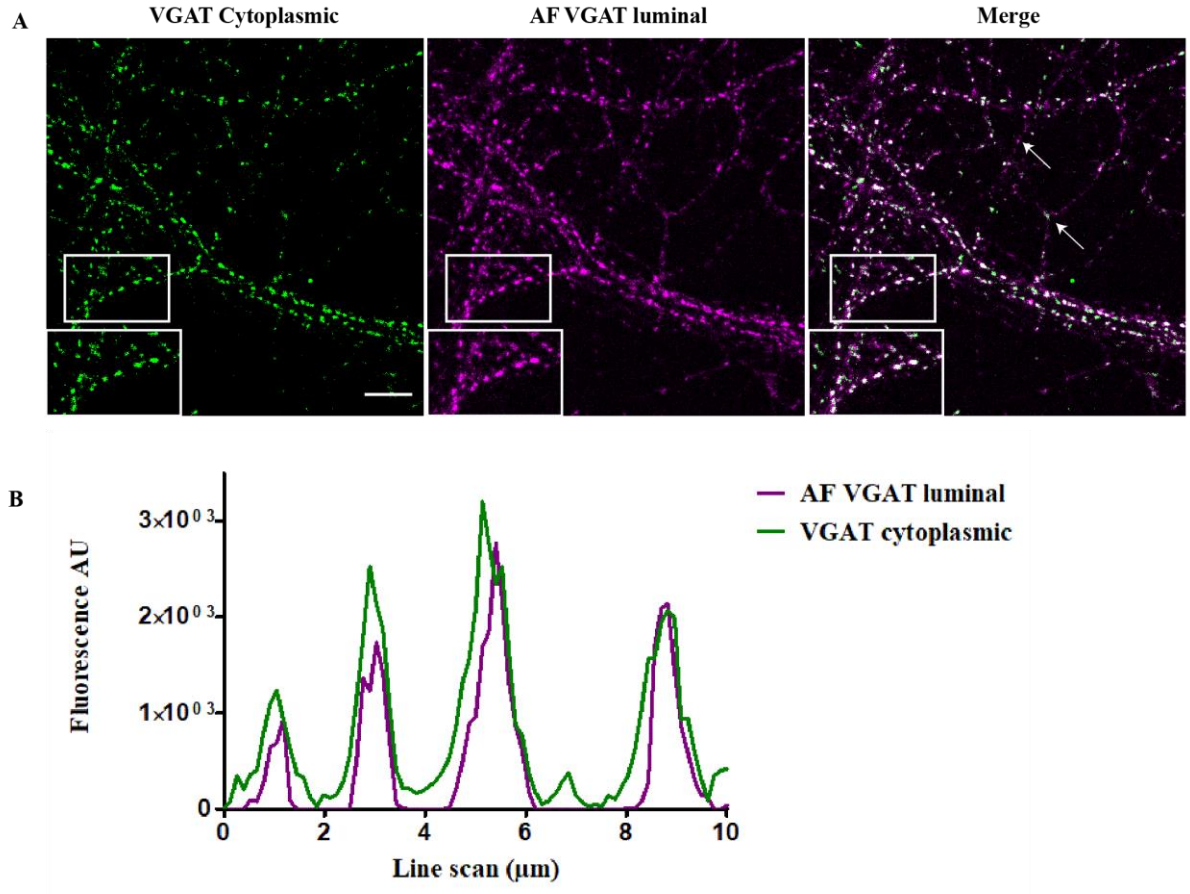

Figure 3. 2 AF conjugated VGAT luminal Ab colocalizes with external VGAT cytoplasmic protein.

(A) Neurons labeled with AF VGAT luminal Ab by spontaneous labeling for 10 minutes at 37°C (Magenta). Cells have then been immunostained with an external VGAT antibody that binds with the cytoplasmic side of VGAT (Green). Merge shows the extent of colocalization visualized by white spots. Note that the arrow points at magenta or green only boutons to confirm that there is little or no bleed through across the channels. (B) Line scans were plotted (by drawing a line in ImageJ and plotting the signal) through boutons found next to each other over a 10-micron distance to show the degree of colocalization between labeled VGAT luminal and immunostained cytoplasmic VGAT Abs. Line scans have been performed on original images without background subtraction. Scale bars: 10 µM.

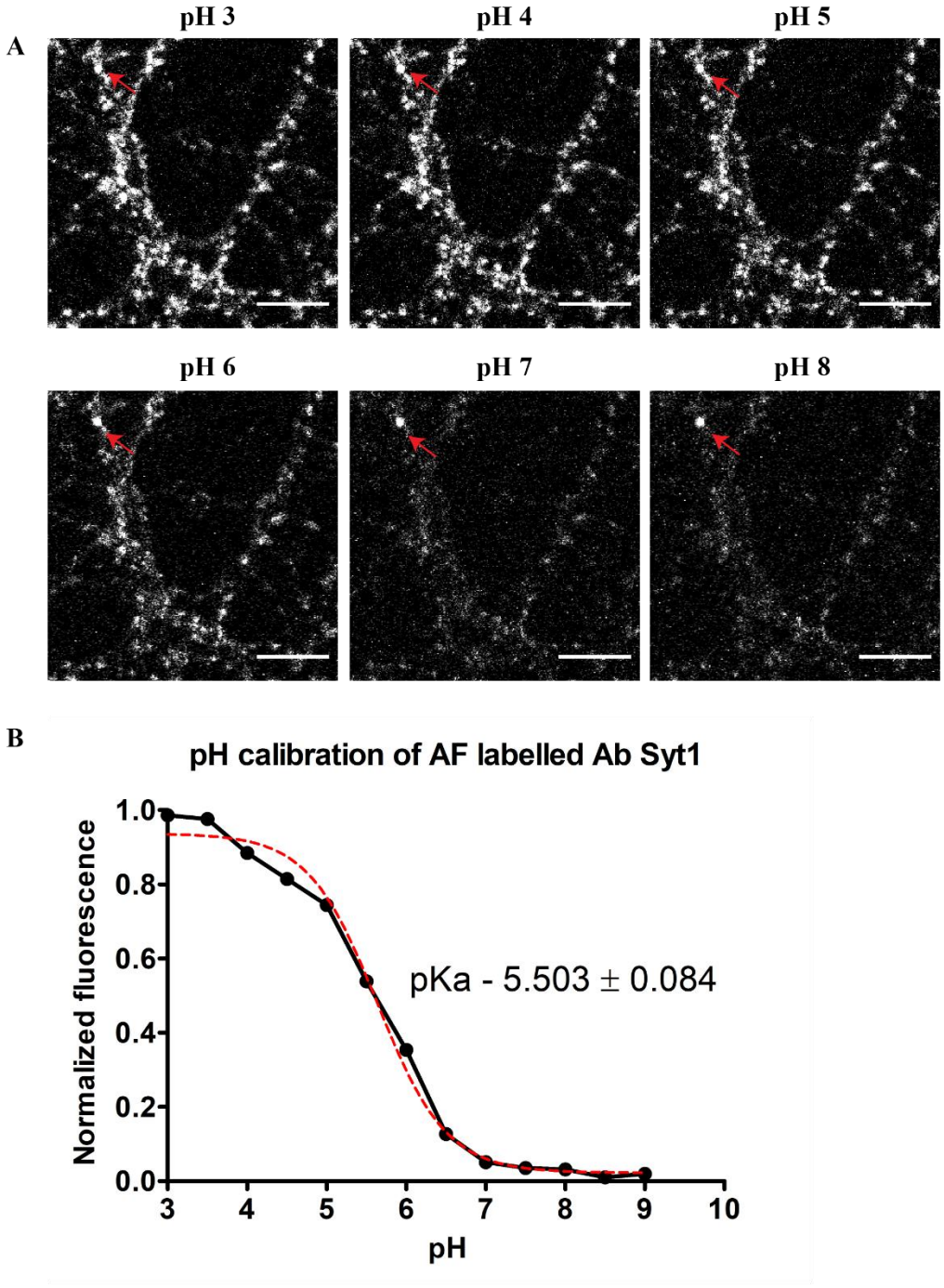

Figure 3. 3 AF responds fast and reversibly with pH changes.

Neurons labeled with AF Syt1 luminal Ab were briefly treated with an ionophore cocktail and subsequently bathed in buffers clamped at specific pH. (A) shows intensity changes at the boutons with changing pH. Note the arrow points at the spot that doesn't change with pH, which is most likely an extracellular dye aggregate. The rest of the boutons show a significant change in signal-to-noise ratio. Media containing the labeled Abs were centrifuged at high speed to get rid of dye aggregates before incubating the neurons in it. (B) quantification of (A) showing the fluorescence change as a function of pH. Data are from 14 cells at least from 3 different coverslips spanning 3 different culture preparations including over 600 synaptic boutons. The red solid line is a fit to the Boltzmann equation on Graph Pad Prism yielding a pKa of 5.503 ± 0.084. Error bars represent s.e.m.; they are barely visible because the values are very close to each other. Scale bar:10 μm.

To further confirm the functionality of the probe in living neurons, neurons labeled with Syt1 AF Ab were electrically stimulated to monitor pH changes during the exo-endocytic cycle. Trains of 6, 60, and 600 action potentials (APs) at 20 Hz were evoked that resulted in a rapid decay of AF fluorescence owing to the quenching of the fluorophore at pH 7.4 (Figure 3.4). At the end of the stimulation, the Abs were retrieved by compensatory endocytosis and unquenched during reacidification of the vesicle lumen (Figure 3.4A). Note that 600APs at 20 Hz have been shown to release the entire recycling vesicle pool in the past (Hua et al., 2010). Inhibitory boutons labeled with VGAT-AF showed similar pKa and similar stimulation profile as the Syt1-AF labeled neurons (refer to Lars Henning Hansen, Bachelor thesis).

Thus, we conclude three points from the above findings: 1) Neurons can be successfully labeled with a pH-sensitive fluorophore AF using the Abs against Syt1 or VGAT proteins. 2) AF probe after internalization is functional and responds fast to pH changes. 3) The pKa of AF is 5.5 which is ideal to study the acidification of the SV in future experiments

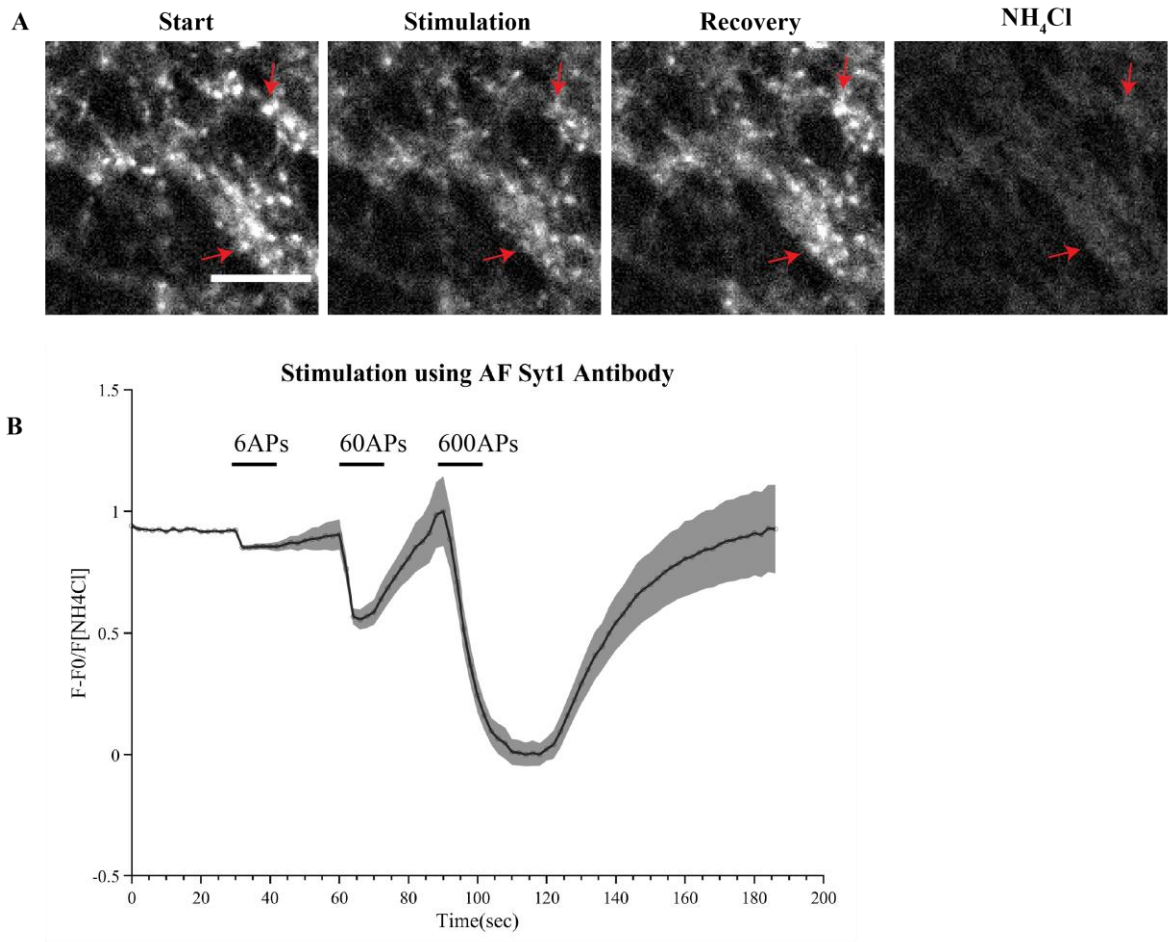

Figure 3. 4 AF Syt1 Ab reliably shows exo-endocytic cycling of SVs in response to electrical stimulation.

(A) AF Syt1 labeled neurons at the start of the stimulation, after 600 action potentials (APs) at 20 Hz of pulses, after a minute of recovery, and after application of 50 mM NH_4Cl. The arrows show individual puncta that are quenched in response to stimulation when exposed to high extracellular pH of 7.4. These puncta then get brighter in the recovery

phase where they get endocytosed and the vesicle reacidifies. Treatment with NH_4Cl alkalinizes the cell and equalizes the pH between outside and inside the cell thus quenching the entire fluorescent signal. This depicts the total pool that was labeled with the AF probe. (B) Neurons were stimulated with a pulse of 6APs followed by 60 and then 600 APs at 20 Hz. Quantification of time series from at least 3 cells over different coverslips and culture preparations. Baseline fluorescence before the 6APs was subtracted and the resulting fluorescence was divided by the NH_4Cl fluorescence to normalize each transient with the total labeled pool. Data were further normalized. Microscope settings were adjusted such that there was minimal or no photobleaching. Minor bleaching was further corrected using a relevant bleach factor. Grey shade depicts the error bars as s.e.m, plotted by MATLAB code written by Tarana Nigam. Scale bar: 10 μm.

3.2 Characterization of Nanobody against luminal Synaptotagmin 1

In the above section, we saw that the Ab against Syt1 can be labeled with a dye and can be efficiently taken up by endocytosis in cultured neurons. To generate an even more versatile tool, we collaborated with Nanotag, Göttingen to produce a nanobody (Nb) against the luminal epitope of Synaptotagmin 1 (Nb Syt1). The Nbs are expected to be encapsulated in the SVs with a higher efficiency due to their smaller size, they can be easily produced in large quantities and they can be engineered with a sequence of choice to customize their usage (for more details, introduction, Section 1.10.2).

Nb Syt1 was fused with GFP or was fused with a HaloTag protein (further details, Results section 3.6.4) so that we can test its specificity and functionality. We characterized the Nb by performing the following four sets of experiments: first, we focused on the binding ability of the Nbs in western blot assays. We investigated whether the Nb binds with purified Syt1 full length and Syt1 lumen proteins. The challenging part of this experiment was the method to visualize the nanobody. This is because, unlike an Ab, a Nb lacks the Fc region (against which secondary Abs are used to visualize the presence of Ab). Various methods of visualization were tested: 1) The Nb construct contains three FLAG tag sequences as linkers between the Nb and conjugated protein of choice (GFP or HaloTag). Thus, membranes were blotted with Nb, followed by Anti-FLAG Ab and then a secondary Ab against the Anti-FLAG Ab. This led to massive amplification and saturated the signal; however, it did help to visualize the binding of Nb with the purified Syt1 proteins (Figure 3.5A). Western blotting using Syt1 Ab (clone 604.2) was used as a control. 2) Another method directly uses the Nb fused with HaloTag to visualize the protein. Nb-Halo was first preincubated to form a complex with the Alexa647-Halo ligand. The complex was used for the protein visualization (Figure 3.5B). However, the background was quite high and due to saturated signals, the blots couldn't be quantified. Note that the purified Syt1 lumen protein (7 kDa) was degraded to a smaller-sized peptide which was also identified by the Nb in both methods of visualization (Figure 3.5).

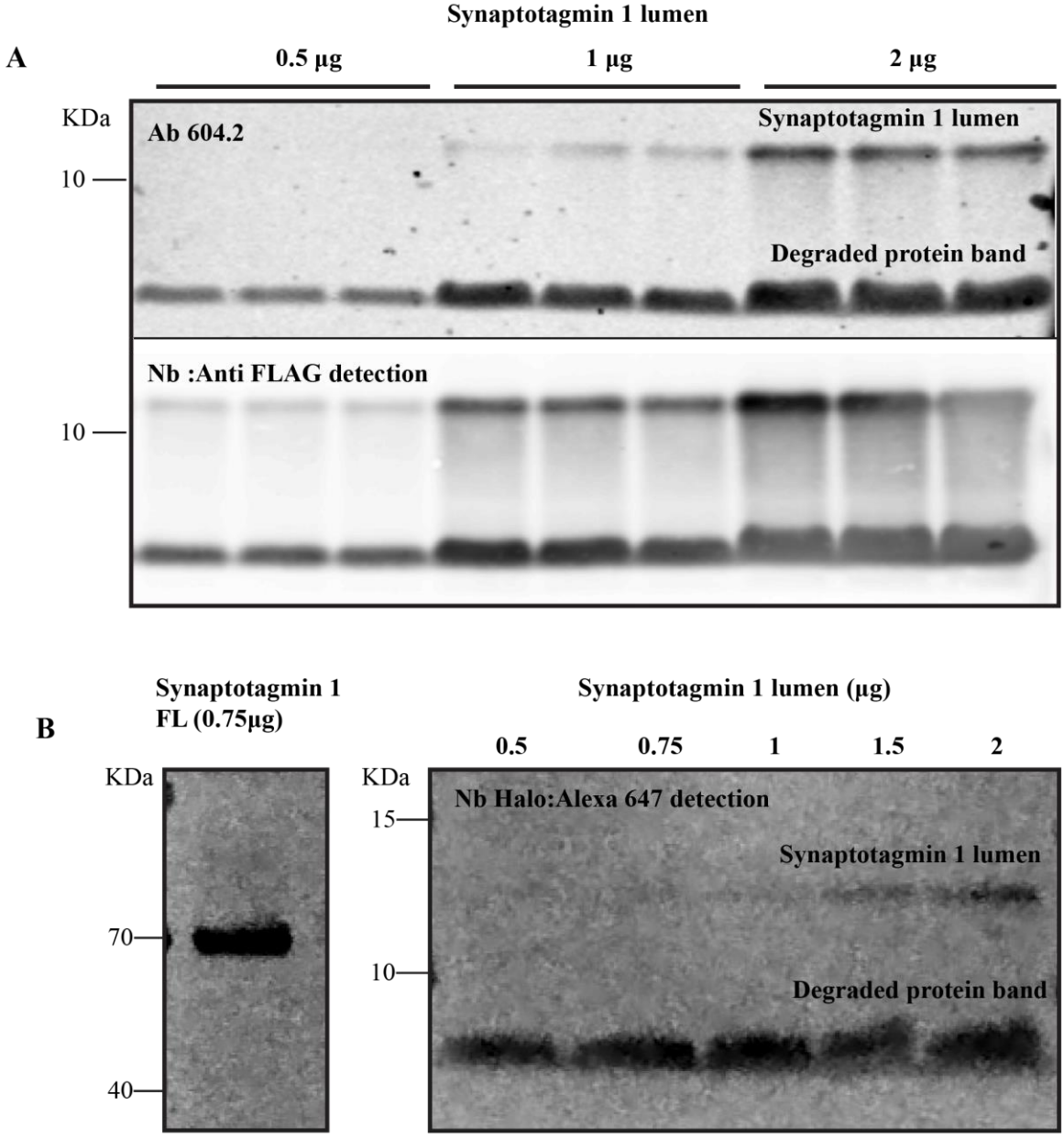

Figure 3. 5 Nanobody (Nb) application in western blotting using purified Syt1 lumen and Syt1 full length (FL) proteins.

Protein was visualized by 2 methods: (A) Membranes were first incubated in Nb, then an antibody against the FLAG tag was used to detect the Nb, finally, a secondary Ab was used to detect the Ab against the FLAG Ab. This led to massive amplification as seen in the saturated signals from the membrane. Protein detected by 604.2 Ab was used as a control. (B) Nb fused with HaloTag was pre-incubated with Halo ligand coupled with Alexa647 dye. The membrane was incubated in milk containing the complex. Membranes were then visualized on a fluorescent scanner. The amount of protein loaded on the gel is given in each lane. Note that the background is quite high in (B) where there is no secondary Ab mediated amplification of the signal. Also, note that the purified Syt1 lumen protein (7 kDa) was degraded to a smaller-sized peptide. FL Syt1 was kindly provided by Dr. Angel Franciso Perera and Syt lumen protein by Dr. Steffen Frey.

Second, we identified the epitope of the Nb, by testing different truncated constructs of Syt1 protein. Equimolar amounts of these peptides spotted on an array were ordered (Genscript) and were detected by GFP fused Nb in dot blot assays (Figure 3.6, performed by Dr. Eugenio Fornasiero). The results indicate that the Nb binds to the sequence KQKFMNELHKIPLPP.

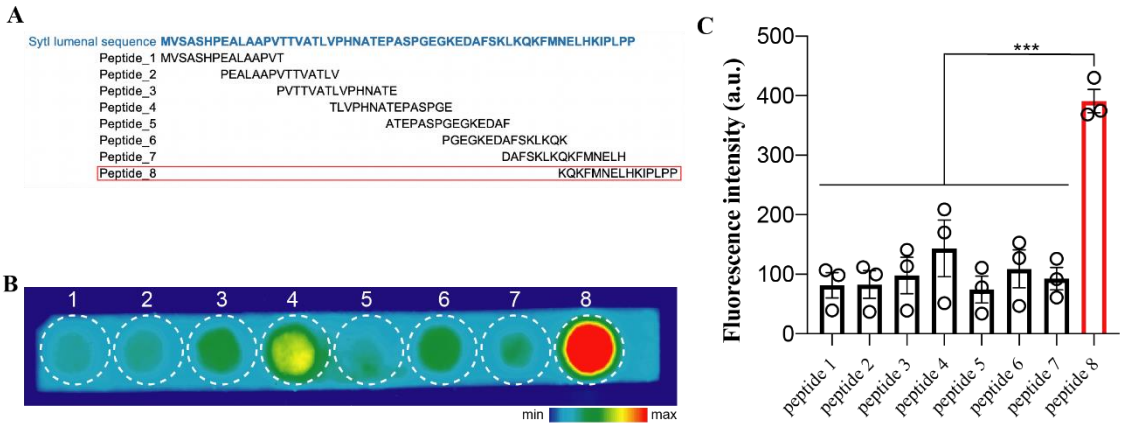

Figure 3. 6 Epitope of Syt1 Nb was identified by dot blot assay

(A) Scheme showing truncated versions of the Syt1 lumen sequence used for the assay (B) Equimolar concentrations of these peptides spotted on an array was purchased (Genscript). Sequence '8' produced the maximum signal. (C) Quantification of B. Experiment was performed by Dr. Eugenio Fornasiero.

Third, we aimed to immunoprecipitate Syt1 from the whole mouse brain lysate by using GFP selector resin bound with GFP Nbs. We successfully immunoprecipitated Syt1 from WT brains while no protein was pulled down from Syt1 knockout (KO) mice brains, thus, confirming the specificity of the Nb (Figure 3.7).

Fourth, we investigated whether the Nb binds with the native protein in living hippocampal neurons. WT and Syt1 KO neurons were labeled with the Nb-pHlourin and a punctate staining pattern, typical of synaptic staining was obtained. Neurons labeled with pHlourin were co-immunostained with an Ab against Synapsin 1/2, a presynaptic marker (Bloom et al., 1979; De Camilli et al., 1983; Cesca et al., 2010). Uptake of the Nb by only the WT neurons indicates its specificity for Syt1 protein. Colocalization with Synapsin 1/2 further validates that the Nb is highly specific (Figure 3.8). Additionally, the same experiment was performed showing colocalization of GFP-Nb with presynaptic marker Bassoon and an SV marker Synaptophysin 1 (Appendix A.1).

Thus, based on the findings from the above experiments, we conclude that the Nb against the luminal domain of Syt1 is a highly specific tool for live-cell imaging.

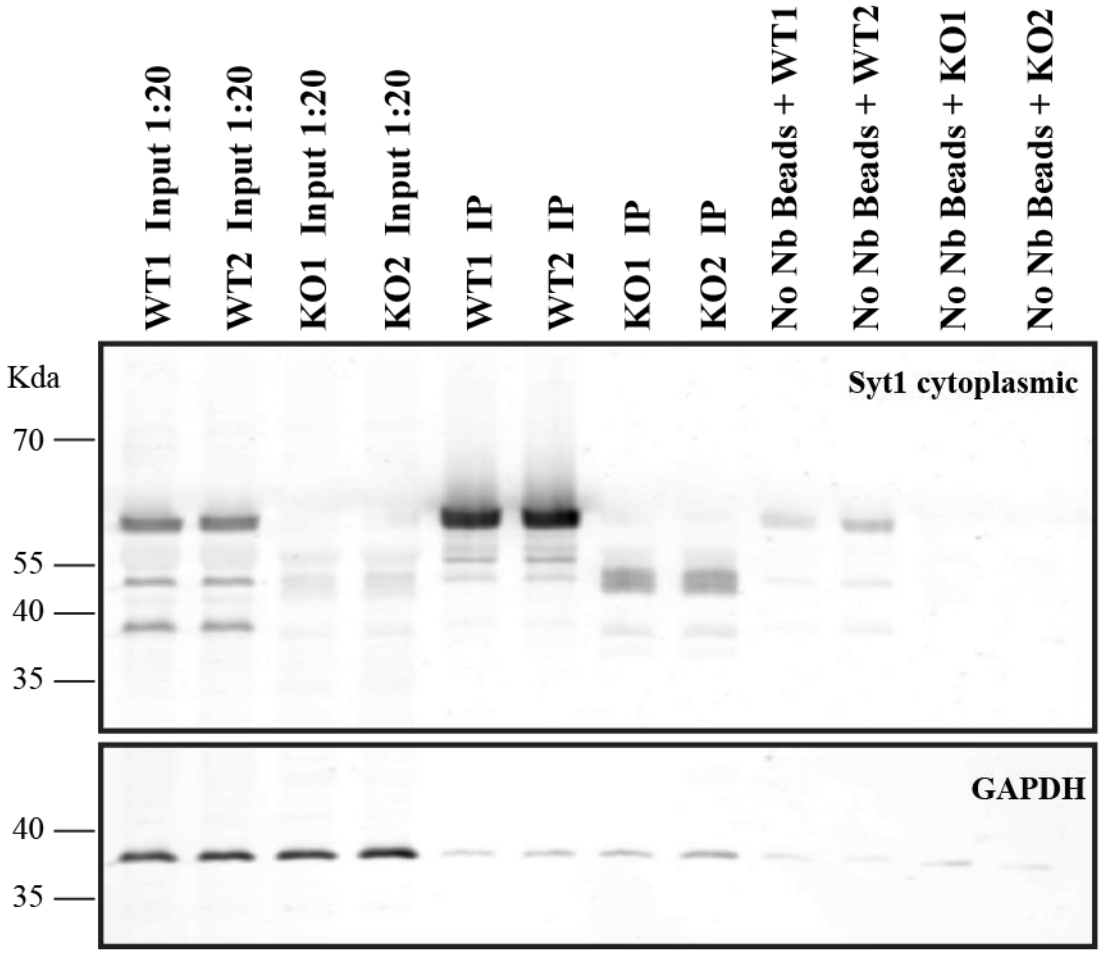

Figure 3. 7 Western Blot of Syt1 immunoprecipitated from WT and KO Syt1 mice brains using GFP-Nb

GFP Selector resin preincubated with Nb-GFP was used to precipitate Syt1 proteins from WT and KO mice brains that were provided by Prof. Volker Haucke. IP was performed in duplicates. Protein concentration was measured in the input sample using the BCA method. Protein concentrations were adjusted between WT and KO lysates to load equal amounts with the beads. Beads bound to Syt1 after IP was directly run on a 10 % Schägger gel. Western blotting was performed and blots were developed for Syt1 cytoplasmic (SySy 105008) and GAPDH (Thermo Scientific, MA5-15738) Abs. Signal was visualized using infrared secondary Abs on an Odyssey scanner. GAPDH was used as a loading control. Note that 'No Nb beads' controls in the last lanes could have been washed further to decrease the background.

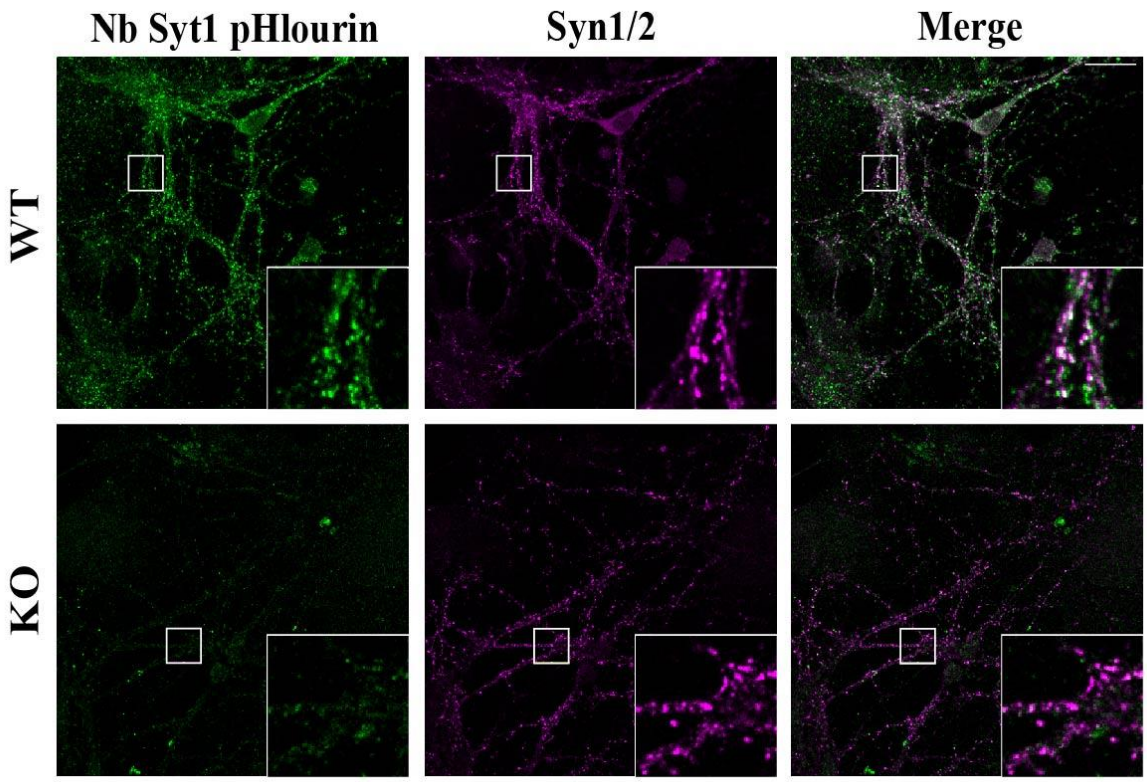

Figure 3. 8 Labeling of WT and Syt1 KO neurons with pHlourin Nb.

Living WT and Syt1 KO neurons (DIV 15) were labeled with Nb fused with pHlourin (1:200, in green). Neurons were fixed and immunostained with a presynaptic marker Synapsin ½ (SySy 106004, in magenta). Colocalized spots in white in WT show the targetability of the Nb to synapses. Specific labeling of WT neurons shows that the Nb is specific to the Syt1 protein. Scale bar: 20 μm. The experiment was performed by Svenja Bolz from the lab of Prof. Volker Haucke, Berlin.

3.3 Nb was fused with the pH-sensitive proteins: pHlourin and mOrange2

The Nb can be used to deliver proteins such as pHlourin and GFP to the SV. This implies that we do not have to genetically modify the neurons to express the proteins in the SV lumen but rather we can use the Nb to target the proteinaceous probes to the recycling vesicles. As mentioned briefly in the introduction, pHlourin and mOrange 2 are pH-sensitive fluorescent proteins that have been used in the past to study the acidification dynamics in an SV. Thus, before trying novel pH probes, we have targeted already existing probes – Nb-pHlourin and Nb-mOrange2 and estimated the resting pH of the vesicle. However, before proceeding with the resting pH estimation, we performed the following three experiments to characterize the Nb fusion protein (with pHlourin/mOrange2) (Figure 3.9A):

1) *In vitro* pKa estimation - The spectral properties of Nb fused with pHlourin and mOrange2 were first characterized *in vitro* using Fluorometry. Purified proteins were diluted in buffers clamped at a specific pH and the emission spectra were measured (Figure 3.9B). The fluorescence change for changing pH yielded a pKa of 7.15 for pHlourin and 6.88 for mOrange2 (Figure 3.9C). The measured pKa is in accordance with the previous study (Egashira et al., 2015).

2) *In vivo* pKa – Labeled neurons were treated with ionophore-containing buffers clamped at a specific pH and images were captured at each pH condition. Images were subjected to bouton analysis and the average fluorescence was plotted against changing pH. The pKa of pHlourin in cells was calculated to be 7.11 and that of mOrange2 was 6.48 (Figure 3.9D).

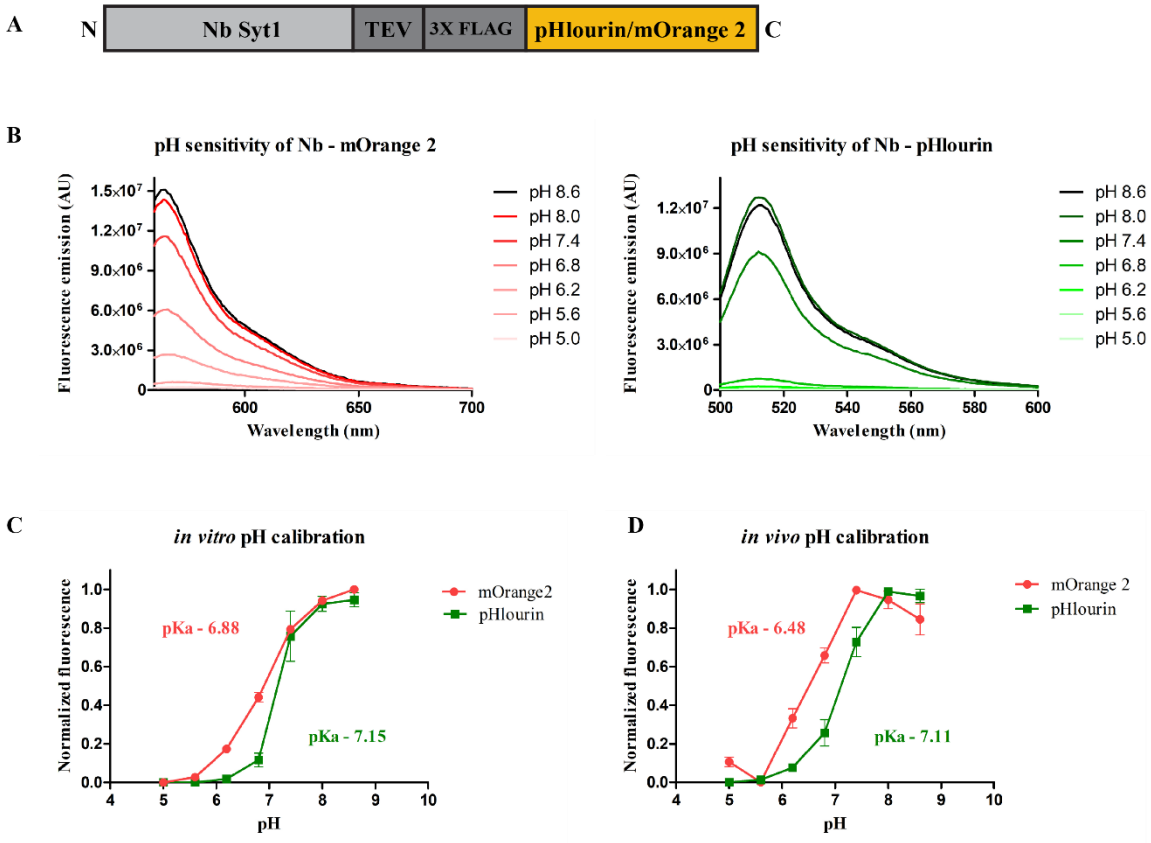

Figure 3. 9 Characterization of Nb fused with pHlourin or mOrange2 proteins.

A) Scheme of Nb Syt1 fused with Nb-pHlourin or Nb-mOrange2 pH-sensitive proteins separated with a TEV and 3X FLAG linker. (B) Emission spectra of 2 µm Nb-pHlourin (Excitation - 488 nm, slit size- 2 nM) and 2 µm Nb-mOrange2 (Excitation- 562 nm, slit size-2 nM) were measured at different pH clamped buffers. (C) Quantification of B. The sigmoidal curve was fitted with the Boltzmann equation using GraphPad Prism to determine the pKa. (D) Neurons labeled with Nb-pHlourin or Nb-mOrange2 probes were treated with buffers containing ionophore cocktails. Images taken at each buffer condition were subjected to bouton analysis and the average fluorescence was plotted against the pH. Images were taken starting from low pH to high pH to avoid the effect of bleaching. Error bars-s.e.m..

3) Removal of the surface pool - the Nb fused with pHlourin or mOrange2 labels the recycling pool of SVs. The fluorescence at a given terminal in our study is thought to be the sum of fluorescence from freshly endocytosed vesicles and the fluorescence from the probe molecules present on the cell surface. We characterized the cleavage of the probe fraction from the cell surface to obtain a clean vesicular signal as described in the next section.

Thus, the data presented above show that the pH-sensitive proteins pHlourin and mOrange can be targeted to the SVs using the Nb and that their pH sensitivity (represented by pKa) is comparable to the previously published literature (Egashira et al., 2015).

3.4 The surface pool of the fluorophore is cleaved with the TEV protease

It has been previously shown that the SV proteins residing on the PM also take part in exo-endocytic recycling and the endocytosed vesicles are largely composed of previously stranded molecules on the PM (Tabares et al., 2007; Wienisch and Klingauf, 2006). As shown in figure 3.1B - there are already existing Syt1 protein molecules on the PM (surface pool) from rounds of exo-endocytosis. In addition, the surface pool contributes to the background fluorescence for studies on vesicular mechanisms. However, by engineering a tobacco etch virus (TEV) cleavage site between the Nb and the fluorophore, the surface pool of the fluorophore can be eliminated by treating the neurons with TEV, and thus, we can obtain a pure vesicular signal of the probe.

We performed a time series of TEV cleavage to monitor the time point at which most of the surface pool is eliminated like how it was performed previously (Wienisch and Klingauf, 2006). We treated neurons with in-house purified TEV enzymes (kindly provided by the lab of Dr. Alexander Stein) and captured images at different time points and observed that the maximum cleavage happens after 3 minutes (Figure 3.10A). To eliminate the contribution from photobleaching, we imaged the neurons at the same time points but without treating them with TEV protease. After comparing the pattern of bleaching (untreated condition), with that of the treated condition, we concluded that 3 minutes of cleavage time is enough to eliminate the surface pool. Additionally, we treated the purified Nb-pHlourin fusion protein with TEV protease at different time points and ran it on a native PAGE gel. This also revealed that the cleavage happens between 2 to 5 minutes (Figure 3.10B). From here on, we used 3 minutes as the cleavage time. Moreover, we tried to reduce the cleavage time from 3 minutes to instantaneous cleavage, by using a super-active form of TEV enzyme called AcTEV™ (#12575015, Thermo Fisher Scientific). However, AcTEV did not work either on the gel or on neurons (data not shown). Thus, we proceeded with the 3-minute cleavage using the TEV enzyme.

To characterize the functionality of neurons after cleaving the surface pool of mOrange2 with the TEV protease, we electrically stimulated the mOrange2 labeled neurons with ('TEV') or without TEV treatment ('control'). We elicited 300APs (action potentials) at 30 Hz, a stimulus condition that releases a significant proportion of the recycling pool (Truckenbrodt et al., 2018). To make sure that the probe is reporting acidification changes, we used the blocker of V-ATPase, Bafilomycin A1 as a control. When the cells were stimulated, we saw a rapid increase in fluorescence owing to an increase in pH during vesicle exocytosis (note that mOrange2 is dark at acidic pH). After stimulation was ended, the nanobodies were retrieved by compensatory endocytosis and the signal got quenched to the baseline fluorescence. We have quantified the recovery rate of the signal after the 90 s from the start of the experiment (% of τ_0). Note that the smaller

the % of τ_0, the closer the recovery is to the initial baseline. The cells treated with Bafilomycin A1 failed to recover (% of τ_0 -103.2 ± 0.26) implying that the quenching of the fluorescence is due to the reacidification of the vesicle lumen. The cells treated with the TEV protease also recovered, albeit not until the initial baseline in the untreated ones (% of τ_0 - 37.9 ± 1.16 versus 13 ± 0.66, $p<0.0001$) (Figure 3.11A). This could be because the endocytosis process brings back a mixed population of mOrange2 fluorophore when cells are stimulated with 300APs: the probe fraction that was already existing at the PM from the previous rounds of exocytosis and the freshly exocytosed fraction. When we add the TEV protease before performing the stimulation, the already existing molecules of fluorophore at the PM are cleaved off. Thus, TEV treatment reduces the observable pool of Syt1 molecules as the fluorophore is chopped off. Note that with TEV treatment, we only get rid of the fluorophore molecules bound to Syt1, while the Syt1 protein molecules remain intact. This means that the rate of endocytosis of Syt1 is the same, but due to a smaller observable pool of fluorophores being endocytosed, we observe a slower recovery in TEV treated compared to untreated cells. This explanation is likely if the vesicle retrieval brings a mixed population of Syt1 proteins: an already existing population of Syt1 from the plasma membrane in addition to the newly exocytosed fraction. To clarify this explanation better, hypothetically, if the vesicle would have brought back only the previously stranded pool of Syt1, we would have seen no recovery in the TEV treated condition as the fluorophores attached to Syt1 are chopped off by TEV.

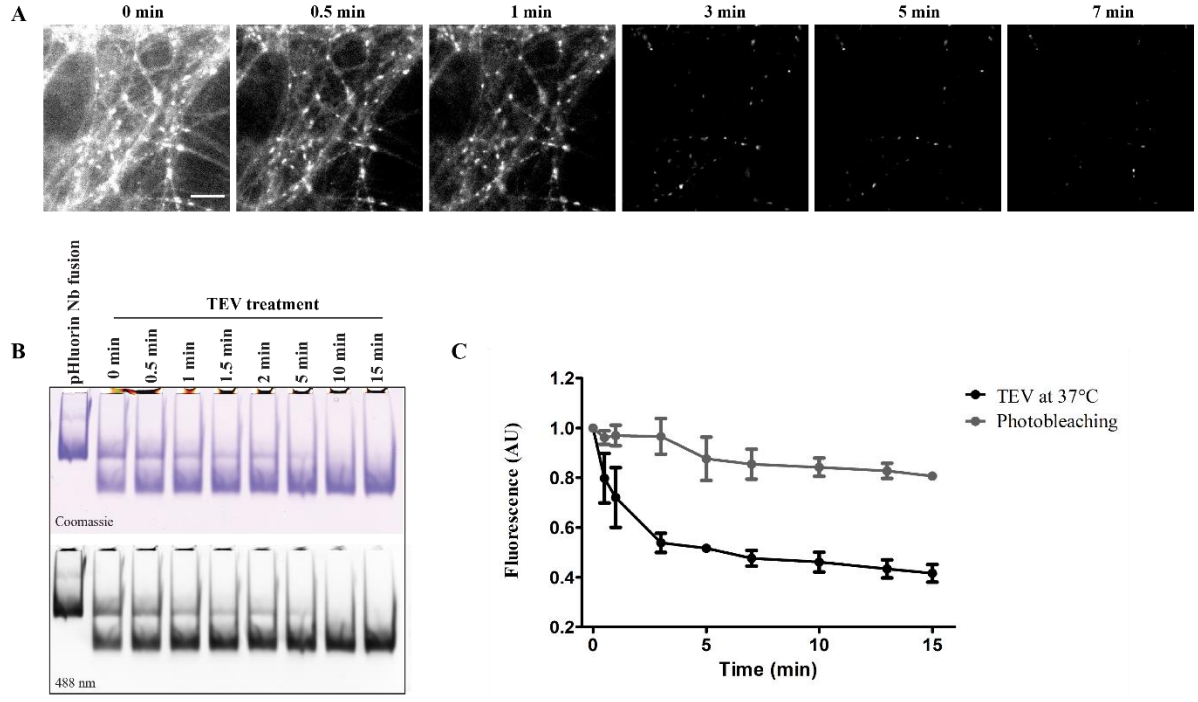

Figure 3. 10 Cleavage of cell surface probe fraction using the TEV protease.

(A) Neurons labeled with Nb-mOrange2 probe were treated with 5 μM TEV protease and images were captured at indicated periods. Note that already after 30 seconds, a substantial amount of probe has been cleaved. (B) Nb-pHlourin fusion protein is treated with TEV at different time points and runs on a Native PAGE. The gel was first scanned on a fluorescence gel reader and then stained with Coomassie. (C) Quantification of A. Images were subjected to bouton analysis and the average fluorescence was plotted against time. Images were also captured for labeled neurons that were not treated with TEV (grey), at the same time points to monitor the extent of photobleaching. Note

that the second half of the decay curve (grey) resembles the second half of the black curve, thus the maximal cleavage already happens after 3minutes. Scale bar- 10 μM. Error bar: s.e.m.

To clarify these observations further, we elicited a smaller stimulus of 40APs at 20 Hz, this has been shown to deplete only the readily releasable pool of docked vesicles (Murthy and Stevens, 1999; Schikorski and Stevens, 1997). Does a stimulus of 40APs bring back the SVs containing only the Syt1 molecules already stranded at the PM or does it bring back a mixed population of already existing and newly endocytosed Syt1 molecules (as shown above using 300APs)? An increase of fluorescence signal was observed with little or no recovery in TEV treated neurons (% of τ_0 of 76.81 ± 0.48 in TEV treated cells versus 6.47 ± 0.93 in the control untreated neurons) (Figure 3.11B). This result indicates that cleaved surface pool (already existing pool) is preferentially retrieved rather than newly exocytosed protein molecules when stimulated with 40APs. These results are in accordance with the results published in the studies elsewhere (Hua et al., 2011). The conclusions from the above set of results are 1) the TEV protease successfully cleaves the surface pool in 3 minutes and that the neurons post-cleavage are still functional to undergo the cycles of exo-endocytosis when electrically stimulated. 2) At a lower stimulation of 40APs, the SVs retrieve the Syt1 protein pool that is already existing at the PM while at a higher stimulus of 300APs, SVs retrieve a mixed population of already stranded Syt1 and newly exocytosed Syt1 molecules. Only the first conclusion is relevant for the upcoming parts of the story.

3.5 Estimation of resting pH using Nb-pHlourin and Nb-mOrange2 probes

The resting pH of the vesicle was estimated in a manner conceptually described in previous studies albeit with some modifications (Egashira et al., 2015). Neurons were labeled with Nb fused with pHlourin or mOrange2 probes and the surface pool was removed by treating the cells with TEV protease for 3 minutes. The image was then captured and labeled as 'resting state'. Cells were treated with buffers containing ionophores clamped at the minimum pH of 5.0 called 'min' and the maximum pH of 8.5 called 'max' values. Then, the same ROI was fixed and immunostained with primary labeled Abs against VGLUT and VGAT. Images were subjected to bouton analysis and processed as described earlier (Methods Section 2.17). By creating a respective map for VGLUT and VGAT, the Glutamatergic and the GABAergic boutons were traced back in the 'resting' and 'min' and 'max' images. A representative image of this workflow is shown in Figure 3.12 A and B for Nb-pHlourin labeling and post-hoc VGAT staining. The same was done with VGLUT positive boutons. Average fluorescence intensities and pKa estimated from the calibration curves were plugged into equation 11 (Methods Section 2.15) and the resting pH was calculated. The above-described procedure was applied to both Nb-pHlourin and Nb-mOrange2 probes. Resting pH of Glutamatergic boutons was significantly lesser than that of GABAergic boutons using both Nb-pHlourin and Nb-mOrange2 probes (Figure 3.12 C and D).

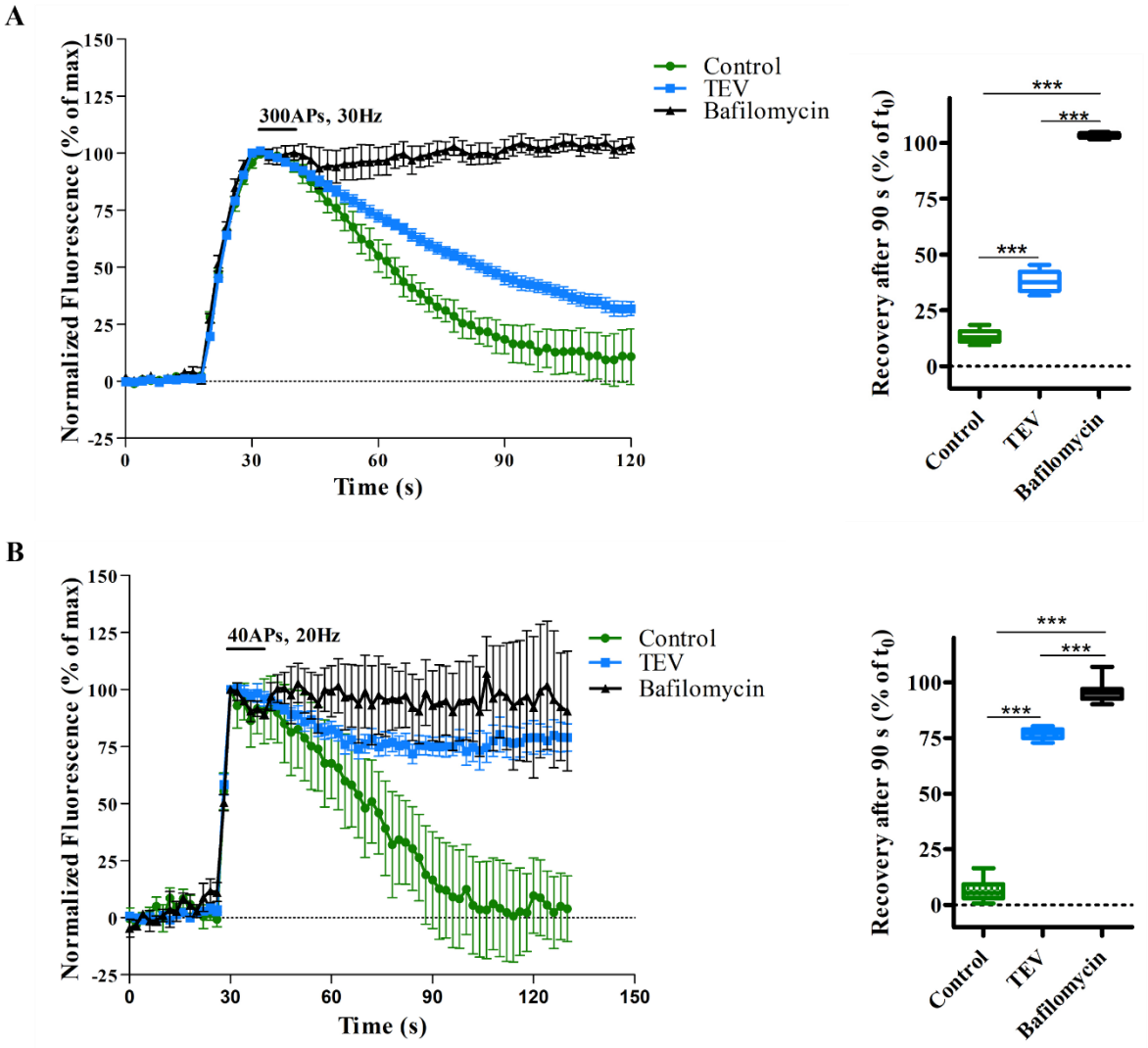

Figure 3. 11 Stimulation of mOrange2 labeled neurons after treatment with TEV protease.

(A) Neurons were labeled with Nb fused with mOrange2 probe and stimulated at 300APs, 30 Hz, (control, green), treated with TEV protease (5 μM) for 3 minutes, washed and then stimulated (TEV, Blue) and treated with 250 nM Bafilomycin (Bafilomycin, Black). % of τ_0 - 13 ± 0.66 in control, 37.9 ± 1.16 in TEV treated and 103.2 ± 0.26 in Bafilomycin A1 treated neurons. (B) Repetition of A but stimulated at 40APs, 20 Hz. % of τ_0 is 6.47 ± 0.93 in the control condition, 76.81 ± 0.48 in TEV treated and 95.43 ± 0.87 in Bafilomycin treated neurons. Data were compared using one-way-ANOVA with multiple comparisons Bonferroni test. *** - $p < 0.0001$. $N \geq 3$, across different neuronal preparations. Error bars: s.e.m.

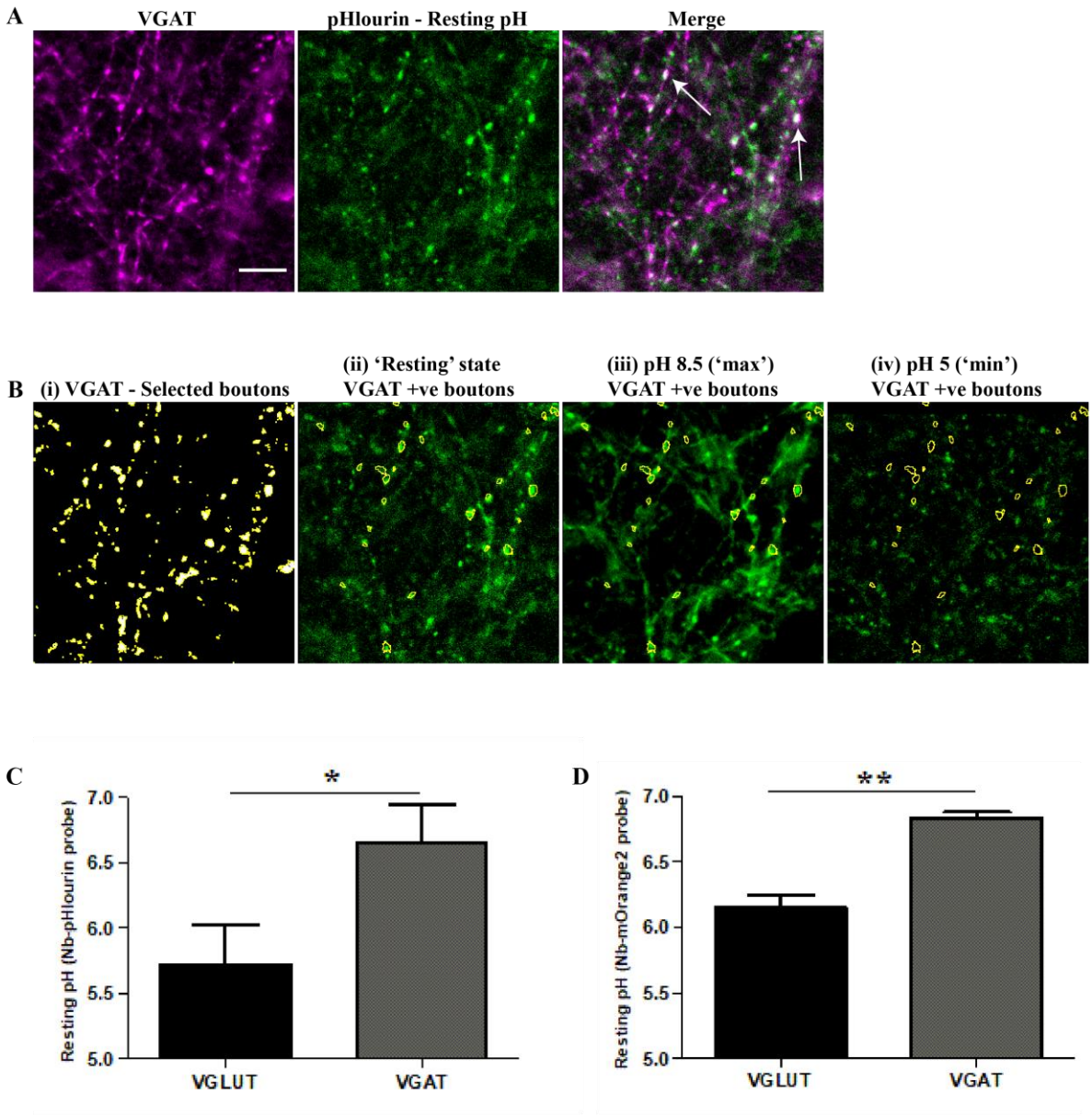

Figure 3. 12 Estimation of resting pH using Nb-pHlourin and Nb-mOrange2 probes.

(A) Post-hoc immunostaining with VGAT Abs (Magenta). Nb-pHlourin labeled neurons after treatment with TEV protease termed as 'Resting' (green). The merge shows pHlourin labeled boutons that are co-positive for VGAT (white spots, indicated by arrows). (B) (i)VGAT image was subjected to intensity threshold 'Triangles' algorithm, and the particles from 0.2-50 microns and 0.2-1 circularity were analyzed. The VGAT image shows the particles that were selected in yellow. (ii) The VGAT selected boutons were recalled into the 'Resting-state image. Then, the particles were manually annotated to make sure that they were pHlourin positive. The same particles were recalled (iii) in 'max' pH 8.5 and (iv) 'min' pH 5 images and the signal was averaged. Before analyses, all images were aligned using the 'Stack Shuffling – Align Slices in Stack' algorithm in Image J (NIH, USA). Scale bar:10 µm. (C) Resting pH estimation using Nb-pHlourin probe and (D) using mOrange2 probe. No. of boutons > 50 from ≥ 3 coverslips across different cultures. Data were analyzed by unpaired t-test. *: $p \leq 0.05$, **: $p \leq 0.001$.

3.6 A flexible system of targeting sensors into SVs

After estimating the resting pH using the conventional probes, we targeted new pH-sensitive fluorophores that have improved properties compared to pHlourin and mOrange2. Here, we developed a flexible system that can be used to target any ion-sensitive probe (pH or Cl^- sensor) into the SV. One approach could be to label the Nb with a required fluorophore like Ab/protein labeling. However, this would require the Nb to be labeled with each fluorophore that is intended to be targeted, separately which would be more time-consuming. Also, when labeled directly, the protein is labeled all over, thus it is impossible to get rid of the plasma membrane pool using the TEV protease. Instead, the short ligands conjugated to fluorophores are easy to produce, simply require one step of mixing with the Nb, and can be easily cleaved from the Nb using the TEV protease. Therefore, to generate a flexible system of targeting fluorophores, we tried 2 strategies: 1) Fusing the Nb Syt1 with another Nb against a small peptide; ALFA Nb, (Götzke et al., 2019) to generate a bispecific Nb 2) Fusing the Nb with Halo/SNAP-tag. Here the Nb Syt1 part acts as the targeting module while the Nb ALFA or Halo/SNAP tags act as the detection module as they can be easily labeled with a ligand conjugated with a fluorophore/ion-sensor.

3.6.1 Fusion of Nb Syt1 with Nb ALFA to generate a bispecific Nb and its binding with GFP-ALFA protein

In a recent publication (Götzke et al., 2019), a Nb against 10 amino acid (aa) peptide called ALFA peptide was developed. We fused the two Nbs: αSyt1 and αALFA to generate a bispecific Nb (Figure 3.13A). Here, the Syt1 Nb would enable targeting to the SVs while the ALFA Nb can bind to any fluorophore that is coupled with the ALFA peptide. The affinity of Nb ALFA to ALFA tag is quite high (K_d is in pM) which makes it an ideal probe such that the probe will not dissociate in the cellular environment.

The bispecific nanobody was cloned and purified (Figure 3.13 B) using ion-exchange chromatography. To test the binding of the bispecific Nb with the ALFA tag, GFP fused with the ALFA tag as a proxy ligand was purified (Figure 3.13 C) using size exclusion chromatography.

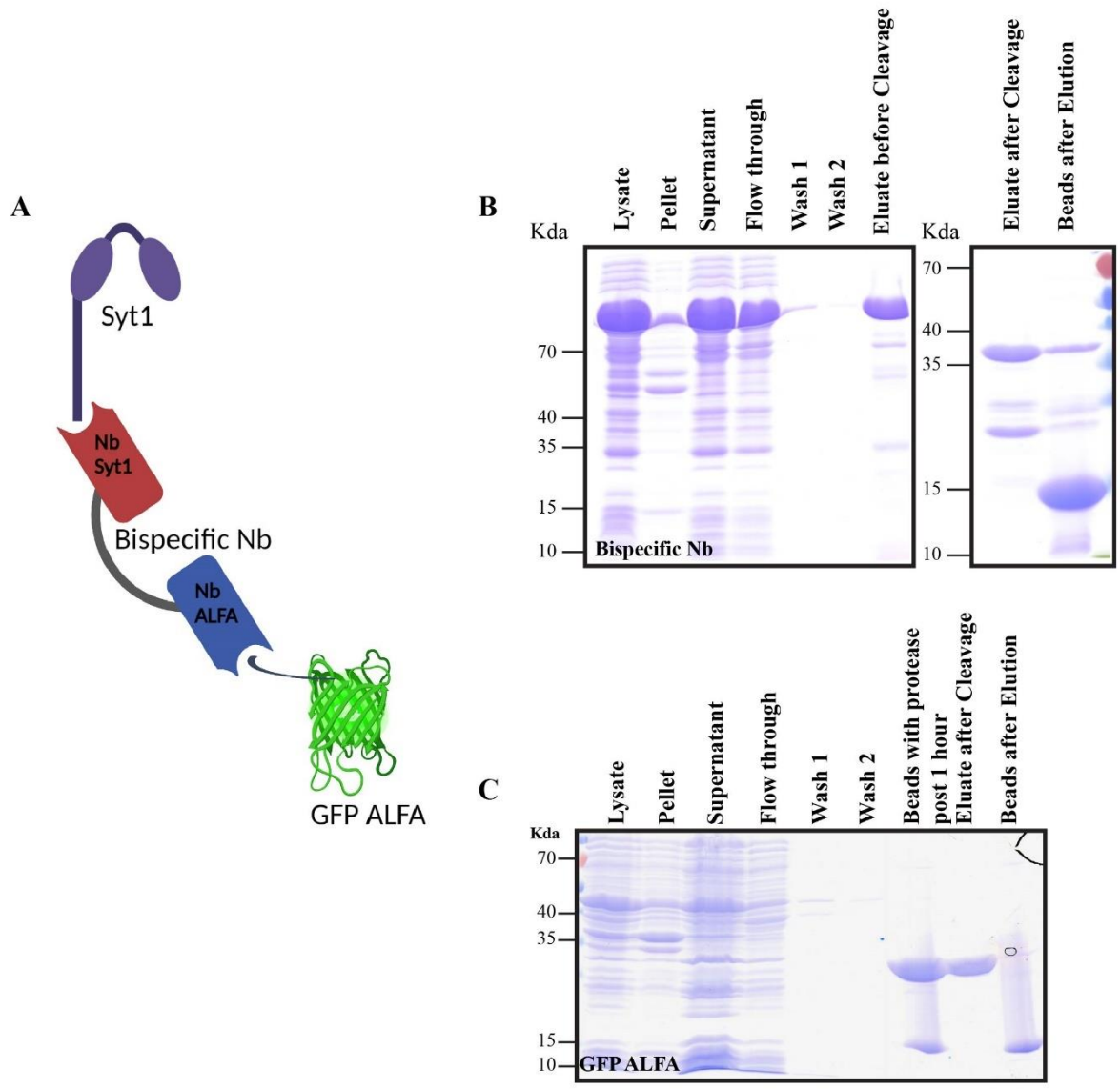

Figure 3. 13 Purification of bispecific Nb and GFP ALFA proteins.

(A) Scheme of bispecific Nb and GFP ALFA. The Nb Syt1 (in red) binds with the luminal domain of Syt1 while the Nb ALFA (in blue) binds with the ALFA peptide (B) Bispecific Nb purification. Note that in B, the cleavage product was run on a separate gel. Cleavage was done with 1µM Ulp1 protease. (C) GFP ALFA purification. 1µM Ulp1 protease was used to perform the on-column protein cleavage.

Bispecific Nb and GFP ALFA were premixed in a 1:1 ratio at RT for 15 minutes to form a complex. The binding of the Nb with GFP-ALFA was confirmed using Native gel electrophoresis (Figure 3.14A). The size shift of the complex in the native gel proved that the complex is successfully formed. The complex was then treated with TEV protease to check whether the TEV site is still accessible. The decrease in molecular weight (MW) after TEV cleavage henceforth shows that the TEV site is indeed accessible (Lane 4, Figure 3.14B Left). The SDS gel (Figure 3.14B right) shows that the interaction of the Nb with GFP ALFA is ionic and thus it is sensitive to SDS detergent.

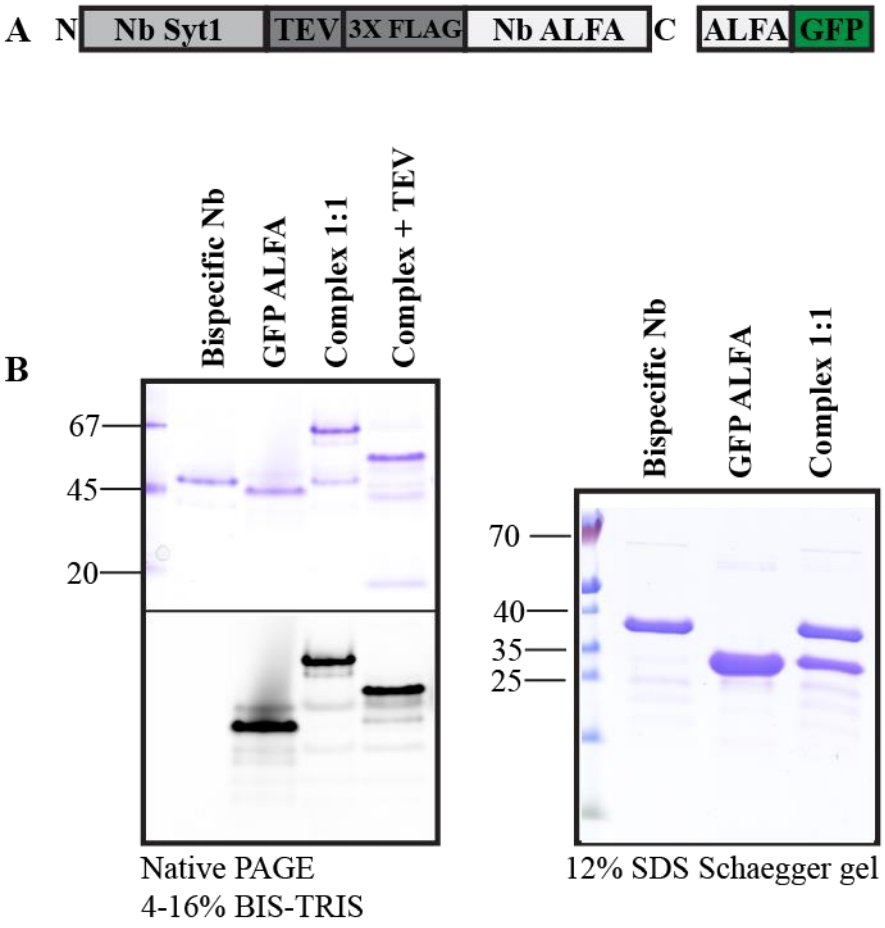

Figure 3. 14 Bispecific Nb and GFP ALFA complex formation

(A) Scheme of Bispecific Nb and GFP ALFA complex formation. 'N' and 'C' mark the N and C terminal of the protein. 'TEV' refers to TEV protease cleavage site, '3X FLAG' – FLAG tag sequence repeated three times and 'ALFA' refers to ALFA peptide (B) Complex formation as confirmed on a native gel (left) and an SDS PAGE (right). The two proteins were mixed in a 1:1 ratio at RT. The complex was treated with 5 µM TEV protease and run on the native gel to confirm the cleavage (Left, lane 4). After Coomassie staining, the same gel was scanned in a fluorescence gel reader. Molecular weights (MW) of Bispecific Nb – 34.5KDa, GFP ALFA – 30.9 KDa. Note that the mobility of the complex at higher MW confirms that the complex formation is successful. As the complex is formed based on ionic interactions, it is a detergent (here SDS) sensitive. Thus, in the SDS PAGE, two bands are visible. The presence of equally sized two bands shows that the proteins were mixed in exactly a 1:1 ratio. Note that the bispecific Nb and GFP ALFA bands in the first 2 lanes of SDS gel (on right) are not equal because of a loading mistake; protein amount loaded is different than protein amount used to form the complex.

3.6.2 Targeting of bispecific Nb-GFP ALFA complex to synaptic vesicles

The complex of bispecific Nb with GFP-ALFA was targeted to neurons by spontaneous labeling, as described before for the Ab and Nb-pHlourin. A puncta-like staining pattern classical for synaptic boutons was seen, in contrast with the 'GFP ALFA only' uptake as the negative control (Figure 3.15). However, it can be observed from these images that 'GFP ALFA only' uptake showed signal in the round dotted pattern instead of oval elongated bouton-like morphology. These are likely the endosomes that take up GFP ALFA

by bulk endocytosis, or clusters of SVs translocating with the microtubules or it could be merely the residual autofluorescence and the free GFP sticking with the membranes despite the washing steps.

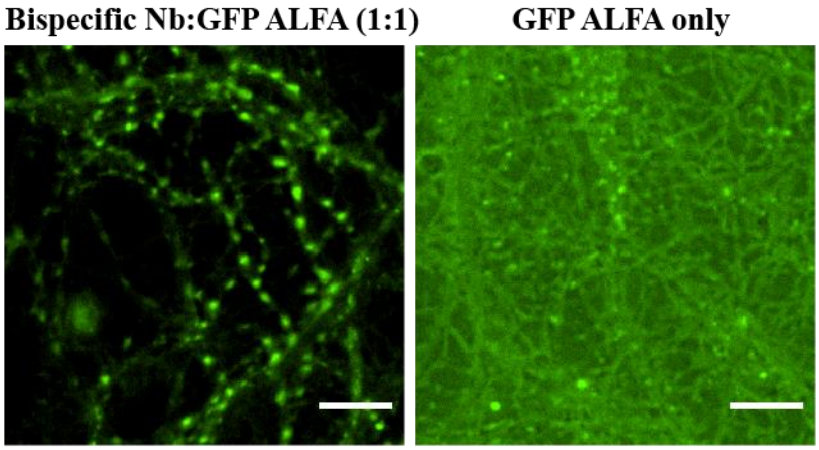

Figure 3. 15 Bispecific Nb and GFP ALFA complex targeting to neurons

Uptake of the complex formed in (A) and GFP ALFA alone as a negative control in cultured neurons. In the left image, the boutons appear as a puncta classical synaptic pattern of staining. Note that in GFP ALFA only control, the green small dots may be endosomes. The signal is a mixture of autofluorescence and background from GFP ALFA-free protein taken up by bulk endocytosis. The two images have been auto-scaled to display the same brightness intensity for comparison. Note the bright green intensity is the background signal, thus the signal-to-noise is extremely weak in the 'GFP ALFA only' image. Scale bar: 10 μM

To confirm the specificity of bispecific Nb-GFP ALFA complex, labeled neurons were fixed and immunostained with external Syt1 cytoplasmic and a presynaptic marker protein Bassoon (Figure 3.16). The high degree of colocalization (white spots in the 'merge') proves that the bispecific Nb-GFP ALFA complex is highly specific to synapses.

Thus, these results indicate that the bispecific Nb successfully binds with GFP-ALFA and targets it to the SVs. In the following section, we attempted to target pH or Cl sensitive fluorophores to SVs, instead of GFP, using the bispecific Nb.

3.6.3 Binding of fluorophore-conjugated to ALFA peptide with the bispecific Nb and its targeting to neurons

The bispecific Nb system worked well for targeting GFP-ALFA and gave us proof of principle. To create a generalized system of targeting fluorophores, we wanted to label the ALFA peptide with a required fluorophore/ion-sensitive probe. ALFA peptide was synthesized and labeled with Alexa488 or TMR fluorophore by Dr. Patrick Menzel in the lab of Prof. Diederichsen (Institute for Organic and Biomolecular Chemistry, Göttingen). Labeled ALFA peptides were mixed with the bispecific nanobody and run on a Native gel to confirm their binding. The labeled bispecific Nb was observed at the same molecular weight

as the bispecific nanobody (Lane5, Figure 3.17B). This is expected as the MW of ALFA peptide labeled with fluorophores is too small to be seen as a size shift. GFP ALFA and its complex with Bispecific Nb were also run on the gel as positive controls (Lanes 1-4, Figure 3.17B).

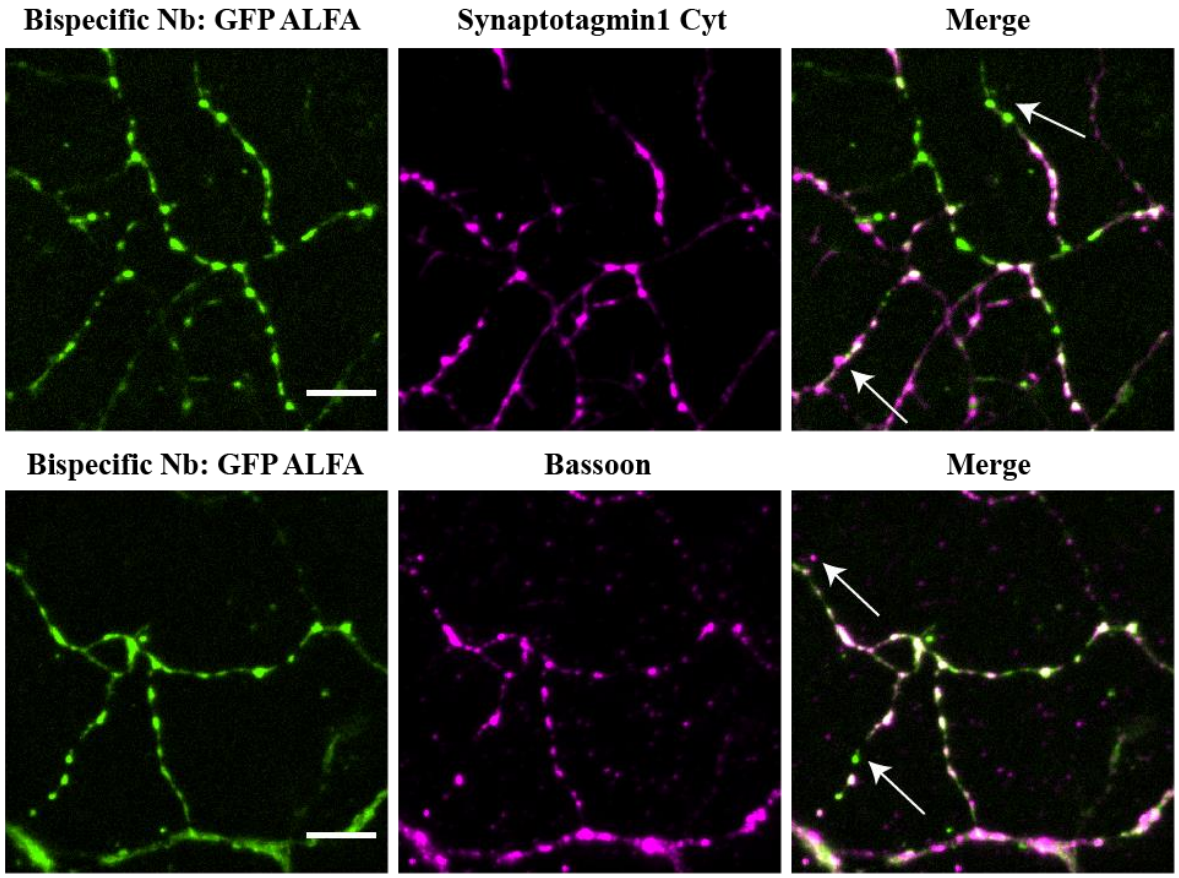

Figure 3. 16 Immunostaining using synaptic markers to confirm the specificity of Bispecific Nb-GFP ALFA complex.

Neurons were stained using Syt1 cytoplasmic (top panel) and Bassoon (bottom panel) antibodies after the uptake of the Bispecific Nb-GFP ALFA complex. The boutons in white in 'merge' show a clear colocalization with the markers proving that the Bispecific Nb is highly specific to synapses. Note that the arrows indicate the boutons and dots that don't colocalize. These are the synapses that could be detected by Ab or Nb. It also confirms that there is no bleed-through in the signal between these channels. Scale bar:10 μM.

However, surprisingly, the complex remains unchanged upon treatment with TEV protease. This is unexpected as the Coomassie staining indicates that the Nb is cleaved by TEV (upper panel, Figure 3.17B), but the fluorophore visualization does not show the same. This observation is enigmatic as it indicates that the fluorophore itself is forming a precipitate (perhaps it is sticky and hydrophobic), independent of the Nb.

We let the neurons uptake the Nb-Alexa 488 complex by spontaneous labeling as described before. It was observed that, despite trying various concentrations and conditions, there was no puncta-like pattern, it was a dotty pattern like 'GFP only' control seen previously (Figure 3.16).

Taken together, the fact that TEV treatment did not show cleavage of the fluorophore-Nb and that neuronal uptake did not work, we conclude that Alexa488-ALFA peptide precipitated or formed a complex by itself (as indicated by the band insensitive to TEV) and thus was not available for its binding with the Nb. To get rid of the precipitate, we employed a few strategies: 1) the fluorophore was centrifuged at 13K g for 10 minutes. This failed, as the precipitate band remained unchanged (Appendix 5.2). 2) Adding a small percentage of detergent (Triton X-100 or SDS) was added to separate the fluorophore molecules and failed to make the fluorophore available. 3) Other fluorophores like TMR were also tried, as the hydrophobicity of Alexa488 may have caused the precipitate formation. However, that did not work either (data not shown). Perhaps, the problem lies with the ALFA peptide itself, which might aggregate when it is tagged to a fluorophore. Thus, the above results show that while the bispecific Nb can be used to target proteins like GFP (perhaps because GFP is more stable than organic dyes), it cannot be used to target organic fluorophores/ion sensors. One needs to employ other strategies to target organic dyes using the Nb system.

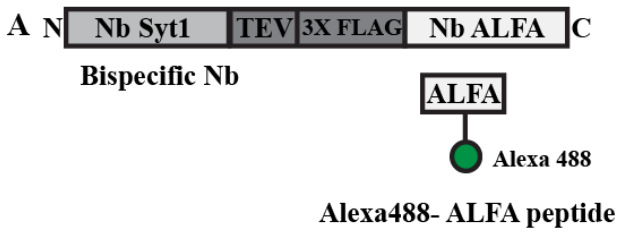

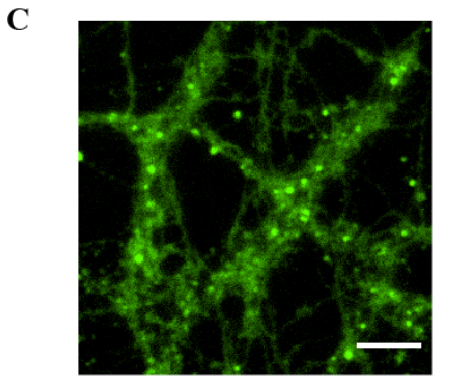

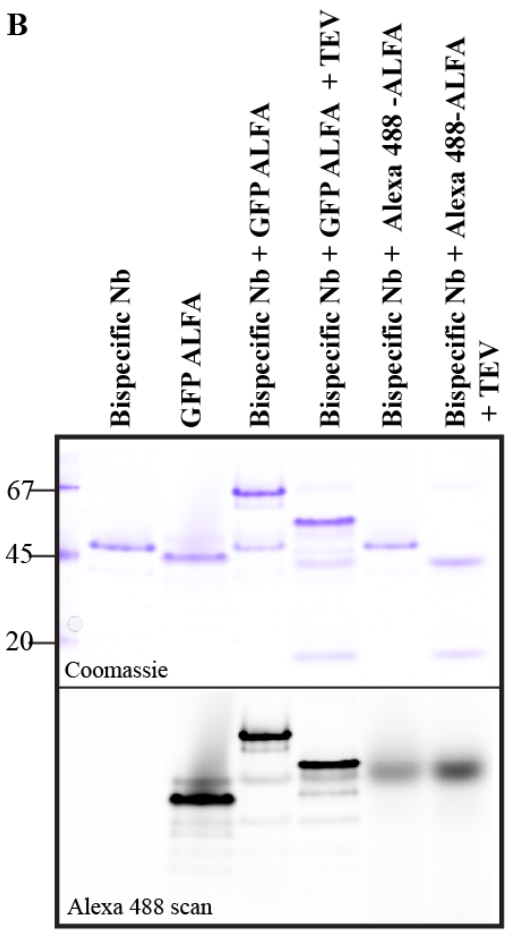

Figure 3. 17 Binding of bispecific Nb with Alexa488 coupled with ALFA peptide and its uptake in neurons.

(A) Scheme showing the binding of the bispecific Nb with the ALFA peptide labeled with Alexa488 (green ball). (B) Bispecific Nb was mixed with the Alexa488-ALFA peptide in a 1:1 ratio at RT for 5 minutes. The complex was run on a Bis-Tris Native Gel before and after treatment with 5 μM TEV Protease (lane 5-6). GFP ALFA and its complex with the Nb were used as a positive control (lanes 1-4). The upper panel is stained by Coomassie, the lower panel is visualized in the Alexa488 channel in the fluorescence gel scanner (C) Uptake of Alexa488-Nb complex in neurons does not result in a punctate pattern but rather just a spotty pattern classical of endosome like morphology. Image has been captured in the Nikon Ti2E epi-fluorescent microscope. Scale bar: 10 μm

3.6.4 Other tags like HaloTag and SNAP tags were fused with the Nb and targeted to SVs

Many protein tags have been developed in the past that bind with small synthetic ligands. HaloTag (Los et al., 2008) and SNAP tags (Keppler et al., 2003) are prime examples that have been widely used for diverse purposes. These systems allow covalent attachment of synthetic ligands onto a protein tag either in cells or in solution. As the bond between the protein tag and the ligand is quite stable (SDS and boiling resistance), it allows several advantages; it can be imaged in living cells for long periods and it can be visualized after fixation thus allowing multiplexing with immunocytochemistry (Los et al., 2008).

Halo and SNAP tags were fused with the Nb (Scheme, Figure 3.18A). Their respective ligands were conjugated with TMR (Promega). Both the tags successfully bound with the ligand coupled with fluorophores (Figure 3.18, Appendix A.3). Treatment with TEV protease shows a nearly full cleavage of the fluorophore from the Nb backbone (Figure 3.18B, Lane 4). Note that in contrast to the cleavage result using the complex of bispecific Nb and labeled ALFA peptide in earlier experiments (Figure 3.17), this time we observed cleavage in both the Coomassie staining and the fluorescence scan (Figure 3.18). The Nb-Halo-TMR complex was successfully taken up in cultured neurons to reveal a synaptic punctate-like pattern. Halo TMR ligand (free or unbound fluorophore) uptake was used as a negative control thus confirming that the labeling is not due to the bulk uptake of the dye or artifactual permeabilization of neurons (Figure 3.18C). Nb fused with HaloTag protein showed better targeting than SNAP-tag fusion protein (Appendix A.3). The system also works with other dyes like Alexa488 and Alexa 647 labeled to Halo ligand (as shown earlier in WB, Figure 3.5). As the Nb-Halo fusion protein can be ligated with fluorophores easily, this system can be used in multicolor imaging. For example, we used Nb-pHlourin together with TMR-Halo Nb or Alexa647-Halo-Nb complex to check the specificity of pHlourin Nb targeting. We saw that many synaptic boutons were colocalized proving that pHlourin Nb was well targeted to the SVs and that multiplex imaging using the Nb tool was possible (Appendix A.4).

To confirm the specificity of Nb Halo targeting, Nb Halo-TMR complex labeled neurons were immunostained with synaptic markers. Boutons co-localized well with markers like Bassoon, Synaptophysin 1, VGLUT, and VGAT (Figure 3.19). These data taken together provide proof that the Nb fused with the HaloTag is a robust system to target fluorophores to SVs.

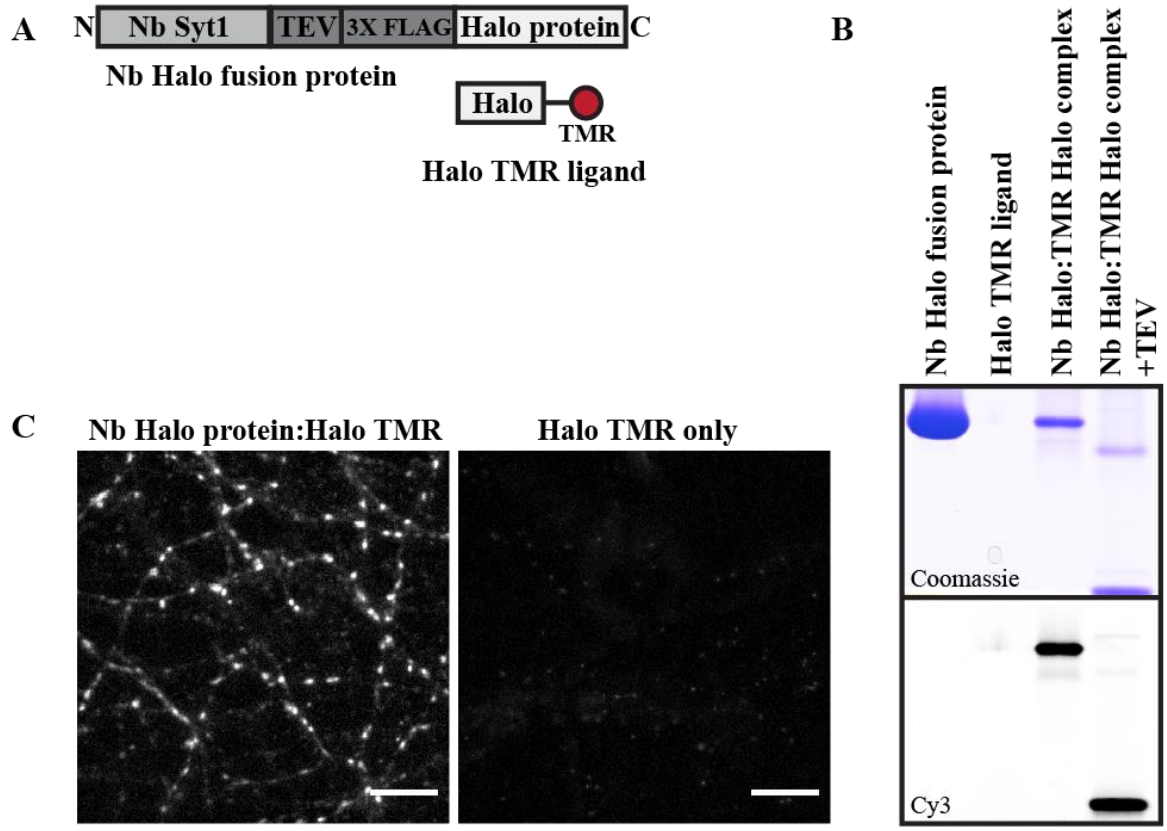

Figure 3. 18 Binding of Nb-Halo fusion protein with Halo ligand labeled with TMR and its targeting to synapses.

(A) Scheme showing the Nb Halo protein tag fusion construct and it's binding with the Halo ligand labeled with TMR fluorophore (red ball). (B) Nb Halo fusion protein and Halo ligand were mixed in a 1:1 ratio at RT for 15 minutes and run on 10 % Native gel to confirm their binding. The complex was treated with 5 μM TEV protease to cleave TMR. The gel was scanned in the Cy3 channel in the fluorescence gel reader to visualize TMR signal and stained with Coomassie to visualize the non-fluorescent proteins. Halo-TMR ligand is too small to be retained on the gel. (C) The complex was taken up in cultured neurons. A clear puncta-like pattern depicting synaptic boutons is seen. Halo TMR ligand-only uptake was used as a negative control. Images were taken on a Nikon Ti2E Epifluorescence microscope. Scale Bar:10 μm.

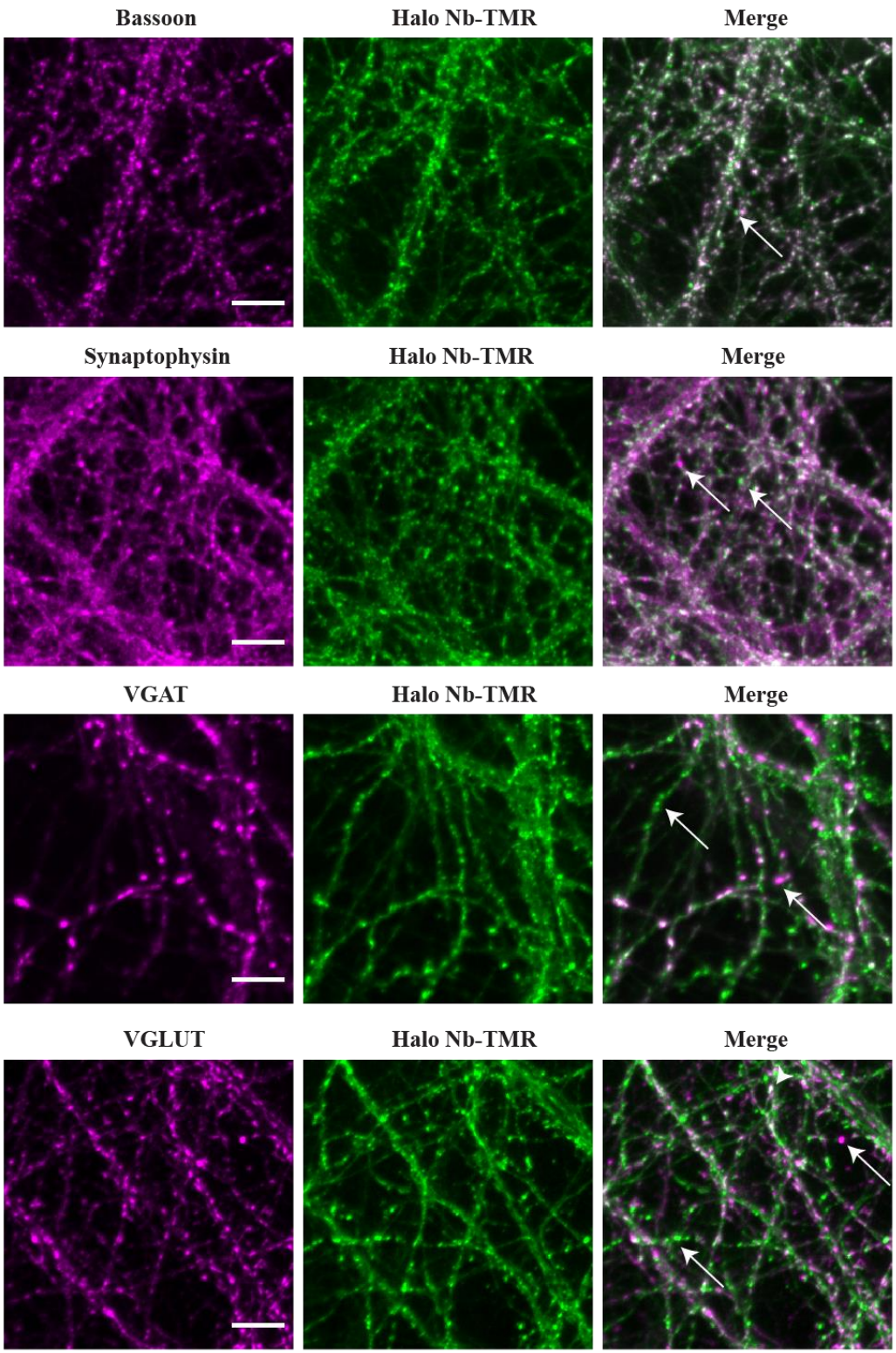

Figure 3. 19 Specificity of Nb Halo-TMR complex confirmed by immunostaining with presynaptic and SV markers.

Neurons were labeled spontaneously with the complex of Nb Halo-TMR. They were then fixed and stained with Abs against presynaptic markers – Bassoon and Synaptophysin1 and SV proteins – VGLUT and VGAT. Images in green show signals from Nb-Halo-TMR while magenta shows the image from each of the markers. The white spots (synaptic boutons) in the 'merge' image indicate the extent of colocalization. White arrows indicate the boutons that DO NOT colocalize to highlight that the images are spectrally well separated. Images are captured on Nikon Ti2E. Scale Bar: 10 μM.

3.7 Targeting of pH-sensitive probes to SVs with the Nb-Halo method

3.7.1 Virginia Orange (VO) – Halo probe

Virginia Orange (VO), 2',7'-difluorocarbofluorescein (λex/λem = 555/582 nm) is a pH-sensitive, high contrast bright fluorophore derived from Fluorescein. Its brightness increases with increasing pH and it has a pKa of 6.75 (Grimm et al., 2016). Halo ligand labeled with VO was obtained from the lab of Prof. Luke Lavis. The binding of VO with the Nb Halo protein was confirmed on a native gel (Figure 3.20B). The complex was successfully targeted to SVs revealing a punctate-like pattern (image not shown). To confirm the functionality of the probe, neurons were electrically stimulated at 300APs, 30 Hz, and the exo-endocytosis pattern was measured. As the probe becomes brighter with increasing pH, the fluorescence of VO increases during exocytosis and decreases during endocytosis. Bafilomycin A1, a blocker of V-ATPase, was used to block the acidification to check if the recovery of signal to the baseline is indeed due to the vesicle acidification (Figure 3.20C).

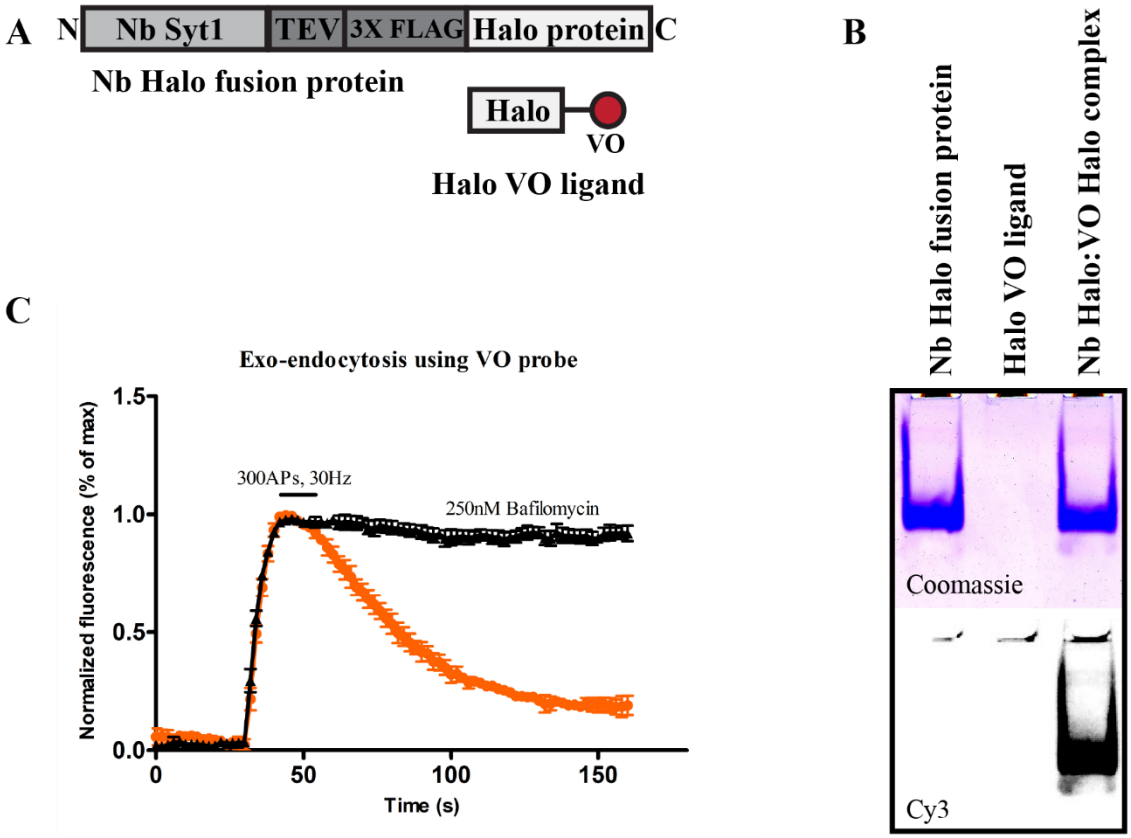

Figure 3. 20 Binding of Nb Halo protein with pH-sensitive fluorophore Virginia Orange (VO) Halo ligand and its uptake in neurons.

(A) Scheme showing the Nb Halo protein tag fusion construct and it's binding with the Halo ligand labeled with VO fluorophore (red ball). (B) Nb Halo fusion protein and Halo ligand were mixed in a 1:1 ratio at RT for 15 minutes and run on 10 % Native gel to confirm its binding. The gel was scanned at the Cy3 channel in the fluorescence gel reader to visualize the VO signal and stained with Coomassie to visualize the non-fluorescent proteins. The Halo-VO ligand is too small to stay on the gel. (C). Neurons labeled with VO were stimulated at 300APs, 30 Hz, to record the exo-endocytic pattern and confirm the functionality of the probe. V-ATPase blocker Bafilomycin A1 was used as the control.

3.7.2 AcidiFluor Orange (AF) – Halo probe

3.7.2.1 Binding and targeting of AF

AF was well characterized in the initial Ab experiments as seen in earlier section 3.1. We went ahead and targeted AF using the Nb Halo method. A great advantage of AF compared to any other pH-sensitive fluorophore used in this study (pHlourin, mOrange2, VO) is that its brightness increases with decreasing pH. This is desirable to estimate a more accurate resting pH of an SV as the other probes may not be able to resolve pH changes in the low acidic range, as described in the Introduction.

Halo Nb binds well with the Halo ligand labeled with AF (commercially available, Goryo Chemicals) (Figure 3.21B). The binding was confirmed on a Native Gel, however, the gel had to be incubated in an acidic buffer to visualize the fluorescence as AF is brighter at low pH. AF was well targeted to presynapse in cultured neurons (Figure 3.21C).

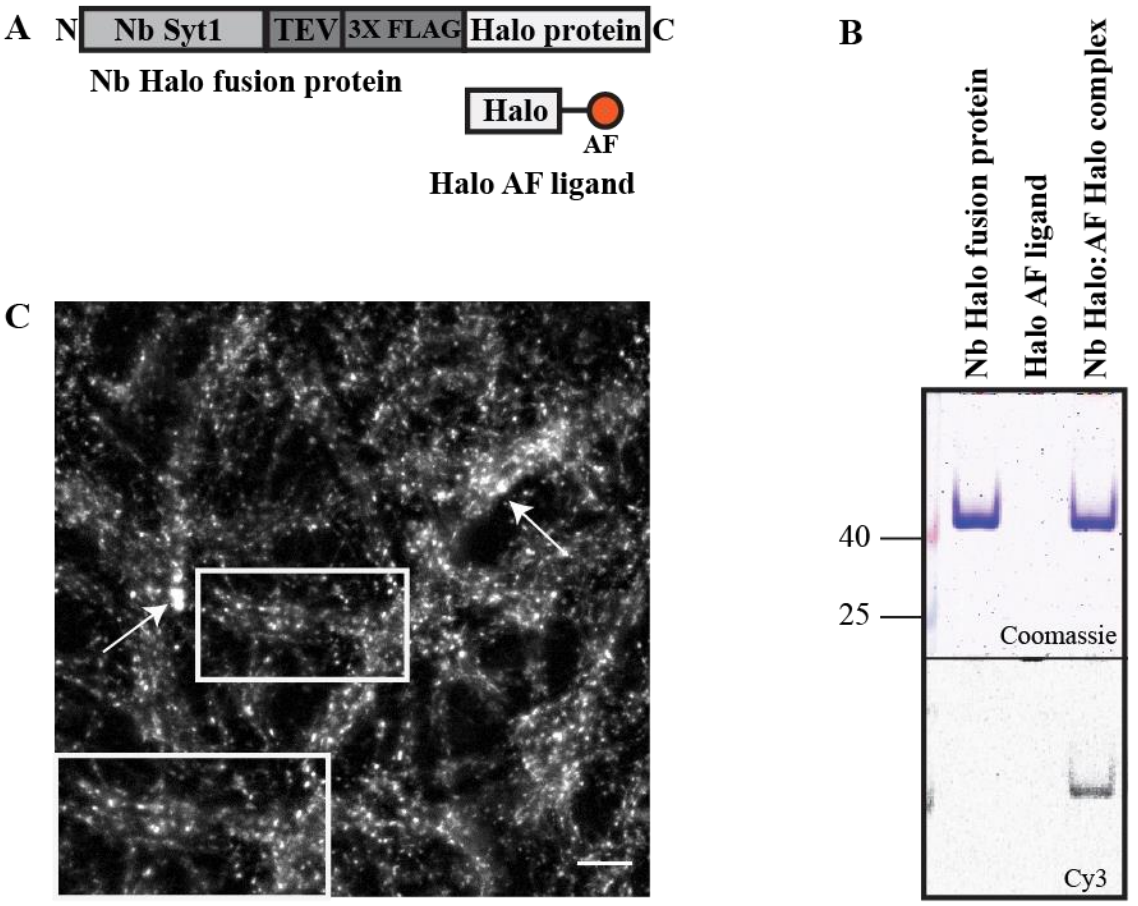

Figure 3. 21 Binding of Nb Halo protein with pH-sensitive AcidiFluor Orange (AF) Halo ligand and its uptake in neurons.

(A) Scheme of Nb Halo fusion protein binding with Halo AF ligand. The orange ball represents the AF fluorophore. (B) Nb and the ligand were mixed in a 1:1 ratio to form the complex and run on a 10 % Native Gel at 200 V for 30 minutes. The gel was incubated in a buffer of pH 5.0 to reveal the fluorescence and imaged in the Fluorescence Gel reader. It was then stained with Coomassie. The gel was run by Margarita Chudenkova. (C) Uptake of Nb Halo-AF complex by spontaneous labeling of the recycling pool of vesicles. The white box zooms a part of the image for better visualization. The white arrows indicate the dye aggregates that couldn't be removed after centrifugation at 13K g for 10 minutes. Scale bar: 10 μM.

3.7.2.2 Estimation of resting pH of recycling SVs using AF probe

Nb-Halo-AF probe was used to estimate the resting pH of Glutamatergic and GABAergic SVs, in a manner conceptually like the one described before with pHlourin and mOrange2 probes (Figure 3.12). Briefly, the neurons labeled with Nb-Halo-AF were treated with TEV protease, and the image captured was referred to as the 'resting' condition. Neurons were briefly treated with an ionophore cocktail containing buffers clamped at a maximum signal pH of 3.2 ('max' image) and a minimum signal image at pH 8.5 ('min' image). The ROI was fixed and immunostained with primary labeled VGLUT and VGAT Abs to classify the synaptic boutons in the 'resting', 'max', and 'min' images into Glutamatergic and GABAergic vesicles. Thus, images were subjected to bouton analysis (Methods), and a map of VGLUT (or VGAT) boutons was traced back to original images, each bouton was then manually annotated in the original 'max' image to be sure, that the selected bouton does contain the Nb-Halo-AF probe. A representative image of this workflow is

shown in Figure 3.22A and B. Average intensities from 'resting', 'max' and 'min' and the pKa estimated before (pKa-5.5) were plugged in equation11 (Methods) to estimate the pH at the 'resting' state. Interestingly, the resting pH obtained using the Nb-Halo-AF probe was 5.21 ± 0.027 for Glutamatergic and 5.11 ± 0.007 for GABAergic boutons (Figure 3.22C). These values are very comparable and they are in contrast with the results from pHlourin and mOrange2 probes used before, where Glutamatergic resting pH was found to be more acidic than the GABAergic SVs (Figure 3.12).

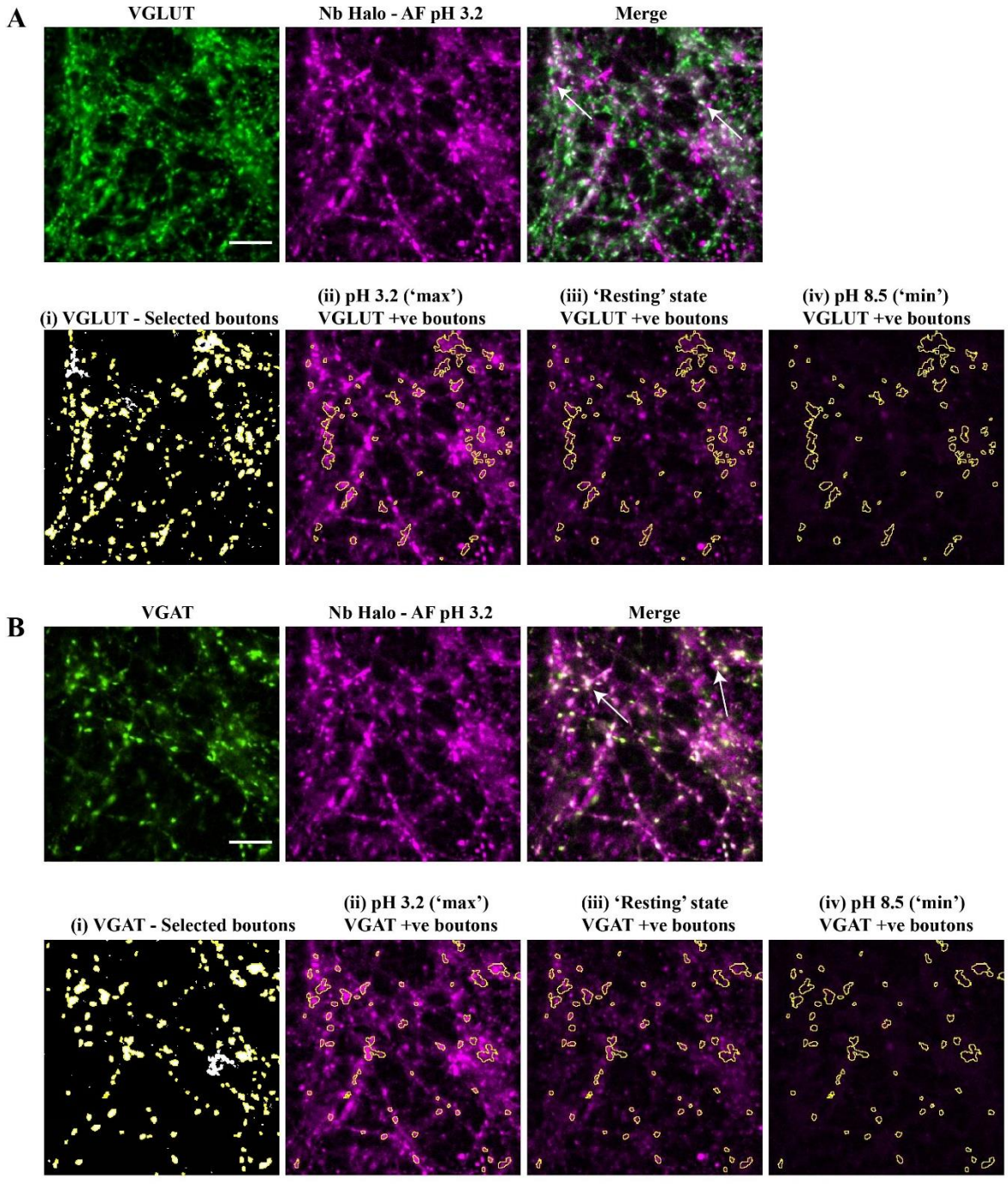
A
VGLUT
Nb Halo - AF pH 3.2
Merge
(i) VGLUT - Selected boutons
(ii) pH 3.2 ('max')
VGLUT +ve boutons
(iii) 'Resting' state
VGLUT +ve boutons
(iv) pH 8.5 ('min')
VGLUT +ve boutons
B
VGAT
Nb Halo - AF pH 3.2
Merge
(i) VGAT - Selected boutons
(ii) pH 3.2 ('max')
VGAT +ve boutons
(iii) 'Resting' state
VGAT +ve boutons
(iv) pH 8.5 ('min')
VGAT +ve boutons

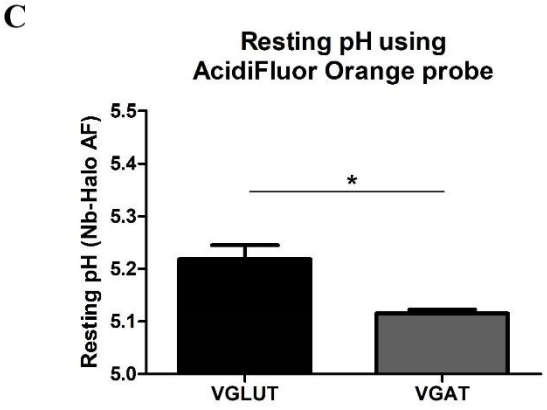
C
Resting pH using
AcidiFluor Orange probe
Resting pH (Nb-Halo AF)
5.5
5.4
5.3
5.2
5.1
5.0
*
VGLUT
VGAT

Figure 3. 22 Estimation of resting pH using Nb-Halo-AcidiFluor Orange probe.

(A) Post-hoc immunostaining with VGLUT Abs (Green). Nb-Halo-AF labeled neurons after treatment with TEV protease termed as 'Resting' (Magenta). The merge shows Nb-Halo-AF labeled boutons that are co-positive for VGLUT (white spots, indicated by arrows). (A) (i)VGLUT image was subjected to intensity threshold 'Triangles' algorithm, and the particles from 0.2-50 microns and 0.2-1 circularity were analyzed. The particles that were selected are highlighted in yellow. (ii) The VGLUT selected boutons were recalled into the 'max' image taken in pH clamped buffer 3.2. Then, each particle was manually annotated to make sure that they were Nb-Halo-AF positive. The same particles were recalled (iii) in the 'resting' state and (iv) in 'min' pH8.5 images and the signal was averaged. Before analyses, all images were aligned using the 'Stack Shuffling – Align Slices in Stack' algorithm in Image J (NIH, USA). (B) Repetition of A but with VGAT. Scale bar:10 μm. (C) Resting pH estimation using Nb-AF probe was obtained to be 5.21 ± 0.027 for Glutamatergic and 5.11 ± 0.007 for GABAergic boutons. No. of boutons > 50 from ≥ 3 coverslips across different cultures. Data were analyzed by unpaired t-test. *: $p \leq 0.05$. Error bars: s.e.m.

3.8 Targeting of Cl^- sensitive probes into SVs with Nb-Halo system

3.8.1 DNA origami-based Cl^- Sensor – 'Clensor'

3.8.1.1 Clensor Formation

Clensor is a pH-independent Cl^- sensor comprised of 3 parts: a sensing module - 12mer Peptide Nucleic Acid (PNA) bound with the Cl^- sensitive fluorophore BAC, a normalizing module - 38 mer DNA oligo D2 labeled with a Cl^- insensitive dye Alexa647 (IBA GmbH, Germany) and a targeting module - 26mer DNA oligo D1. Clensor was previously targeted to lysosomes using an aptamer against transferrin receptor (Saha, 2015). In this study, we have modified the Clensor construct to have a Halo ligand attached to the D1 DNA strand (Biomers, Germany) instead of the aptamer in the original construct. (Figure 3.23A).

Clensor synthesis was examined by running the oligos D2, D1+D2, and D1+D2+PNA on a native polyacrylamide gel to compare the shift in size. The D1+D2+PNA complex ran higher than both D2 alone and the D1 (Halo)+D2 complex (Figure 3.23C) confirming that the Halo-Clensor was successfully formed. The PNA amount was titrated in every single experiment to find the concentration that gives the maximum yield. The emission spectra of BAC and Alexa647 were measured to confirm the fluorophore characteristics (Figure 3.23B). The Cl^- and the pH sensitivity of Halo-Clensor was measured using fluorometry. It was seen that Halo-Clensor was sensitive to Cl^- in the range of 0-100 mM Cl^- and insensitive to pH in the physiological range. The ratio of fluorescence of Cl^- insensitive Alexa647 (R) to the fluorescence of Cl^- sensitive fluorophore BAC (G) was plotted against changing Cl^- concentrations. The R/G ratio showed a linear graph and the values were normalized to 0 mM Cl^-. The relationship between the normalized R/G ratio and the Cl^- concentration had an intercept at 1. It was then fitted with a linear regression model to estimate the slope which corresponds to a Stern Volmer constant of 27.45 ± 2.65 M^{-1} (Figure 3.24).

The above set of experiments show that Clensor was successfully synthesized and it is Cl^- sensitive while being pH insensitive in the physiological range

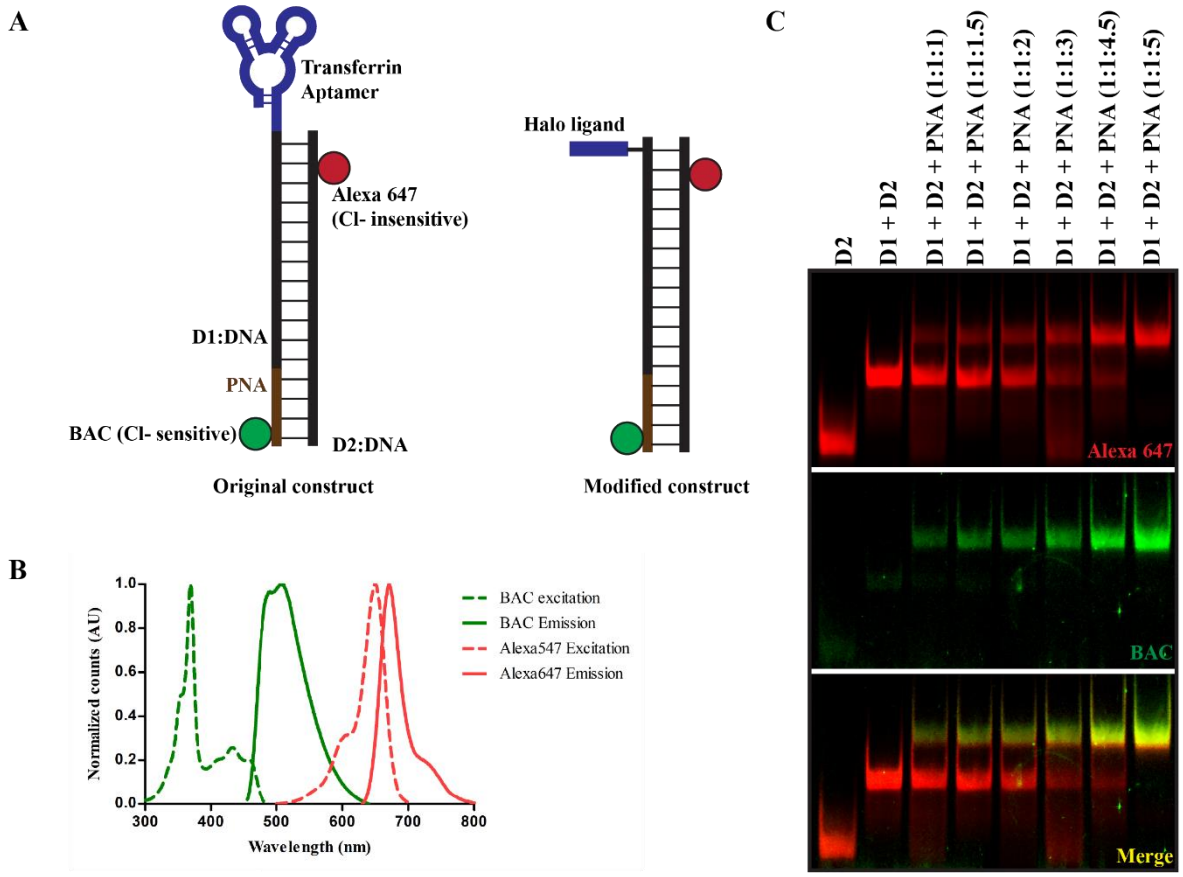

Figure 3. 23 Halo-Clensor formations was confirmed using gel mobility shift assay

(A) Scheme showing a comparison of original Clensor construct from (Saha, 2015) containing the D1 DNA oligo with a transferrin aptamer with the modified Clensor construct used in this study, containing D1 with a Halo ligand. (B) Excitation and emission spectra of BAC in green (measured on Fluorolog) and Alexa647 in red (retrieved from Thermo Fisher Scientific Spectra Viewer) (C) 10 µM of DNA oligos D2, D1+D2, and D1+D2+PNA were run on a 10 % Polyacrylamide Native gel in 1X TBE buffer at 200 V for 30 minutes. The gel was imaged in Cy5 and Alexa488 channels in a fluorescence gel reader to visualize Alexa647 and BAC respectively.

3.8.1.2 Binding of Halo-Clensor with the Halo Nb fusion protein

The Clensor sample showing the highest yield (Lane 8, Figure 3.23C) was used to form a complex with the Nb Halo fusion protein by mixing them in 1:1, 1:2, and 2:1 (Nb: Clensor) ratios for 15 minutes at RT. This was followed by an analysis of a native gel to confirm the formation of the complex (Figure 3.25). The shift in the size of the Nb-Clensor compared to 'only Nb' or 'only Clensor' confirms that the Nb-Halo protein binds with Halo-Clensor. The gel was stained with Coomassie to reveal the non-fluorescent (i.e., unbound Nb). We observed that the binding reaction is not very efficient as in the 1:1 molar ratio, there were both unbound Nb and unbound Clensor. Thus, the complex was further purified using size exclusion chromatography (Appendix A.5).

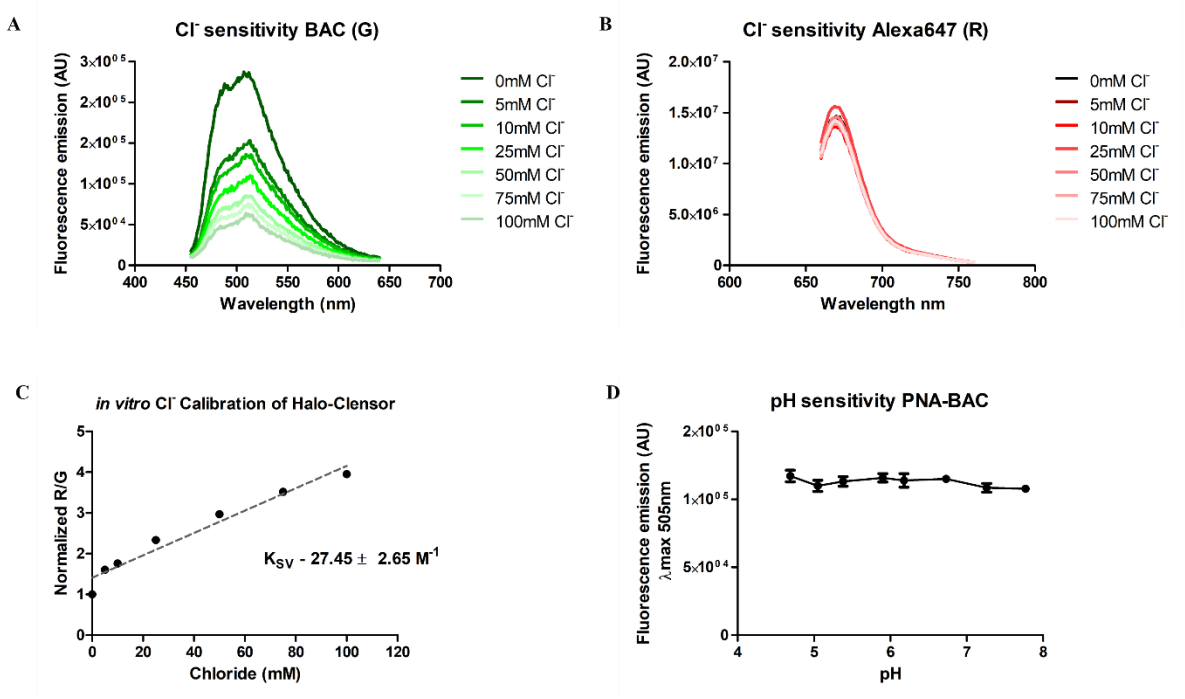

Figure 3. 24 *in vitro* Cl⁻ and pH sensitivity of Halo-Clensor

10 μM Clensor-Halo complex was diluted in buffers containing different Cl⁻ concentrations. The emission spectra of (A) BAC (G) and (B) Alexa 647 (R) are measured by exciting BAC at 434 nm, 5 nm slit size, and Alexa647 at 650 nm, slit size of 2 nm. (C) R/G ratios are plotted as a function of increasing chloride concentrations and normalized to the value at 0 mM Chloride so that the graph intercepts at 1 on the Y-axis. The graph obtained was fitted with a linear regression model to determine the Stern Volmer constant Ksv of 27.45 M^{-1}. (D) BAC-PNA was diluted in pH clamped buffers and the counts at λ_{max} at 505 nm were plotted as a function of changing pH. Error bars- s.e.m

To check whether the binding of the Nb with Clensor preserves its properties or not, we further characterized the Nb-Clensor complex using Fluorometry. The emission spectra of BAC and Alexa647 were measured in the free Clensor and the Nb-Halo-Clensor (called as Nb-Clensor) complex (Figure 3.26). Spectra of the two dyes, BAC and Alexa were measured in each of the two samples: Clensor and Nb-Clensor complex. The samples were diluted either in 0 mM Cl⁻ or in 162 mM Cl⁻ buffers (See Methods section for details) to compare the Cl⁻ sensitivity in Clensor alone versus Nb-Clensor complex. The ratio of Alexa647 emission (R) to BAC emission (G) was plotted as a readout of Cl⁻ sensitivity. It was observed that the fluorescence counts in the Alexa647 channel in Clensor and Nb-Clensor complex were identical at 0 mM Cl⁻ as well as 162 mM Cl⁻ (Figure 3.26A, right). This proves two things: 1) The Alexa fluorophore is intact even after Clensor is bound with the Nb. 2) Alexa is insensitive to Cl⁻. The fluorescence counts in the BAC channel were identical between Clensor and Nb-Clensor complex at 0 mM Cl⁻ and 162 mM Cl⁻. This shows that the fluorescent properties of BAC are also preserved when the sensor is bound with the Nb. Moreover, the BAC counts are higher in 0 mM Cl⁻ compared to 162 mM Cl⁻ showing that BAC is Cl⁻ sensitive. The R/G ratio of Clensor in 0 mM Cl⁻ is 7.83 and that in 162 mM Cl⁻ is 43. Thus, the R/G of the sensor is decreased by ~5.5 times when 162 mM Cl⁻ is added (Figure 3.26B).

These results prove that the properties of Clensor are intact when Clensor has bound with the Nb and that the complex is highly sensitive to Cl^-.

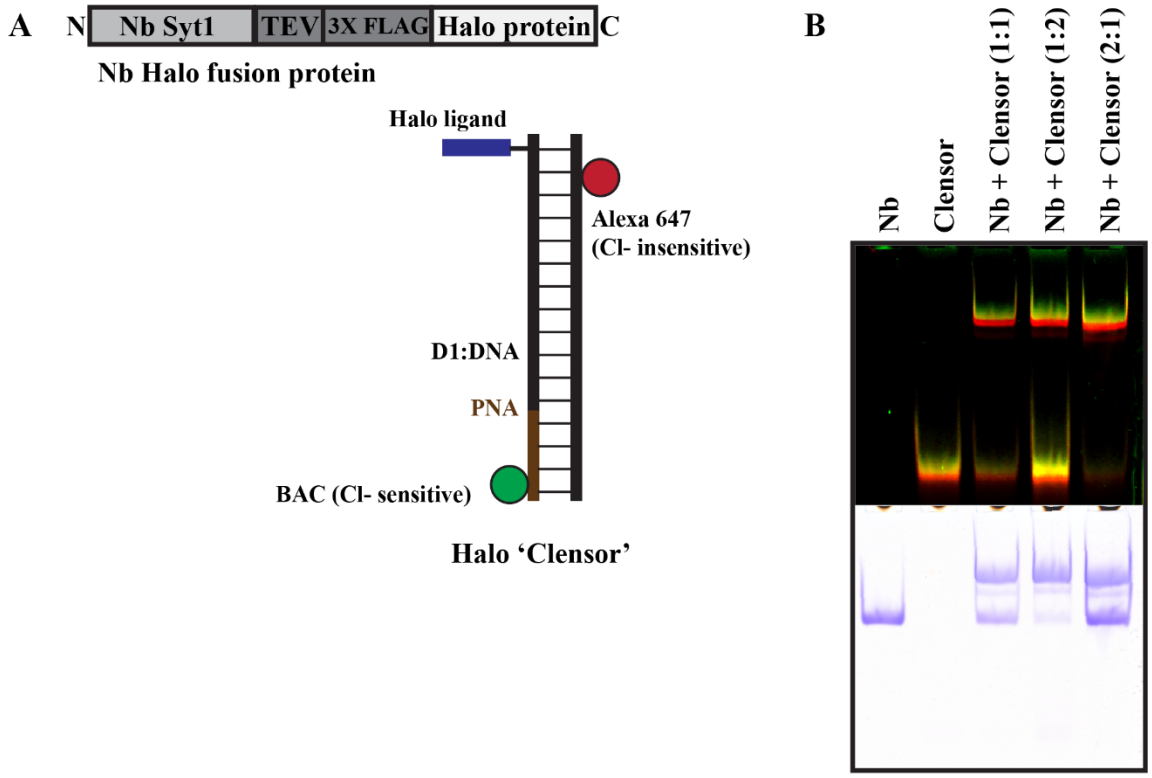

Figure 3. 25 Nb-Halo and Halo Clensor complex formation.

(A) Scheme showing the binding of Nb Halo fusion protein and the Halo Clensor. (B) 10 µM of Nb-Halo and Halo Clensor were mixed in 1:1, 1:2, 2:1 ratio, and 3µL of 10 µM sample were run on the 10 % Native Polyacrylamide Gel. The gel was visualized in Cy5 and Alexa 647 channels of the fluorescence gel reader to visualize Alexa647 and BAC. Only the Merge of the two channels is shown (top panel). The gel was further stained with Coomassie to visualize the non-fluorescent protein bands (lower panel). Note that it appears as if the green and red bands poorly colocalize, however, this appears because the intensity from the Alexa channel (red band) is much higher compared to that from the BAC channel (green band).

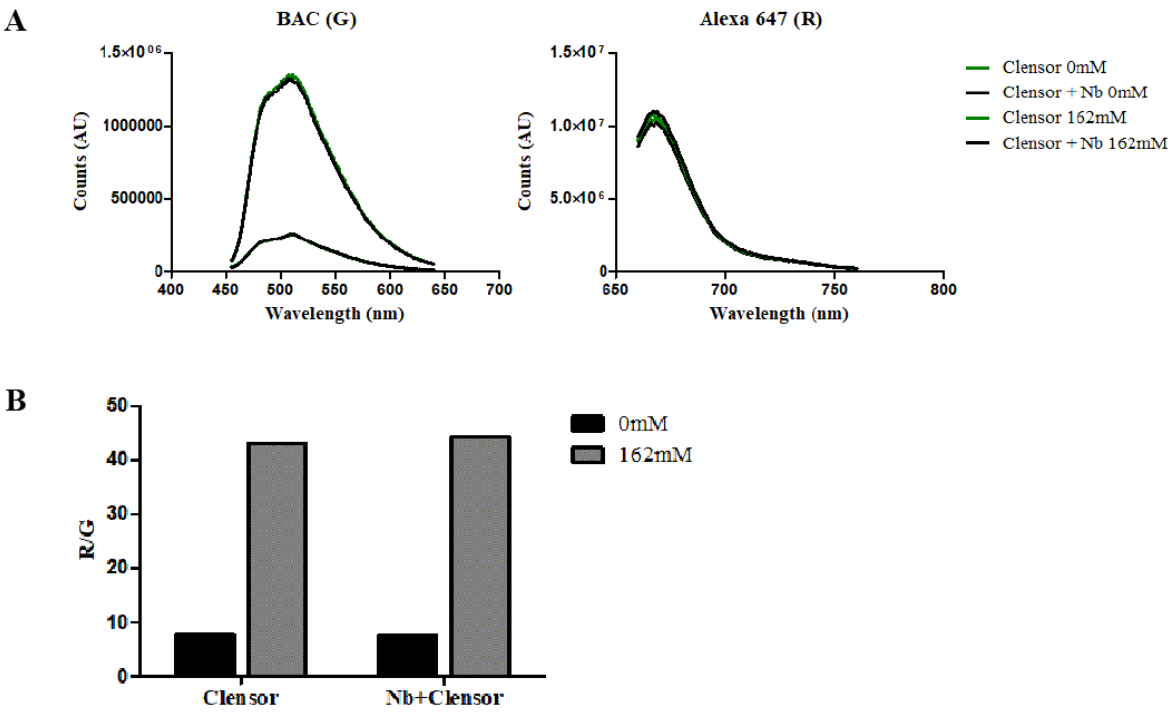

Figure 3. 26 Nb-Halo-Clensor complex behaves identically to Clensor alone.

(A) Emission spectra of BAC and Alexa647 of 5 µM Clensor alone (green) versus Nb-Clensor complex (black) in 0 mM and 162 mM Cl^- containing buffers. The full overlap of black and green plots makes the green plots less visible. The fluorescence counts on the Y-axis are raw counts and have not been normalized to show that Clensor behaves identically with the Nb-Clensor complex. Spectra are measured by exciting BAC at 434 nm, 5nm slit size, and Alexa647 at 650 nm, slit size of 2 nm. (B) Quantification of A by plotting the Alexa (R) by BAC (G) ratio at 0 mM (black) and 162 mM (grey) Chloride concentrations.

3.8.1.3 Uptake of Halo-Clensor complex in neurons

Clensor was targeted into SVs by spontaneously labeling cultured neurons with the Nb-Clensor complex. It was observed that the signal-to-noise ratio (SNR) was high in the Alexa647 channel yielding a punctate pattern. The SNR in the BAC channel was quite low. However, the Alexa channel was used to navigate and find the synapses containing the sensor molecules. Unlabeled neurons were used as a negative control as well as a marker for autofluorescence. Unfortunately, SNR in the BAC channel was so low that it couldn't be differentiated from the autofluorescence signal in the BAC channel (Figure 3.27).

To understand the lack of measurable signal in the BAC channel, we tried the following possibilities:

1) Clensor was dissociated in live cells such that only the D1+D2 complex containing Alexa647 fluorophore got targeted while the PNA part containing BAC got disassembled.

This seems unlikely as the authors had used it in lysosomes (Chakraborty et al., 2017; Osei-Owusu et al., 2021) which, perhaps, has an even harsher environment compared to an SV. If the Alexa647 SNR is good, it means that both D1 (containing the Halo ligand) and D2 (containing the Alexa fluorophore) were targeted

together. This is because the targeting module (Halo ligand) is at D1 while the Alexa fluorophore is at D2. PNA-DNA interactions are even stronger than DNA-DNA interactions, making the dissociation only for PNA-BAC highly unlikely.

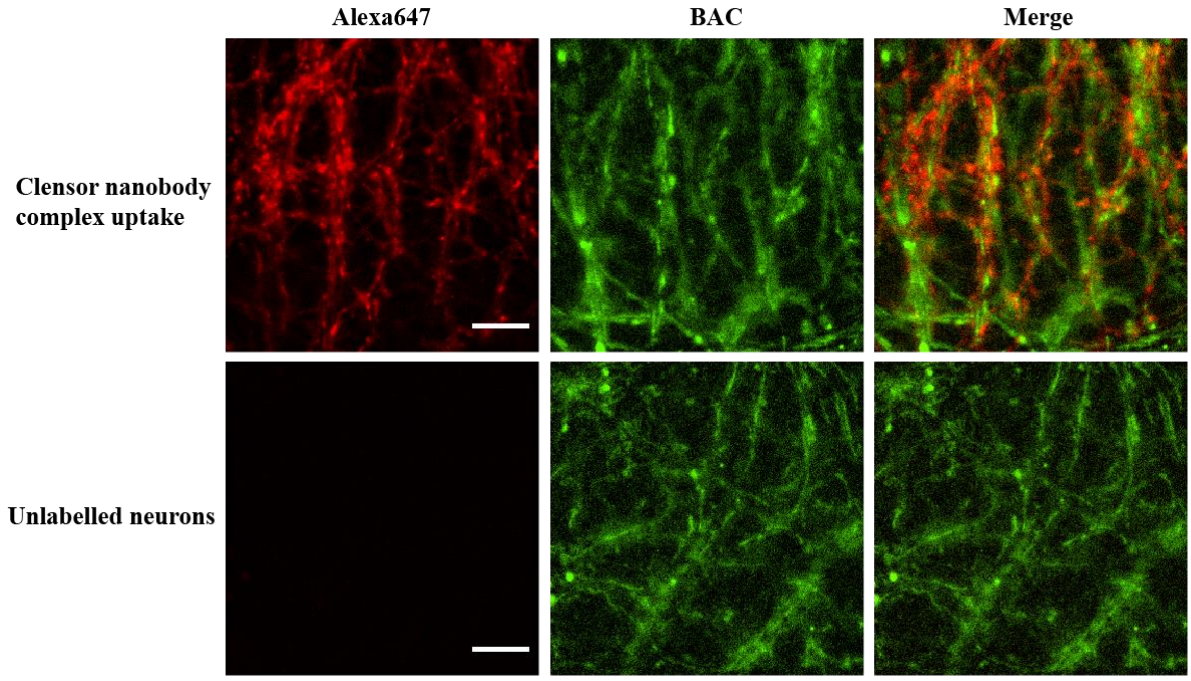

Figure 3. 27 Targeting of Nb-Halo-Clensor to SVs in cultured neurons.

Neurons were bathed in their media containing 20 μM Nb Halo-Halo Clensor complex for 10 minutes at 37°C. Cells were imaged using the Nikon Ti-2E system in Alexa 647 channel (Exc 628/40, BA 692/40, red) and GFP channel (Exc 472/30, BA 520/35, green) for BAC visualization. Unlabeled cells were imaged in the same conditions and were used as a negative control. Note that the signal-to-noise ratio in the BAC channel is so poor that it resembles the signal in the unlabeled cells owing to the autofluorescence. Scale bar: 10 μm.

2) Clensor was never targeted specifically and the signal in Alexa 647 channel was merely an artifact due to Clensor molecules sticking unspecifically to the membrane.

To assess this possibility, neurons labeled with Nb-Halo-Clensor were fixed and immunostained with presynaptic marker Bassoon. We observed that some boutons in the Alexa647 channel colocalized with boutons positive for Bassoon. Clensor alone was given for uptake as a negative control ('Clensor only'). 'Clensor only' uptake showed barely any signal in the Alexa647 channel indicating that the Clensor is targeted to synapses only with the help of the Nb; it isn't sticking to the membranes or is being endocytosed in bulk. Thus, the Nb-mediated targeting of Clensor is specific to synapses (Figure 3.28). Signal in the 'BAC' channel was comparable between 'Clensor only' uptake (negative control) and in unlabeled cells (in Cyan, Figure 3.28). This is perhaps due to the autofluorescence of neurons when cultivated for 14-18 DIV.

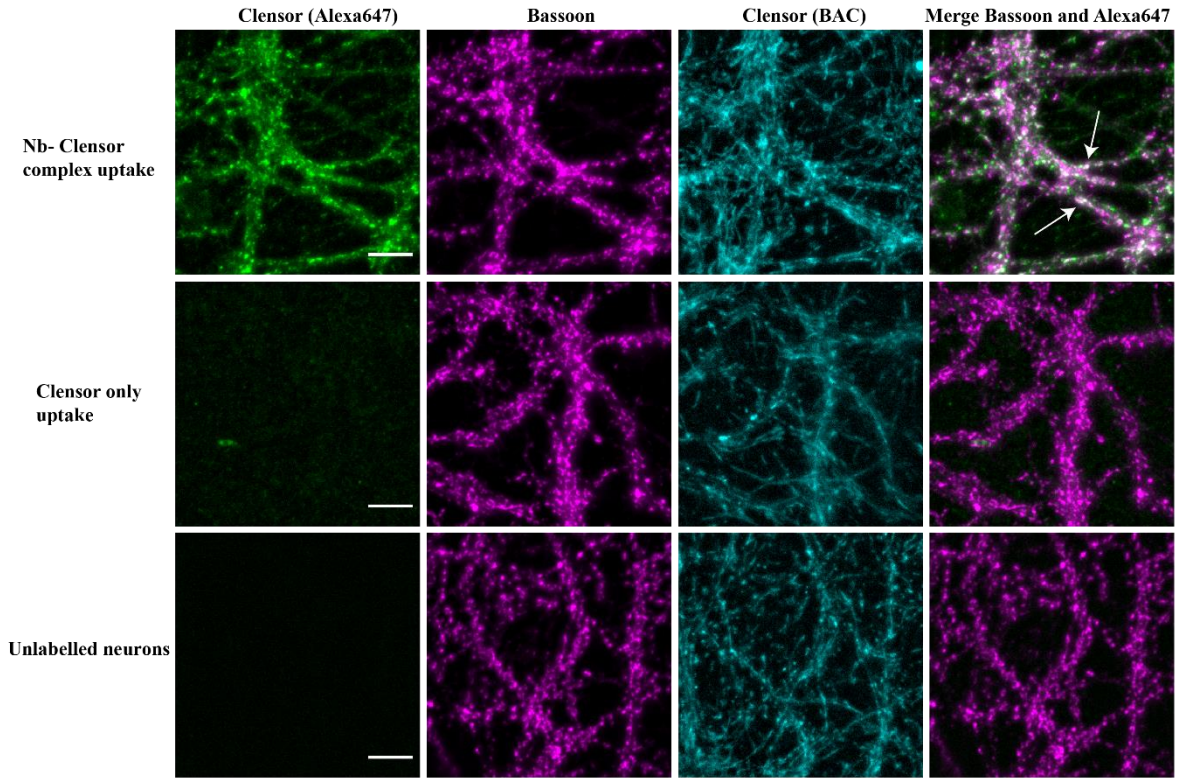

Figure 3. 28 Nb-Halo-Clensor targetings are specific for presynapse.

15 μM Nb-Halo-Clensor complex and Clensor alone without the Nb was taken up in cultured neurons by spontaneous labeling. Post labeling, neurons were fixed in 4 % PFA+4 % Sucrose and immunostained for presynaptic marker Bassoon (Magenta). Alexa647 (in green) and BAC (in cyan) fluorophores from Clensor were imaged. White boutons in the 'Merge' image are co-positive for Alexa647 and Bassoon. Image intensity has been scaled at the same brightness settings in individual color channels so that they are comparable. Scale Bar: 10 μM.

Furthermore, neurons labeled with Nb-Clensor complex were immunostained for SV markers VGAT, Synaptophysin 1, and VGLUT (Figure 3.29). Many boutons labeled with Clensor (Alexa647 channel) are positive for SV markers. A line plot of VGAT colocalized boutons shows a high degree of colocalization (Appendix A.6). This conclusively proves that Clensor is targeted specifically to SVs using the Nb-Halo targeting system. However, the SNR in the BAC channel is quite low and even comparable to the autofluorescence from unlabeled cells. Note that the signal from the BAC channel (in cyan) appears more like a mesh, instead of synaptic punctae. This is perhaps due to the mitochondrial network formation, and the autofluorescence coming from the mitochondria. However, more experiments need to be performed to confirm the source of autofluorescence.

3) Imaging is performed where live neurons are bathed in Tyrode's buffer which has 140 mM Cl^-. During the recycling process, the SVs containing the Clensor molecules have high Cl^- concentration, thus the BAC molecules are already quenched.

To assess the third possibility, we performed the following experiments. (i) Clensor labeled living neurons or neurons briefly fixed with PFA were incubated in an ionophore containing buffer clamped at 0 mM Cl^-

or 162 mM Cl^- for one hour. Note that it was shown in a previous study that mild PFA fixation (2.5 % PFA) for a couple of minutes before treating them with the ionophore cocktail can also be used for measuring the calibration profile to keep the cells intact (Saha, 2015). This is because the state of the neurons treated with ionophore cocktail is already not physiological and is thus comparable with those of mildly fixed ones. Saha et al had also shown that BAC is unaffected by PFA fixation. Images in both Alexa647 (R) and BAC (G) were captured in each buffer condition and a ratio of R/G was compared between the two buffers. We observed no difference in R/G ratios (Figure 3.30). It seems that the signal observed in the BAC channel is indeed merely due to autofluorescence. While there is a ~5.5-fold difference in R/G ratios between 0 mM and 162 mM Cl^-, in vitro, (Figure 3.26) there is barely any difference in cellular imaging. (ii) Living neurons were imaged in 0 mM Chloride containing buffers even though this is extremely harsh for the cells. (iii) Neurons were spontaneously labeled with Nb-Clensor complex in 0 mM Chloride containing buffer instead of their media containing the probe. These experiments were extremely harsh and instantly resulted in cell death.

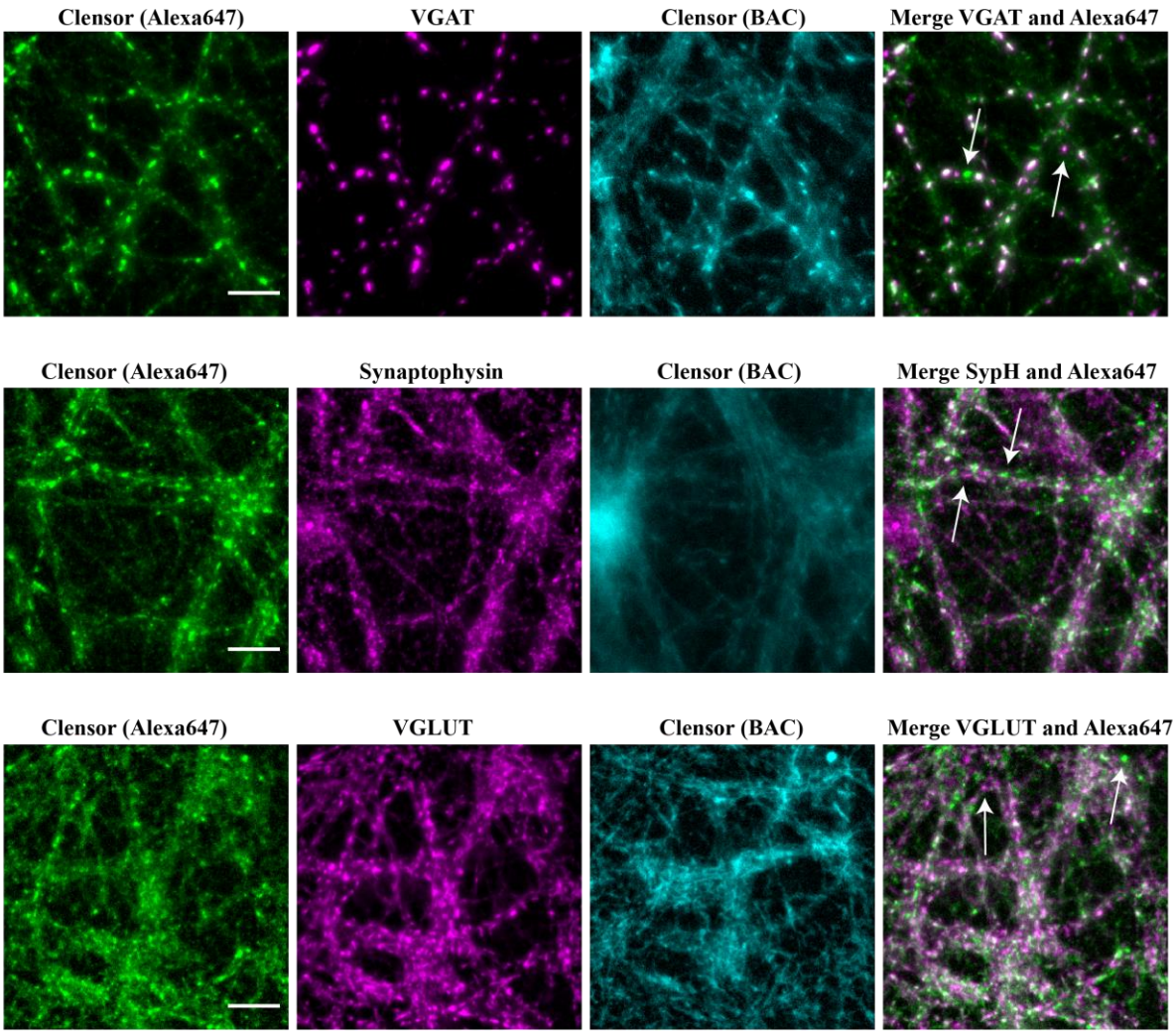

Figure 3. 29 Co-labeling of Nb-Halo-Clensor positive boutons with presynaptic and SV markers.

Neurons were labeled with Nb-Halo-Clensor complex and then immunostained with presynaptic markers-VGAT, Synaptophysin, and VGLUT (in magenta). The white spots in the merged image represent the boutons that are co-positive for Clensor (Alexa647) and presynaptic marker. The white arrow indicates spots that do not colocalize. This shows that the images are spectrally well separated and there is no bleed-through of the signal through the channels. Scale Bar:10 μM.

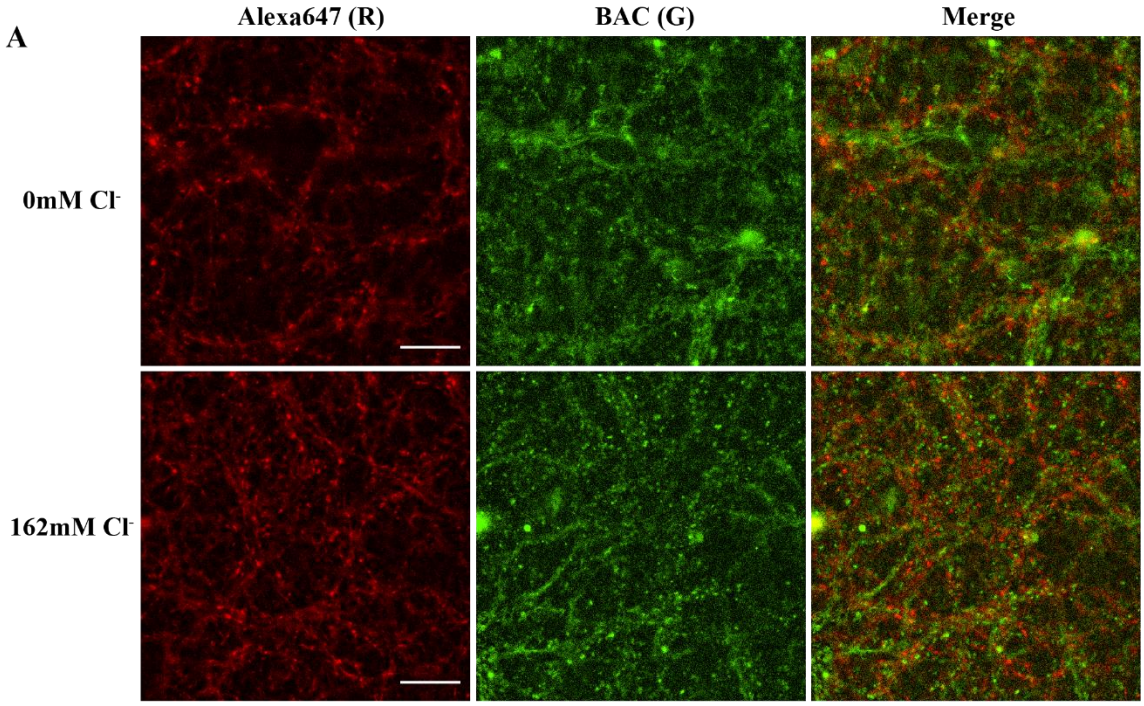

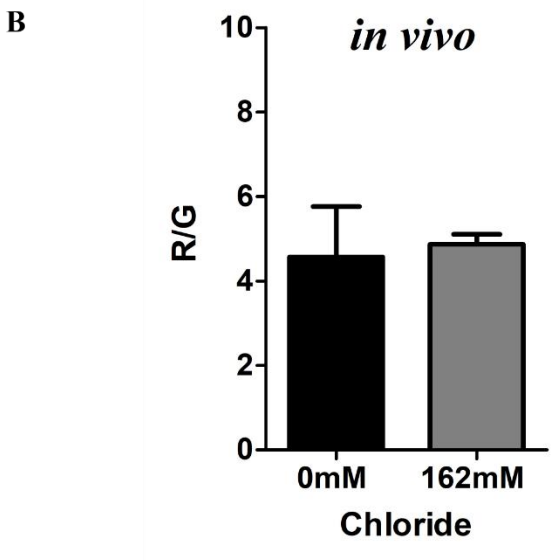

Figure 3. 30 Cl^- sensitivity of Nb-Halo-Clensor in neurons.

Neurons were labeled with Nb-Clensor complex by spontaneous labeling. Cells were then mildly fixed with 2.5 % PFA for a couple of minutes and bathed in ionophore containing buffers clamped at 0 mM or 162 mM Chloride for 1 hour at 25°C. A) Representative images of Clensor; Alexa647 (red) and BAC (green) in 0 mM or 162 mM Chloride.

(B) Quantification of A over at least 3 individual cells across 3 coverslips. Images were subjected to bouton analysis (Methods). Scale Bar: 20 μM.

4) Clensor did get correctly targeted but the Clensor molecules were not enough per vesicle to give a substantial amount of signal.

Clensor is targeted using the Nb against Syt 1 protein. The copy number of Syt1 in an SV is ~15 (Takamori et al., 2006) Considering that the length of the Clensor molecule is ~12 nm in length while the SV is about 40-50nm in diameter, we calculated if 15 molecules of Clensor can indeed fit in a vesicle. Given that a DNA double helix is ~2.37nm wide, and assuming that Clensor is a rod-like cylindrical molecule ~12 nm in length, the volume of Clensor is ~ 52.9 X 10^{-27} m^3. Assuming an SV is 40 nm in diameter, the volume of an SV is ~ 33.49 X 10^{-24} m^3 (or 33.49 zeptoliters; $1m^3$ = 1000L). If Clensor was to fit in the SV perfectly, without any steric constraint, assuming that the SV lumen is empty, then ~633 molecules of Clensor can fit. Thus, theoretically, 15 Clensor molecules can fit easily in an SV. However, the fact that we did not see any fluorescence indicated we required a different strategy. Thus, instead of using the entire Clensor construct, we labeled BAC directly to the Halo ligand and used the Nb-Halo targeting system to target the BAC fluorophore, directly to the vesicle. This may lead to a greater number of fluorophores as the steric hindrance from Clensor (if any) might have reduced. However, as Alexa647 would not be there, internal normalization is not possible. Additionally, as BAC is quenched by increasing [Cl^-], it is harder to perform intensity-based imaging and corresponding correction for photobleaching. Fluorescence Lifetime Imaging (FLIM) has recently gained momentum as it is independent of the number of fluorophores and is not affected by bleaching. Thus, there is no need for an internal normalizing control such as Alexa647, if one is measuring the lifetime of the fluorophore (next section).

3.8.2 Cl^- sensitive fluorophore BAC and Fluorescence Lifetime Imaging (FLIM)

3.8.2.1 Binding of Halo-BAC with the Nb Halo fusion protein and its characterization

BAC fluorophore (Generon, Slough, UK) was conjugated with the Halo ligand (Chemical Facility, MPI) (Figure 3.31A). Since BAC is a symmetrical molecule with two carboxyl groups (Figure 3.31A), its ligation with Halo ligand yielded two products: Mono-Halo BAC (having one Halo ligand) and Di-Halo-BAC (having two Halo ligands). We then investigated the binding of both the products with the Nb on a native PAGE. Each di-Halo BAC molecule was bound with two molecules of Nb and thus ended up dimerizing the Nb (Appendix A.7). To avoid any artifacts due to Nb dimer, we went ahead with the Mono-Halo-BAC (referred to as Halo BAC from here on) construct.

Halo BAC was incubated with the Halo-Nb in a 1:1 ratio at RT to form a complex. The complex formation was confirmed by running it on a Native gel. The fluorescence signal corresponding to the Nb Halo protein confirmed that Halo-BAC successfully binds with the Halo-Nb protein (Figure 3.31C).

To compare the Cl^- sensitivity of Halo BAC and Nb-Halo BAC complex, its emission spectra were measured in 0 mM and 162 mM Cl^- containing buffers. The spectral shape between the ligand alone and its complex with the Nb remained the same (Figure 3.31D). Note that the emission spectra of Halo BAC are slightly lower than the emission spectra of the Nb-Halo-BAC complex at 0 mM Cl^- (top curves in Figure 3.31D). This is perhaps due to pipetting error, as the raw fluorescence counts have been plotted. The addition of 162 mM Cl^- decreases the fluorescence in both the ligand and the complex by approximately 8 folds (Figure 3.31E).

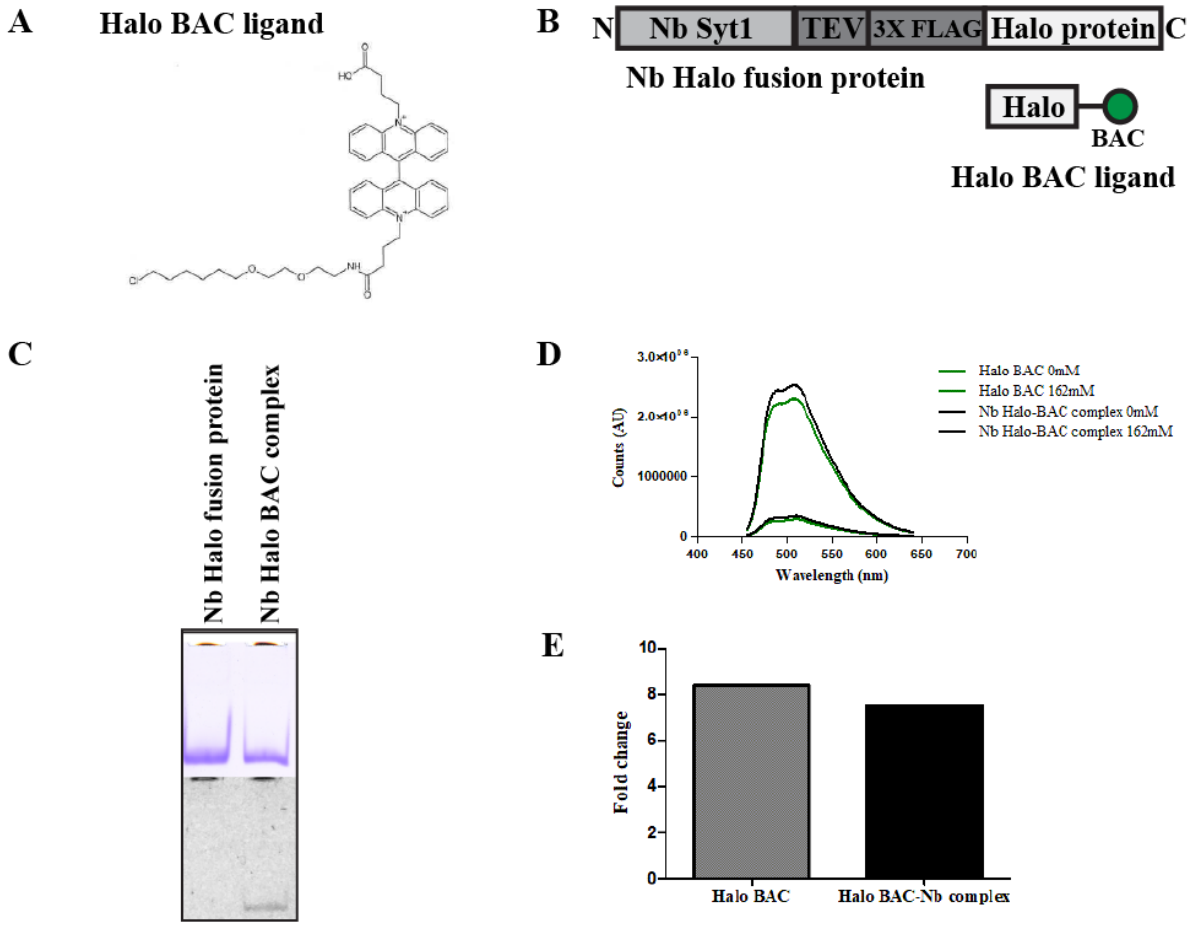

Figure 3. 31 Binding of Nb Halo with Halo-BAC ligand and its spectral characteristics.

A) BAC fluorophore was ligated with the HaloTag ligand to generate Halo-BAC. (B) Scheme of Nb Halo fusion protein binding with Halo-BAC (green ball) ligand. (C) 5 µM Nb Halo and its complex with Halo BAC ligand were run on a 10 % polyacrylamide native gel. The gel was first scanned in the Alexa488 channel of the fluorescence gel reader (bottom panel) followed by Coomassie staining to reveal the unbound Nb (top panel). (D) The emission spectra of Halo BAC ligand (green) and Nb-Halo BAC complex (black) at 0 mM and 162 mM Cl^-. (E) Quantification of D. Comparison of fold change in Cl^- sensitivity of Halo BAC and Nb-Halo Complex.

After the initial characterization using fluorometry, we measured the fluorescence lifetime changes of Halo-BAC with increasing [Cl-]. The lifetime of Halo-BAC changes quite dramatically from 5.2 ns to 0.7 ns when Cl^- was increased from 0 mM to 162 mM (Figure 3.32). The inverse of a lifetime was plotted against the Cl^- concentrations and the values were normalized to 0 mM Cl^-. The relationship between the normalized R/G ratio and the Cl^- concentration had an intercept at 1. It was then fitted with a linear regression model to estimate the slope which corresponds to a Stern Volmer constant of 37.99 ± 0.8164 M^{-1}. Halo-BAC lifetimes were also measured at different pH clamped buffers. As expected, lifetimes do not change and BAC is confirmed to be pH insensitive (Appendix A.8). These results are taken together imply that the properties of BAC are perfectly intact even when it is bound with the Nb and that BAC is highly sensitive to Cl^- while being pH insensitive.

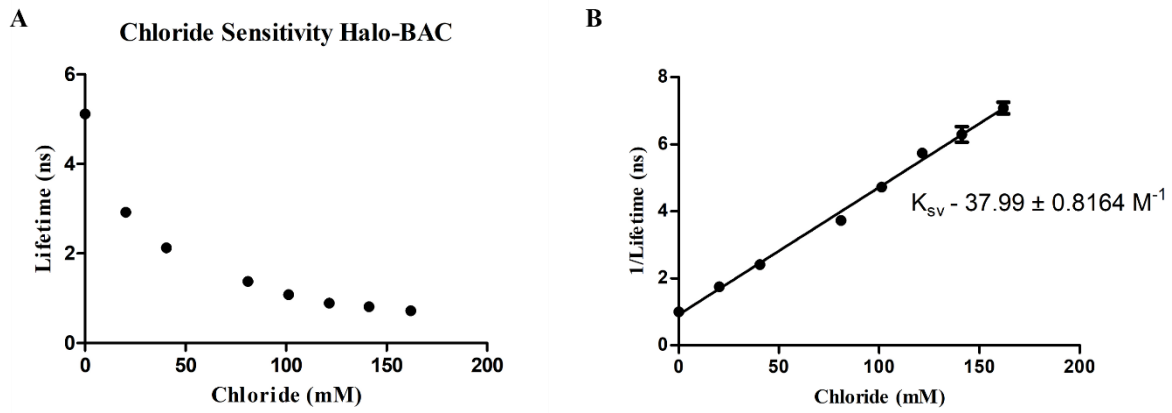

Figure 3. 32 Fluorescence Lifetime of Halo-BAC with increasing Cl^- concentration.

The Halo-BAC probe was diluted with buffers clamped at specific Cl^- concentration at a final concentration of 2 nM and imaged in 8 well dishes containing a glass bottom (Ibidi). The lifetime of each sample was measured and fit to a monoexponential decay function. (A) The plot of average lifetimes of Halo-BAC at different Cl^- concentrations. (B) The inverse of values from A was plotted against Cl^- concentration and fit with a linear regression model to estimate the slope (K_{sv}). Imaging was done on a Leica SP8 microscope.

3.8.2.2 Uptake of Halo-Clensor complex in neurons

Halo BAC was targeted to the SVs using the Nb-Halo system of targeting probes. Images were captured in the Nikon Ti2E epifluorescence microscope as well as on the Leica SP8 FLIM setup. Unfortunately, like the Clensor targeting experiments, BAC still did not give a measurable SNR (Figure 3.33A). The signal is comparable to the signal in unlabeled cells and perhaps is due to the autofluorescence. Note that the morphology looks slightly different in labeled and unlabeled neurons. In the unlabeled neurons, the structures look more elongated; however, this is only an artifact or rather the specific part of the cell (example mitochondria) under observation. When seen in many images, both the dotty and elongated structures are present in both labeled and unlabeled cells. The same problem that BAC's fluorescence is comparable to autofluorescence happened again. Thus, we next attempted to record the emission spectra

of autofluorescence and compared them with that of BAC-PNA to see a possible window where imaging can be performed without interference from autofluorescence. Emission spectra were recorded by selecting the ROI at neurites and cell bodies. The spectra quite overlapped between the neurites, cell body, and BAC-PNA (Figure 3.33B), thus it is difficult to separate them, to obtain the true signal from the BAC channel.

We also recorded the lifetime of autofluorescence from neurites, cell bodies and compared it with the BAC-PNA lifetime. The average lifetime of BAC-PNA was 3.22 ns while that of neurite was 2.8 ns (Figure 3.33C). The autofluorescence lifetime is quite hard to separate from the true signal as 2.8 ns lie in the chloride calibration in Figure 3.32A, especially because the autofluorescence lifetime lies in the linear range of Cl^- sensitivity. Thus, these results taken together prove that BAC cannot be used for measuring Cl^- in SVs.

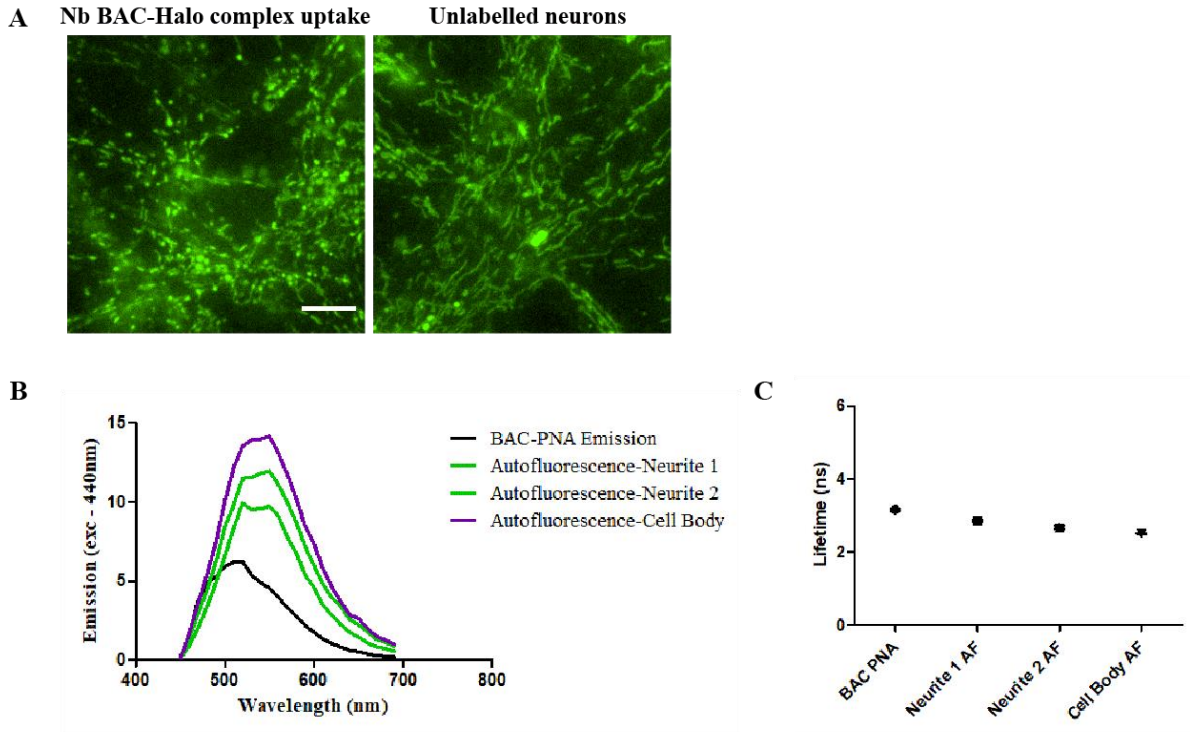

Figure 3. 33 Uptake of Nb-Halo-BAC complex and characteristics of autofluorescence.

(A) Neurons were bathed in their media containing 5 μM Nb-Halo-BAC complex for 10 minutes at 37°C in the incubator spontaneous labeling of the probe. Images were captured in a Nikon Ti2E microscope. Scale bar:10 μm. (B) Autofluorescence spectra were recorded from neurites and cell bodies in unlabeled neurons. As a comparison with BAC fluorophore, the spectra were recorded for BAC-PNA alone. (C) Lifetimes of samples in B. The spectra and lifetimes were recorded at Leica SP8 microscope by exciting the sample with 440 nm laser (PicoQuant).

4 Discussion

In this project, we have devised a new method to target fluorescent probes into synaptic vesicles (SVs) using nanobodies (Nbs) directed against the luminal domain of Syt1, which is a major intrinsic SV protein. We observe that the fluorescent signal from the Nb uptake in cultured hippocampal neurons colocalizes with other SV proteins, such as Synapsin 1/2, Synaptophysin 1, and Bassoon. This shows that the Nb specifically targets SVs. The Nb probe can be customized to flexibly detect various ionic species present in SVs, such as H^+ and Cl^-. By probing the ion dynamics inside the SV, this method can lead to a better understanding of SV filling with neurotransmitters. In the section below, I discuss the advantages of this method over other existing approaches, the main findings, and important considerations required for measuring pH and Cl^- in SVs.

4.1 Targeting of ion sensors to SVs

We have presented here a fast and flexible method to target small molecule sensors into SVs using an Nb-based probe, in which a fluorescent sensor for a specific ionic species is covalently fused with the Nb via a HaloTag protein linker. As the fluorescent signal comes from exogenously applied probes, the method is free from overexpression artifacts that may occur. Additionally, the probe design allows to effectively remove non-specific fluorescence emanating from the surface pool of probes that are not internalized during endocytosis and stranded on the PM using TEV protease. This helps in enhancing the specificity and signal-to-noise of the fluorescence signal. Thus, the above probe offers a modular system whereby any existing or newly developed sensor can be easily attached to the Nb, which acts as a ferry to target the sensor to the SV lumen.

It can be argued that instead of having a Halo protein tag attached to the Nb, alternatively, the Nb can be directly labeled with the required fluorophore (like a labeled Ab). However, this has several problems: (i) As the Ab is labeled all over, it is impossible to get rid of the PM pool using TEV protease. Additionally, the Ab can also get labeled at the site where it binds to its epitope which might affect its ability to recognize its epitope (ii) Each time the Nb will have to be labeled separately with a required fluorophore, which is time-consuming. Instead, the Halo ligand conjugated fluorophores are easy to produce (some are commercially available, Promega) and simply require one step of mixing with the Nb-Halo protein in a 1:1

molar ratio. In most cases, the unbound dye is not an issue. For example, when neurons were incubated with only the ligand (Halo TMR) without the Nb, we did not observe any puncta-like pattern (Figure 3.18C, Page 66). In other cases, the unbound dye can be separated using size exclusion chromatography. (iii) Most Ab labeling procedures involve binding of the amino group (on the protein) with succinimidyl ester form of the fluorophore. This method is highly imprecise and it is often hard to calculate the number of fluorophores conjugated with the protein. This point is particularly relevant for performing quantitative studies. (iv) Many fluorophores lose their function or sensitivity when they are bound directly with the protein. For example, BAC loses its Cl^- sensitivity when bound with a protein (Prakash et al., 2016). Change of probe functionality can also happen with binding to the Halo ligand, but the chances are low as the Halo ligand has been shown to conjugate with a variety of fluorophores (Promega website).

4.2 Resting pH of the vesicle

The resting pH of SVs has been estimated in many studies previously. In cultured hippocampal neurons, a pH_{sv} of 5.67 ± 0.71 was determined using pHlourin (Miesenböck et al., 1998) and a pH_{sv} of 5.80 ± 0.04 in Glutamatergic and a much higher pH of 6.55 ± 0.03 in GABAergic vesicles using mOrange 2 (Egashira et al., 2016). In isolated SVs containing pHlourin, a pH_{sv} of 6.4 -7.0 was obtained in Glutamatergic and 6.6-7.2 in GABAergic vesicles (Farsi et al., 2016). This discrepancy could arise because of a potential difference in ionic content of isolated SVs and SVs present in living neurons.

The currently available pH sensors have a low sensitivity in the late acidic phase of the vesicle life cycle. pHlourin has a pKa of 7.1 and thus lacks sensitivity below pH 6. In comparison, mOrange 2 exhibited a pKa of 6.5 and thus, it could only measure pH as low as 5.5 (Egashira et al., 2015). Additionally, these sensors are dark or weakly fluorescent in the acidic range. The pH of the SV may be much lower than 5.6 and the established tools until now are unable to measure it. Additionally, a FRET-based pH-sensitive protein called Cerulean was fused with Synaptobrevin II to report a pHsv of 5.5- 5.7 in cultured hippocampal neurons (Ph.D. thesis, Ralf Felix Beinlich, Munich, Germany, 2018 (Beinlich, 2018)). Cerulean has many advantages: 1) Its pKa is 5.3. 2) FLIM measurements were performed using this sensor, so the absolute pH values reported were independent of factors such as the number of fluorophores and photobleaching. However, Cerulean had some pitfalls: 1) It had overexpression artifacts, up to 30% of the sensor accumulated at the plasma membrane. 2) It was difficult to remove the PM fraction of Cerulean even with a TEV protease (due to unknown reasons). Furthermore, they measured a pHsv of 4.5 in the beginning which further increased to a pH of 5.7. While the method offers many advantages, it is complicated, and so far, cannot be used to study GABAergic pH_{sv} as the sensor was preferentially expressed in Glutamatergic vesicles.

We tried two pH-sensitive fluorophores: pHrodo (Miksa et al., 2009) (Figure A.9), and AcidiFluor Orange (AF, GC3011; Goryo Kayaku, Sapporo, Japan). An *in vitro* and *in vivo* pH calibration curve was plotted to

obtain the dynamic range of the probe. Previously, pHrodo was conjugated with lipid and yielded a pKa of 5.6 (Kemmer et al., 2015), however, when it was labeled with Ab or Halo ligand, was shown to exhibit a modified pKa of 7.04 (Figure A.9). This did not fit with our pKa requirement in the range between 5.2 and 5.7. The change in sensor characteristics (pKa) was perhaps caused by an associated Ab or Halo ligand. In contrast, AF exhibited a pKa of 5.5 and was brighter at a lower pH, which is ideal to measure the late phase of SV acidification. Using AF, the pHsv was measured to be 5.21 ± 0.027 in Glutamatergic and 5.11 ± 0.007 in GABAergic boutons. To our knowledge, this is the first time that such a low pH is obtained separately for Glutamatergic and GABAergic SVs. This means that the ΔpH (difference between cytoplasmic and vesicular pH) is 2.3 which is considerably higher than the earlier reported value of 1.8. The actual resting pH of an SV could be even lower (<5.1) than our measured values, which needs further future investigations. Nevertheless, the comparable pH for GABAergic and Glutamatergic vesicles requires explanation considering that a differential pH was observed earlier in this study using Nb-pHlourin and Nb-mOrange2 probes (Figure 3.12, Page 58) and studies elsewhere (Egashira et al., 2015; Farsi et al., 2016; Miesenböck et al., 1998). Complementary studies using another variation of the sensor, such as VGAT luminal antibody tagged with AF, are needed to confirm this observation.

Additionally, mass spectrometry did not reveal much difference in the SV proteome between Glutamate and GABA SVs (Gronborg et al., 2010). Thus, the molecular composition of Glutamatergic and GABAergic is possibly comparable, except for the respective transporter. Therefore, any difference in their resting ionic state can be explained partly by the difference in the transporter's coupling with specific ions. However, with advanced single vesicle imaging methodologies (Upmanyu et al., 2021) and the discovery of new vesicular proteins by improvements in mass spectrometry (Taoufiq et al., 2020). Glutamatergic and GABAergic SVs might be more different than what we had anticipated. Thus, a separate pH calibration profile for Glutamatergic and GABAergic vesicle populations are required to systematically compare the pHsv of the two populations in future experiments.

4.3 Targeting of Cl^- sensor into the SV and estimation of luminal Cl^- concentration

Clensor is a DNA origami-based quantitative Cl^- a sensor that contains a Cl^- sensitive fluorophore BAC and a Cl^- insensitive fluorophore Alexa647 for normalization (Prakash et al., 2016a; Saha, 2015). The Halo Clensor was bound with the Nb and was successfully targeted to SVs (Figure 3.28). Additionally, Nb binding did not change the functionality of Clensor. We measured a 5.5-fold change in the Nb-Clensor complex when measured from 0 mM to 162 mM Cl^-. This system of targeting DNA origami-based ratiometric sensors can be used for other fluorophores such as pH-sensitive fluorophores where intensity-based imaging might be a problem and thus requires an internal normalizing control. Speculatively, the fact that Clensor could be targeted to SVs using the spontaneous uptake also supports the model of full vesicle

fusion with the PM compared to the 'Kiss and run' model of fusion, as it is hard to imagine the uptake of bulky molecules like Clensor through a narrow pore (Rizzoli and Jahn, 2007).

In this study, we have measured the lifetime of BAC-Halo with an increasing Cl^- concentration. Nb binding did not change the functionality of BAC directly. We measured an 8-fold change in the Nb-BAC complex when measured from 0 mM to 162 mM Cl^-. Additionally, in the dynamic quenching process, both the fluorescence intensity and the lifetime of the fluorophore decrease (Geddes, 2001). This can be illustrated by the following equation which is an extension from equations 8 and 9, mentioned in the introduction.

$$\frac{I_0}{I} = \frac{\tau_0}{\tau} = 1 + k_q \tau_0 [Q] = 1 + K_{SV}[Q] \quad (12)$$

Thus, our data show that both the fluorescence intensity and the lifetime of BAC decrease with the presence of Cl^- ions (Figure 3.24 and Figure 3.32). This is not the case in static quenching as the uncomplexed fluorophore still has the same lifetime, thus there is no change in the lifetime readout and $\tau_0/\tau = 1$ (Geddes, 2001). This concludes that BAC indeed works by dynamic quenching in our experiments.

The average fluorescence lifetime of BAC-PNA and Clensor was reported to be 7.35 and 7.40 ns respectively in 10 mM phosphate buffer, pH7.2 (Prakash et al., 2016a). We measured an average lifetime of BAC-Halo to be 5.2 ns in 1X Cl (-) buffer (120 mM KNO_3, 20 mM $NaNO_3$, 1 mM Ca $(NO_3)_2$, 1 mM Mg $(NO_3)_2$, 20 mM HEPES, pH 7.4). Reported K_{sv} of Clensor was 58.6 ± 0.3 M^{-1} while we measured a Ksv of 27.45 ± 2.65 M^{-1} in Halo-Clensor and 37.99 ± 0.8164 M^{-1} in Halo-BAC ligand. This is not surprising, as FLIM is highly sensitive and both small chemical modifications and buffer composition can alter the reported lifetimes. Our lifetime measurements are reliable as we used a standard fluorophore, Oregon Green 488, to calibrate the microscope each time before the measurement.

However, this system ultimately could not be used to estimate the luminal $[Cl^-]$, neither through intensity-based imaging of Clensor nor through lifetime measurements in BAC-Halo. This is because there was barely any measurable signal from the BAC channel. Previously, it was also reported that the structure of BAC can change with OH- or negatively charged ions in the cytoplasm (Biwersi et al., 1994). This does not justify the lack of fluorescence as two studies are reporting the Cl^- concentration in lysosomes, and they were able to visualize individual lysosomes (Chakraborty et al., 2017; Osei-Owusu et al., 2021). In the following sections, we discuss possible reasons that hinder our system and prevent the measurement of Cl using BAC.

4.3.1 There are not enough BAC fluorophores to give a measurable signal

It has been estimated that the number of SVs in the presynaptic terminal of cultured hippocampal neurons is approximately 200 (Schikorski and Stevens, 1997). However, it is possible that in our experiments we label only the readily releasable pool containing ~5-20 vesicles (Schikorski and Stevens, 2001). Now, while that may be enough to get a measurable signal from Alexa 647 (molar extinction coefficient, E = 270,000 $cm^{-1}M^{-1}$, retrieved from Invitrogen.com), the signal was not strong enough from BAC, likely due to its low quantum yield (of BAC, E = 7500 $cm^{-1}M^{-1}$ (Biwersi et al., 1994)). In contrast, Saha et al were able to visualize

BAC in lysosomes. The diameter of lysosomes is ~10 times bigger than an SV resulting in a 1000-fold increase in the volume. Considering the low quantum yield of BAC, it is likely that we could not obtain enough labeled SVs. Future experiments using a high-intensity stimulation-based uptake can help in labeling the entire SV pool in the neuron as performed previously in a study (Hua et al., 2010).

4.3.2 Autofluorescence spectrum overlap with the BAC spectrum.

Autofluorescence is the basal level of fluorescence that is unspecific to any antigen-antibody interaction and predominantly occurs near the ultraviolet light spectrum (Dolman and MacLeod, 1981). Doman and McLeod also describe the following properties of autofluorescence. It can come from proteins, from organelles like mitochondria and lysosomes, and from a lipid-containing pigment called Lipofuscin that accumulates in the cytoplasm of the cells during aging (Dolman and MacLeod, 1981). With the increasing age of cells, lipofuscin increases and becomes darker in color. Lipofuscin mostly accumulates in the postmitotic cells like nerve cells and myocardium it was first observed in human nerve cells. Brain lipofuscin mainly contains polymeric lipids and phospholipids, along with amino acids bound to lipids or included in proteins. It was suggested that lipofuscin is the product of polymerization of unsaturated fatty acids and intracellular peroxidation

Autofluorescence can mask the expression of lowly expressed targets or dim dyes if they overlap in their spectra. This is perhaps what happened with our experiments. The autofluorescence spectra from neurites fully overlap with the BAC-PNA spectrum. Additionally, the average fluorescence lifetime of BAC-PNA (with 20 mM Chloride) measured was 3.1 ns, which is comparable to that of the autofluorescence from neurites measured as 2.8 ns.

Autofluorescence may explain the discrepancy between our study and previous studies of Clensor in lysosomes (Saha, 2015). Neurons may be more autofluorescent than other cell types including Drosophila hemocytes (used in the previous studies). Neurons form massive networks and are used after 14 DIV when the synapses have fully matured. Thus, it is possible that in addition to a low number of fluorophores in synaptic boutons, autofluorescence in our system is higher and does not allow us to visualize BAC. Perhaps, the development of more Cl^- sensitive fluorophores in the spectra with longer wavelengths will be beneficial to perform Cl^- measurements in SVs.

4.4 Limitations

1. **NbSyt1 cannot recognize its epitope in PFA fixed neurons -** The epitope sequence that the Nb recognizes: KQKFMNELHKIPLPP, contains many Proline and Lysine residues which inhibits the crosslinking using aldehyde fixation like PFA. Thus, the Nb is incapable of recognizing the epitope after fixation and can only work in the live-cell application. This is in contrast with the Ab against Syt1 lumen (604.2) which can very well detect the epitope even after fixation.

2. **The Nbs bind well with the Syt1 epitope in Rat and Mouse neurons but don't identify the human Syt1 epitope.** The epitope that the Nb binds in Mouse/Rat is KQKFMNELHKIPLPP, which is the 43-57th amino acid from the N terminal in a 57 amino acid luminal part of Syt1. This sequence differs by 3 amino acids in human Syt1 epitope KEKFMNELHKIPLP (which lacks the last Proline). Unfortunately, the Nb does not bind with the human epitope in our experiments. We had differentiated human-induced pluripotent stem cells (hiPSCs) to neurons and tested the Nb. While the differentiation protocol worked quite well, the Nb did not recognize the human epitope (Refer to Margarita Chudenkova, Lab Rotation Report).
3. **Photostability of fluorescent dyes-** In this study, we have used AcidiFluor Orange for resting pH detection. While this works, it was also clear that AcidiFluor Orange is prone to photobleaching. It was much better than previously reported CypHer dye (Hua et al., 2011), but it was still prone to bleaching. For this reason, we used low exposure times to capture the images in different pH clamped buffers for the resting pH estimation, which compromised the signal-to-noise ratio and was problematic for image processing. In the end, we need to bear in mind that no system is perfect to match all the needs in a biological system as every system comes with advantages and disadvantages depending upon the context.

4.5 Conclusions and perspectives

The process of neurotransmitter filling and storage inside an SV is the least studied process but as crucial as the fusion of SV with the PM or binding of neurotransmitters with the postsynaptic receptors for neurotransmission. We know that the neurotransmitter transporters directly and allosterically interact with the ions like Cl^- and H^+ to transport, concentrate and store neurotransmitters into the lumen of an SV. Thus, it is extremely valuable to resolve the ionic content of an SV using fluorescent probes that can be particularly targeted inside its lumen. In this study, we have used the Nb-Halo probe to target pH and Cl^- sensors into SVs. We can use this system to target any other ion sensor to the vesicle, which will allow mapping the SV ionic composition to understand the ion dynamics during SV recycling. Additionally, we have generated a pipeline to perform FLIM measurements. This will enable us to estimate absolute ion concentrations using changes in the fluorescence lifetime of the ion-sensitive fluorophore. A combination of targeting novel fluorescent sensors and quantitatively mapping the ionic composition of an SV will certainly lead to a clearer understanding of the dependence of neurotransmitter transporters on changing ionic fluxes. In this project, we have used an Nb against the SV protein Syt1. Complementary studies with luminal Abs or Nbs against VGLUT or VGAT directly will help to confirm the findings in this study. Recently six mice monoclonal Abs against different parts of VGLUTs have been reported (Eriksen et al., 2021). Five of the Abs bind against the luminal domain of VGLUT thus, they can be labeled with the AF pH probe to visualize the Glutamatergic boutons specifically. Due to the lack of VGLUT specific inhibitors, precise inactivation of the transporter has not been possible in the past. But now, one of the

new VGLUT Abs against the luminal domain can be used to inhibit the Cl^- conductance in VGLUT. Therefore, it can aid us to study the change in resting ion concentration when VGLUT's activity is impaired, and thus help us address the role of pH and Cl^- behind the mechanistic functioning of VGLUT. Additionally, Nbs against the cytoplasmic domain of VGLUT can be used to inhibit its function, although its mechanism of inhibition is unknown (Schenck et al., 2017). Thus, with the continued development of exciting new ion-sensitive fluorescent probes, antibodies, and nanobodies, there are possibilities of multiplexing measurements. This will help us to model the loading and storage of SVs with neurotransmitters and arrive at a comprehensive and quantitative ionic map of the SV.

Appendix

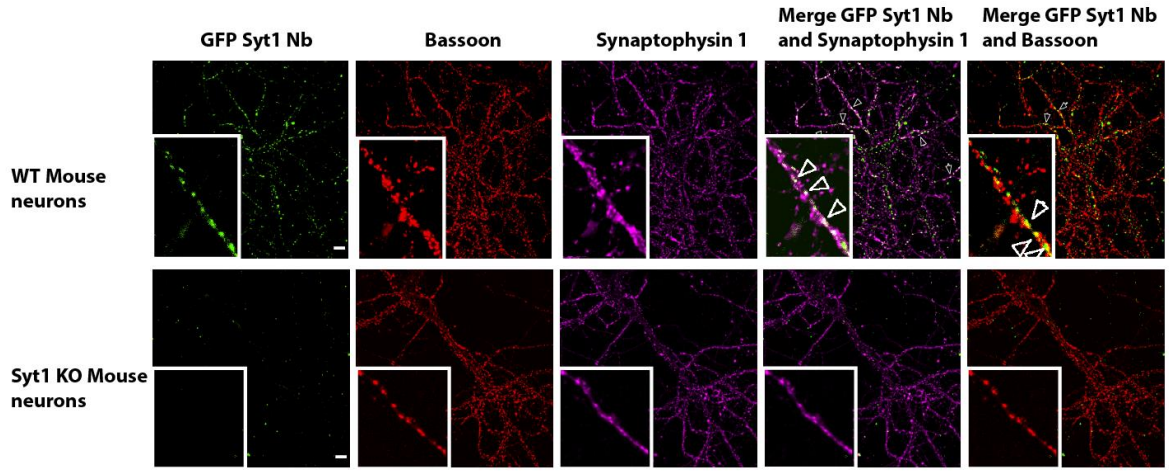

Figure A. 1 Immunostaining of Nb-Syt1 -GFP labeled neurons with Ab against presynaptic marker Bassoon and SV marker Synaptophysin 1.

Living WT and Syt1 KO neurons (DIV 13-18) were labeled with Nb fused with GFP (1:200, in green). Neurons were fixed and immunostained with a presynaptic marker Bassoon (in red) and an SV marker (Synaptophysin 1). Colocalized spots in white in the merged image show the spots that are labeled with the Nb and are positive for Synaptophysin 1. The yellow colocalized spots in the second merge image show the spots that were labeled with Nb are positive for Bassoon. Specific labeling of WT neurons shows that the Nb is specific to the Syt1 protein. Scale bar:10 μm.

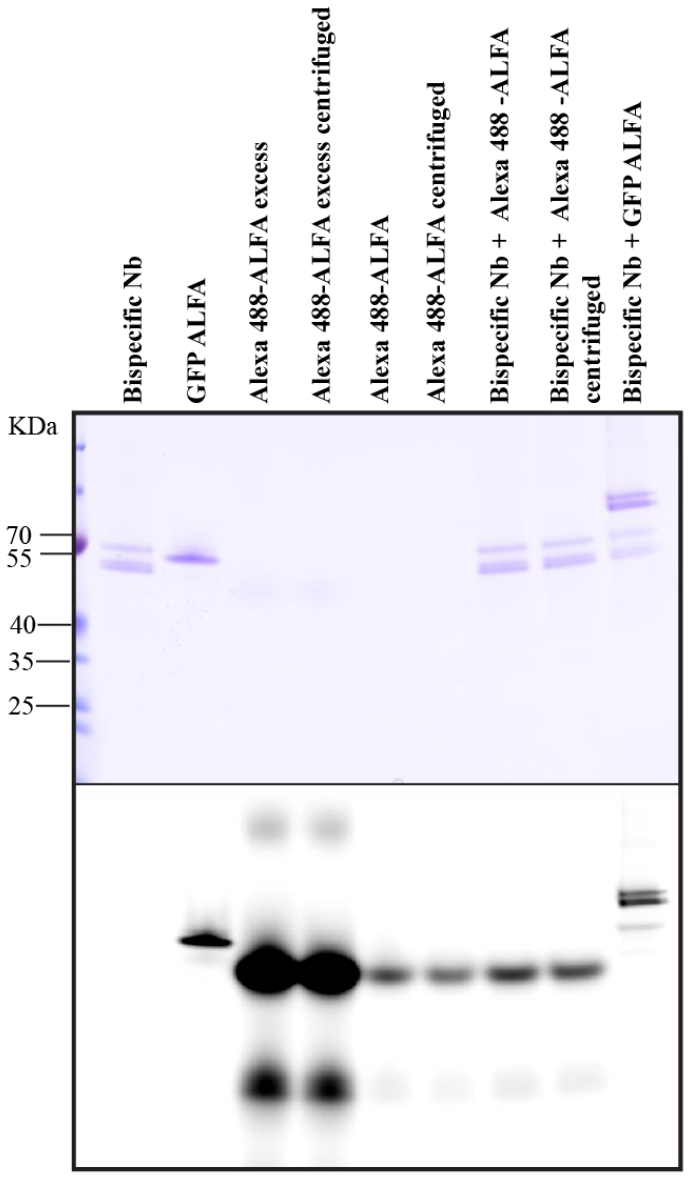

Figure A. 2 Precipitation of ALFA tag labeled with Alexa488.

Bispecific Nb was mixed with GFP ALFA and ALFA-Alexa488 in a 1:1 ratio at RT for 15minutes. While the complex formation between bispecific Nb (Lane 1) and GFP ALFA (Lane 2) works (Lane 9), the bulky dark band between lanes 3-8 represents the precipitate that Alexa488-ALFA forms by itself, even without the Nb (Lanes 3-6). High-speed centrifugation (13K g) did not help to cleave off the precipitate that was unavailable to bind with the bispecific Nb. The gel was scanned in the GFP channel in the fluorescence scanner (bottom panel) followed by Coomassie staining to visualize the unbound/non-fluorescent protein (top panel).

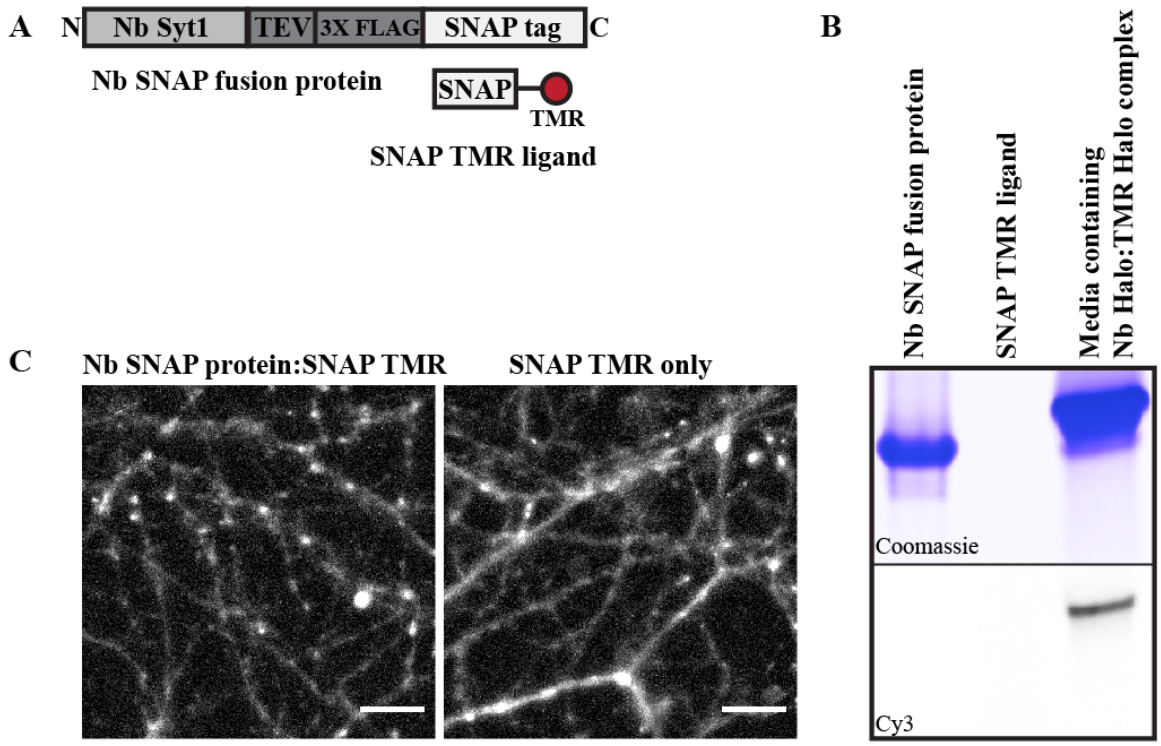

Figure A. 3 Binding of Nb-SNAP fusion protein with SNAP ligand labeled with Tetramethyl Rhodamine (TMR) and its targeting to synapses.

(A) Scheme showing the Nb SNAP protein tag fusion construct and it's binding with the SNAP ligand labeled with TMR fluorophore (red ball). (B) Nb SNAP fusion protein and SNAP ligand were mixed in a 1:1 ratio at RT for 15 minutes and run on 10 % Native gel to confirm its binding. The gel was scanned at the Cy3 channel in the fluorescence gel reader to visualize TMR signal and stained with Coomassie to visualize the non-fluorescent proteins. SNAP-TMR ligand is too small to be retained in the gel. (C) Uptake of the complex in cultured neurons, but the SNR is lower than the Halo-Nb targeting. SNAP TMR ligand only uptake was used as a negative control, however, unlike Halo ligand, it showed a substantial signal. Images were taken on a Nikon Ti2E Epifluorescence microscope. Scale Bar:10 μm.

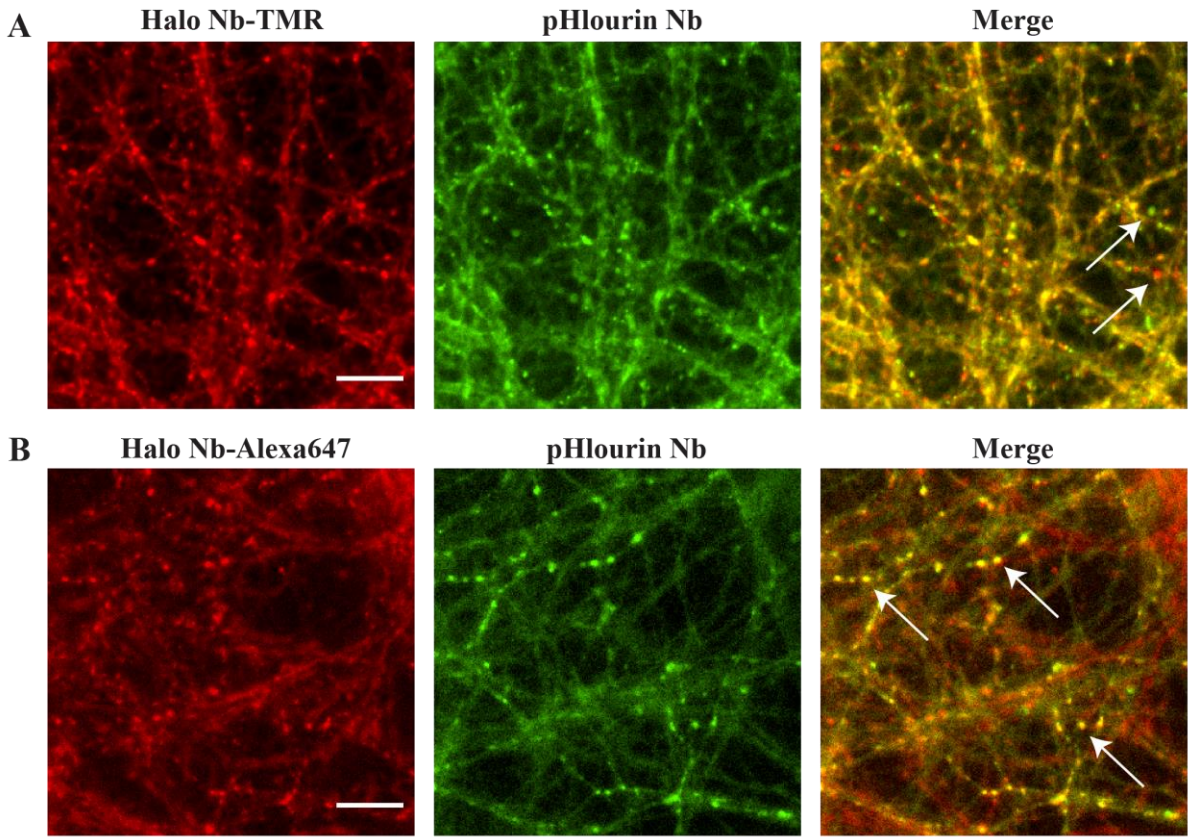

Figure A. 4 Co-uptake of Nb pHlourin and Nb-Halo-TMR/Alexa 647 complex

Cultured neurons (13-18DIV) were spontaneously labeled with 5 μM pHlourin Nb (in green) and 5 μM of Halo-Nb-TMR (A) /Alexa647 (B) complex (in red) simultaneously to confirm the specificity of pHlourin Nb. Many synaptic boutons colocalized with each other. In (A) the yellow spots show a high degree of colocalization. The arrows indicate red and green spots that do not colocalize with each other showing that the two channels of imaging are spectrally well separated. In (B) the arrows indicate the yellow spots that do colocalize with each other. Scale bars: 10 μM. Note that imaging was performed after fixing and mounting the neurons, hence the images are taken at pH7.4, thereby revealing the pHlourin labeled pool as bright punctae.

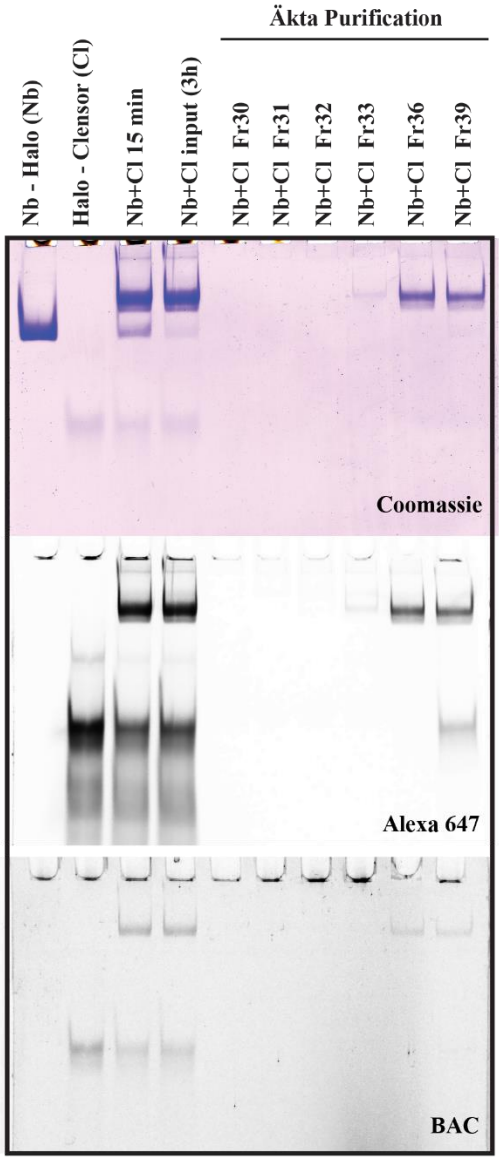

Figure A. 5 Size exclusion chromatography of Nb-Halo – Clensor complex.

10 μM of Nb-Halo and Clensor-Halo were mixed in a 1:1 molar ratio for 15 minutes at RT to form the Nb-Clensor-Halo complex. The complex was kept at RT for 3 hours and subjected to size exclusion chromatography (AKTA, Superdex 200) to separate the complex from Nb and Clensor alone. The fractions collected from AKTA were run on a 10 % Native polyacrylamide gel to visualize the separated bands. The gel was first scanned in Alexa647 and BAC channels followed by Coomassie staining to visualize the non-fluorescent protein bands. Note that Fraction (Fr) 36 is the purest and was used for uptake experiments in cultured neurons. This experiment was performed by Margarita Chudenkova.

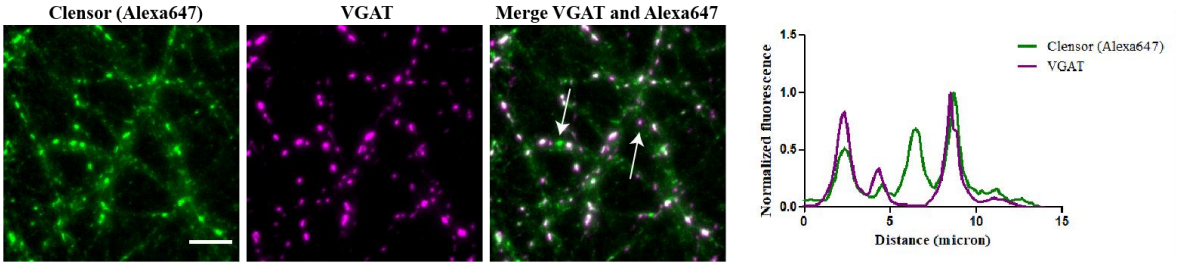

Figure A. 6 Nb-Halo-Clensor targeting is specific for GABA SV.

15 μM Nb-Clensor complex was taken up in cultured neurons by spontaneous labeling. Post labeling, neurons were fixed in 4 % PFA+4 % Sucrose and immunostained for presynaptic marker VGAT (Magenta). Alexa647 from Clensor were imaged (Green). White boutons in the 'Merge' image are co-positive for Alexa647 and VGAT. The line plot on the right shows that there are boutons that fully overlap in the two channels, while there are some that don't fully overlap (middle green peak) Scale Bar: 10 μM.

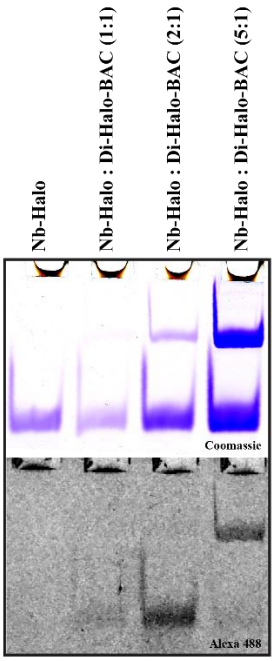

Figure A. 7 Formation of Nb-Halo and Di-Halo-BAC complex leads to dimerization of the Nb.

5 μM Nb Halo and its complex with Di-Halo BAC ligand were run on a 10 % polyacrylamide native gel. The gel was first scanned in the Alexa488 channel of the fluorescence gel reader followed by Coomassie staining to reveal the unbound Nb. The amount of Di-Halo BAC was titrated against the Nb-Halo to reveal the Nb dimerization behavior better. The experiment was performed by Margarita Chudenkova.

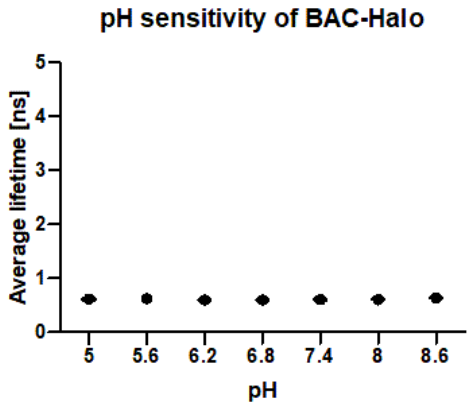

Figure A. 8 pH sensitivity of Halo-BAC using FLIM

Halo-BAC probe was diluted in buffers clamped at specific pH to a final concentration of 2 nM and imaged in 8 well-glass-bottomed Ibidi dishes. The lifetime of each sample was measured and fit to a monoexponential decay function. Imaging was done on a Leica SP8 microscope. Note that the lifetime is as low as 0.6 ns, as all the pH clamped buffers contained a high concentration of sodium chloride. However, the graph shows that the lifetime of BAC does not change with pH, making it a pH-insensitive nanodevice.

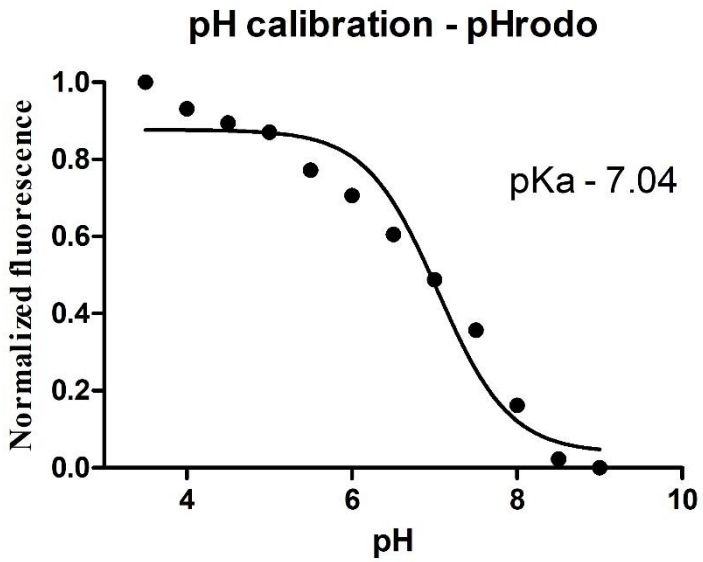

Figure A. 9 *in vivo* pH calibration of Nb-Halo pHrodo

Neurons labeled with Nb-Halo pHrodo complex were treated with ionophore-containing buffers clamped at a specific pH. Images from at least three cells were captured at each pH condition at the Nikon Ti2E microscope. Fluorescence change as a function of pH was plotted. The black solid line is a fit to the Boltzmann equation on Graph Pad Prism yielding a pKa of 7.04.

5 Bibliography

Abcam (1998). Immunocytochemistry and immunofluorescence protocol. Abcam 1–6.

Abcam (2010). Immunoprecipitation Protocol. EBiosciences 1–4.

Accardi, A., and Miller, C. (2004). Secondary active transport mediated by a prokaryotic homologue of ClC Cl- channels. Nature *427*, 803–807.

Ahnert-Hilger, G., Höltje, M., Pahner, I., Winter, S., and Brunk, I. (2003). Regulation of vesicular neurotransmitter transporters. Rev. Physiol. Biochem. Pharmacol. *150*, 140–160.

Alabi, A.A., and Tsien, R.W. (2013). Perspectives on Kiss-and-Run: Role in Exocytosis, Endocytosis, and Neurotransmission. Annu. Rev. Physiol. *75*, 393–422.

Arosio, D., Ricci, F., Marchetti, L., Gualdani, R., Albertazzi, L., and Beltram, F. (2010). Simultaneous intracellular chloride and pH measurements using a GFP-based sensor. Nat. Methods *7*, 516.

Atluri, P.P., and Ryan, T.A. (2006). The kinetics of synaptic vesicle reacidification at hippocampal nerve terminals. J. Neurosci. *26*, 2313–2320.

Azevedo, F.A.C., Carvalho, L.R.B., Grinberg, L.T., Farfel, J.M., Ferretti, R.E.L., Leite, R.E.P., Filho, W.J., Lent, R., and Herculano-Houzel, S. (2009). Equal numbers of neuronal and nonneuronal cells make the human brain an isometrically scaled-up primate brain. J. Comp. Neurol. *513*, 532–541.

Bal, W., Kurowska, E., and Maret, W. (2012). The Final Frontier of pH and the Undiscovered Country Beyond. PLoS One *7*, 7–10.

Balaji, J., and Ryan, T.A. (2007). Single-vesicle imaging reveals that synaptic vesicle exocytosis and endocytosis are coupled by a single stochastic mode. Proc. Natl. Acad. Sci. U. S. A. *104*, 20576–20581.

BCA Protein Assay (2020). BCA Protein Assay Kit 23225. 0–3.

Beinlich, M.R.F. (2018). Mechanisms Underlying Biphasic Synaptic Vesicle Acidification in Glutamatergic Synapses. Mech. Underlying Biphasic Synaptic Vesicle Acidif. Glutamatergic Synapses *Dissertati*, Heinrich-Heine Universität Düsseldorf.

Bellocchio, E.E., Reimer, R.J., Jr, R.T.F., and Edwards, R.H. (2000). Uptake of Glutamate into Synaptic Vesicles by an Inorganic Phosphate Transporter. *289*, 957–961.

Ben-Ari, Y., Khalilov, I., Kahle, K.T., and Cherubini, E. (2012). The GABA excitatory/inhibitory shift in brain maturation and neurological disorders. Neuroscientist *18*, 467–486.

Bennett, M.V.., and Zukin, R.S. (2004). Electrical Coupling and Neuronal Synchronization in the

Mammalian Brain. Neuron *41*, 495–511.

Bertani, G. (1951). Studies on lysogenesis. I. The mode of phage liberation by lysogenic Escherichia coli. J. Bacteriol. *62*, 293–300.

Bianchini, L., and Pousségur, J. (1994). Molecular structure and regulation of vertebrate Na+/H+ exchangers. J. Exp. Biol. *196*, 337–345.

Biwersi, J., and Verkman, A.S. (1991). Cell-Permeable Fluorescent Indicator for Cytosolic Chloride. Biochemistry *30*, 7879–7883.

Biwersi, J., Tulk, B., and Verkman, A.S. (1994). Long wavelength Cl sensitive Fluorescent indicators. 139–143.

Blakely, R.D., and Edwards, R.H. (2012). Vesicular and Plasma Membrane Transporters for Neurotransmitters. Cold Spring Harb. Perspect. Biol. *4*, a005595–a005595.

Bloom, F.E., Ueda, T., Battenberg, E., and Greengard, P. (1979). Immunocytochemical localization, in synapses, of protein I, an endogenous substrate for protein kinases in mammalian brain. Proc. Natl. Acad. Sci. *76*, 5982–5986.

Bloom, O., Evergren, E., Tomilin, N., Kjaerulff, O., Löw, P., Brodin, L., Pieribone, V.A., Greengard, P., and Shupliakov, O. (2003). Colocalization of synapsin and actin during synaptic vesicle recycling. J. Cell Biol. *161*, 737–747.

Burger, P.M., Mehl, E., Cameron, P.L., Maycox, P.R., Baumert, M., Lottspeich, F., De Camilli, P., and Jahn, R. (1989). Synaptic vesicles immunoisolated from rat cerebral cortex contain high levels of glutamate. Neuron *3*, 715–720.

Burger, P.M., Hell, J., Mehl, E., Krasel, C., Lottspeich, F., and Jahn, R. (1991). GABA and glycine in synaptic vesicles: storage and transport characteristics. Neuron *7*, 287–293.

Burkhardt, P., Hattendorf, D.A., Weis, W.I., and Fasshauer, D. (2008). Munc18a controls SNARE assembly through its interaction with the syntaxin N-peptide. EMBO J. *27*, 923–933.

De Camilli, P., Harris, S.M., Huttner, W.B., and Greengard, P. (1983). Synapsin I (Protein I), a nerve terminal-specific phosphoprotein. II. Its specific association with synaptic vesicles demonstrated by immunocytochemistry in agarose-embedded synaptosomes. J. Cell Biol. *96*, 1355–1373.

Del Castillo, J., and Katz, B. (1954). Action, and spontaneous release, of acetylcholine at an inexcitable nerve-muscle junction. J. Physiol. *126*, 27P.

Ceccarelli, B., and Hurlbut, W.P. (1980). Vesicle hypothesis of the release of quanta of acetylcholine. Physiol. Rev. *60*, 396–441.

Cesca, F., Baldelli, P., Valtorta, F., and Benfenati, F. (2010). The synapsins: Key actors of synapse function and plasticity. Prog. Neurobiol. *91*, 313–348.

Chakraborty, K., Leung, K.H., and Krishnan, Y. (2017). High lumenal chloride in the lysosome is critical for lysosome function. Elife *6*, 1–21.

Chang, R., Eriksen, J., and Edwards, R.H. (2018). The dual role of chloride in synaptic vesicle glutamate transport. Elife *7*, 1–16.

Chapman, E.R. (2008). How Does Synaptotagmin Trigger Neurotransmitter Release? Annu. Rev. Biochem. *77*, 615–641.

Chapman, E.R., and Jahn, R. (1994). Calcium-dependent interaction of the cytoplasmic region of synaptotagmin with membranes. Autonomous function of a single C2-homologous domain. J. Biol. Chem. *269*, 5735–5741.

Chatterjee, D., Chakraborty, M., Leit, M., Neff, L., Jamsa-Kellokumpu, S., Fuchs, R., Bartkiewicz, M., Hernando, N., and Baron, R. (1992). The osteoclast proton pump differs in its pharmacology and catalytic subunits from other vacuolar H(+)-ATPases. J. Exp. Biol. *172*, 193–204.

Clayton, E.L., Evans, G.J.O., and Cousin, M.A. (2007). Activity-dependent control of bulk endocytosis by protein dephosphorylation in central nerve terminals. J. Physiol. *585*, 687–691.

Cousin, M.A., and Robinson, P.J. (2001). The dephosphins: dephosphorylation by calcineurin triggers synaptic vesicle endocytosis. Trends Neurosci. *24*, 659–665.

Denker, A., Krohnert, K., Buckers, J., Neher, E., and Rizzoli, S.O. (2011). The reserve pool of synaptic vesicles acts as a buffer for proteins involved in synaptic vesicle recycling. Proc. Natl. Acad. Sci. *108*, 17183–17188.

Djamgoz, M.B.A., and Laming, P.J. (1987). Micro-electrode measurements and functional aspects of chloride activity in cyprinid fish retina: Extracellular activity and intracellular activities of L- and C-type horizontal cells. Vision Res. *27*, 1481–1489.

Dolman, C.L., and MacLeod, P.M. (1981). Lipofuscin and its Relation to Aging. In Advances in Cellular Neurobiology, (ACADEMIC PRESS, INC.), pp. 205–247.

Doyon, N., Vinay, L., Prescott, S.A., and De Koninck, Y. (2016). Chloride Regulation: A Dynamic Equilibrium Crucial for Synaptic Inhibition. Neuron *89*, 1157–1172.

Van Dyke, R.W., and Belcher, J.D. (1994). Acidification of three types of liver endocytic vesicles: Similarities and differences. Am. J. Physiol. - Cell Physiol. *266*.

Edwards, R.H. (2007). The Neurotransmitter Cycle and Quantal Size. Neuron *55*, 835–858.

Egashira, Y., Takase, M., and Takamori, S. (2015). Monitoring of Vacuolar-Type H+ ATPase-Mediated Proton Influx into Synaptic Vesicles. J. Neurosci. *35*, 3701–3710.

Egashira, Y., Takase, M., Watanabe, S., Ishida, J., Fukamizu, A., Kaneko, R., Yanagawa, Y., and Takamori, S. (2016). Unique pH dynamics in GABAergic synaptic vesicles illuminates the mechanism and kinetics of GABA loading. Proc. Natl. Acad. Sci. U. S. A. *113*, 10702–10707.

Egholm, M., Buchardt, O., Christensen, L., Behrens, C., Freier, S.M., Driver, D.A., Berg, R.H., Kim, S.K., Norden, B., and Nielsen, P.E. (1993). PNA hybridizes to complementary oligonucleotides obeying the Watson–Crick hydrogen-bonding rules. Nature *365*, 566–568.

Eiden, L.E., Schäfer, M.K.H., Weihe, E., and Schütz, B. (2004). The vesicular amine transporter family (SLC18): Amine/proton antiporters required for vesicular accumulation and regulated exocytotic secretion of monoamines and acetylcholine. Pflugers Arch. Eur. J. Physiol. *447*, 636–640.

Erickson, J.D., Schafer, M.K., Bonner, T.I., Eiden, L.E., and Weihe, E. (1996). Distinct pharmacological properties and distribution in neurons and endocrine cells of two isoforms of the human vesicular monoamine transporter. Proc. Natl. Acad. Sci. *93*, 5166–5171.

Eriksen, J., Chang, R., McGregor, M., Silm, K., Suzuki, T., and Edwards, R.H. (2016). Protons Regulate Vesicular Glutamate Transporters through an Allosteric Mechanism. Neuron *90*, 768–780.

Eriksen, J., Li, F., Stroud, R.M., and Edwards, R.H. (2021). Allosteric Inhibition of a Vesicular Glutamate Transporter by an Isoform-Specific Antibody. Biochemistry *60*, 2463–2470.

Evans, G.J.O., and Cousin, M.A. (2007). Activity-Dependent Control of Slow Synaptic Vesicle Endocytosis by Cyclin-Dependent Kinase 5. J. Neurosci. *27*, 401–411.

Farinas, J., and Verkman, A.S. (1999). Receptor-mediated targeting of fluorescent probes in living cells. J. Biol. Chem. *274*, 7603–7606.

Farsi, Z., Preobraschenski, J., Van Den Bogaart, G., Riedel, D., Jahn, R., and Woehler, A. (2016). Single-Vesicle imaging reveals different transport mechanisms between glutamatergic and GABAergic vesicles. Science (80-.). *351*, 981–984.

Farsi, Z., Jahn, R., and Woehler, A. (2017). Proton electrochemical gradient: Driving and regulating neurotransmitter uptake. BioEssays *39*, 1–9.

Fesce, R., Grohovaz, F., Valtorta, F., and Meldolesi, J. (1994). Neurotransmitter release: fusion or 'kiss-and-run'? Trends Cell Biol. *4*, 1–4.

Fievet, P. (2015). Donnan Potential. In Encyclopedia of Membranes, (Berlin, Heidelberg: Springer Berlin Heidelberg), pp. 1–3.

Fletcher, T.L., Cameron, P., De Camilli, P., and Banker, G. (1991). The distribution of synapsin I and

synaptophysin in hippocampal neurons developing in culture. J. Neurosci. *11*, 1617–1626.

Fornasiero, E.F., and Opazo, F. (2015). Super-resolution imaging for cell biologists. BioEssays *37*, 436–451.

Frankær, C.G., Rosenberg, M., Santella, M., Hussain, K.J., Laursen, B.W., and Sørensen, T.J. (2019). Tuning the p K a of a pH Responsive Fluorophore and the Consequences for Calibration of Optical Sensors Based on a Single Fluorophore but Multiple Receptors. ACS Sensors *4*, 764–773.

Futai, M., Oka, T., Sun-Wada, G.H., Moriyama, Y., Kanazawa, H., and Wada, Y. (2000). Luminal acidification of diverse organelles by V-ATPase in animal cells. J. Exp. Biol. *203*, 107–116.

Gaffield, M.A., Tabares, L., and Betz, W.J. (2009). Preferred Sites of Exocytosis and Endocytosis Colocalize during High- But Not Lower-Frequency Stimulation in Mouse Motor Nerve Terminals. J. Neurosci. *29*, 15308–15316.

Gandhi, S.P., and Stevens, C.F. (2003). Three modes of synaptic vesicular recycling revealed by single-vesicle imaging. Nature *423*, 607–613.

Gasnier, B. (2004). The SLC32 transporter, a key protein for the synaptic release of inhibitory amino acids. Pflugers Arch. Eur. J. Physiol. Arch. Eur. J. Physiol. Arch. Eur. J. Physiol. *447*, 756–759.

Geddes, C.D. (2001). Optical halide sensing using fluorescence quenching: theory, simulations and applications - a review. Meas. Sci. Technol. *12*, R53–R88.

Goh, G.Y., Huang, H., Ullman, J., Borre, L., Hnasko, T.S., Trussell, L.O., and Edwards, R.H. (2011). Presynaptic regulation of quantal size: K+/H+ exchange stimulates vesicular glutamate transport. Nat. Neurosci. *14*, 1285–1292.

Götzke, H., Kilisch, M., Martínez-Carranza, M., Sograte-Idrissi, S., Rajavel, A., Schlichthaerle, T., Engels, N., Jungmann, R., Stenmark, P., Opazo, F., et al. (2019). The ALFA-tag is a highly versatile tool for nanobody-based bioscience applications. Nat. Commun. *10*, 1–12.

Grabe, M., and Oster, G. (2001). Regulation of organelle acidity. J. Gen. Physiol. *117*, 329–343.

Granseth, B., and Lagnado, L. (2008). The role of endocytosis in regulating the strength of hippocampal synapses. J. Physiol. *586*, 5969–5982.

Grimley, J.S., Li, L., Wang, W., Wen, L., Beese, L.S., Hellinga, H.W., and Augustine, G.J. (2013). Visualization of synaptic inhibition with an optogenetic sensor developed by cell-free protein engineering automation. J. Neurosci. *33*, 16297–16309.

Grimm, J.B., Gruber, T.D., Ortiz, G., Brown, T.A., and Lavis, L.D. (2016). Virginia Orange: A Versatile, Red-Shifted Fluorescein Scaffold for Single- And Dual-Input Fluorogenic Probes. Bioconjug. Chem. *27*, 474–480.

Gronborg, M., Pavlos, N.J., Brunk, I., Chua, J.J.E., Munster-Wandowski, A., Riedel, D., Ahnert-Hilger, G., Urlaub, H., and Jahn, R. (2010). Quantitative Comparison of Glutamatergic and GABAergic Synaptic Vesicles Unveils Selectivity for Few Proteins Including MAL2, a Novel Synaptic Vesicle Protein. J. Neurosci. *30*, 2–12.

Hallermann, S., Fejtova, A., Schmidt, H., Weyhersmüller, A., Silver, R.A., Gundelfinger, E.D., and Eilers, J. (2010). Bassoon Speeds Vesicle Reloading at a Central Excitatory Synapse. Neuron *68*, 710–723.

Hamer-Casterman, Atarchouch, T, C., Muyldermans, S., Robinson, G., Hamers, C., Bajyana, E., Bendahman, N., and Hamilton, R. (1993). Naturally occurring antibodies devoid of light chains. Nature *363*, 446–448.

Harris, R.A., and Allan, A.M. (1985). Functional coupling of γ-aminobutyric acid receptors to chloride channels in brain membranes. Science (80-.). *228*, 1108–1110.

Hartinger, J., and Jahn, R. (1993). An anion binding site that regulates the glutamate transporter of synaptic vesicles. J. Biol. Chem. *268*, 23122–23127.

Haucke, V., Neher, E., and Sigrist, S.J. (2011). Protein scaffolds in the coupling of synaptic exocytosis and endocytosis. Nat. Rev. Neurosci. *12*, 127–138.

Hell, J.W., Edelmann, L., Hartinger, J., and Jahn, R. (1991). Functional Reconstitution of the γ-Aminobutyric Acid Transporter from Synaptic Vesicles Using Artificial Ion Gradients. Biochemistry *30*, 11795–11800.

Heuser, J.E., and Reese, T.S. (1973). Evidence for recycling of synaptic vesicle membrane during transmitter release at the frog neuromuscular junction. J. Cell Biol. *57*, 315–344.

Heuser, J.E., and Reese, T.S. (1981). Structural changes after transmitter release at the frog neuromuscular junction. J. Cell Biol. *88*, 564–580.

Hinshaw, J.E., and Schmid, S.L. (1995). Dynamin self-assembles into rings suggesting a mechanism for coated vesicle budding. Nature *374*, 190–192.

Hoopmann, P., Punge, A., Barysch, S. V., Westphal, V., Bückers, J., Opazo, F., Bethani, I., Lauterbach, M.A., Hell, S.W., and Rizzoli, S.O. (2010). Endosomal sorting of readily releasable synaptic vesicles. Proc. Natl. Acad. Sci. U. S. A. *107*, 19055–19060.

Hua, Y., Sinha, R., Martineau, M., Kahms, M., and Klingauf, J. (2010). A common origin of synaptic vesicles undergoing evoked and spontaneous fusion. Nat. Neurosci. *13*, 1451–1453.

Hua, Y., Sinha, R., Thiel, C.S., Schmidt, R., Hüve, J., Martens, H., Hell, S.W., Egner, A., and Klingauf, J. (2011). A readily retrievable pool of synaptic vesicles. Nat. Neurosci. *14*, 833–839.

Huang, H., and Trussell, L.O. (2014). Presynaptic HCN Channels Regulate Vesicular Glutamate

Transport. Neuron *84*, 340–346.

Ishikawa, T., Sahara, Y., and Takahashi, T. (2002). A single packet of transmitter does not saturate postsynaptic glutamate receptors. Neuron *34*, 613–621.

Jahn, R., and Fasshauer, D. (2012). Molecular machines governing exocytosis of synaptic vesicles. Nature *490*, 201–207.

Jayaraman, S., Haggie, P., Wachter, R.M., Remington, S.J., and Verkman, A.S. (2000). Mechanism and cellular applications of a green fluorescent protein-based halide sensor. J. Biol. Chem. *275*, 6047–6050.

Jentsch, T.J., and Pusch, M. (2018). CLC chloride channels and transporters: Structure, function, physiology, and disease. Physiol. Rev. *98*, 1493–1590.

Jentsch, T.J., Neagoe, I., and Scheel, O. (2005). CLC chloride channels and transporters. Curr. Opin. Neurobiol. *15*, 319–325.

Jia, Y., Jucius, T.J., Cook, S.A., and Ackerman, S.L. (2015). Loss of Clcc1 Results in ER Stress, Misfolded Protein Accumulation, and Neurodegeneration. J. Neurosci. *35*, 3001–3009.

Johnson, R.G. (1988). Accumulation of biological amines into chromaffin granules: A model for hormone and neurotransmitter transport. Physiol. Rev. *68*, 232–307.

Johnson, R.G., Carty, S.E., and Scarpa, A. (1981). Proton: Substrate stoichiometries during active transport of biogenic amines in chromaffin ghosts. J. Biol. Chem. *256*, 5773–5780.

Juge, N., Yoshida, Y., Yatsushiro, S., Omote, H., and Moriyama, Y. (2006). Vesicular glutamate transporter contains two independent transport machineries. J. Biol. Chem. *281*, 39499–39506.

Juge, N., Muroyama, A., Hiasa, M., Omote, H., and Moriyama, Y. (2009). Vesicular inhibitory amino acid transporter is a Cl-/ γ-aminobutyrate co-transporter. J. Biol. Chem. *284*, 35073–35078.

Juge, N., Gray, J.A., Omote, H., Miyaji, T., Inoue, T., Hara, C., Uneyama, H., Edwards, R.H., Nicoll, R.A., and Moriyama, Y. (2010). Metabolic Control of Vesicular Glutamate Transport and Release. Neuron *68*, 99–112.

Jung, N., and Haucke, V. (2007). Clathrin-mediated endocytosis at synapses. Traffic *8*, 1129–1136.

Kaneko, H., Putzier, I., Frings, S., Kaupp, U.B., and Gensch, T. (2004). Chloride accumulation in mammalian olfactory sensory neurons. J. Neurosci. *24*, 7931–7938.

Katz, B. (1971). Quantal mechanism of neural transmitter release. Science (80-.). *173*, 123–126.

Kemmer, G.C., Bogh, S.A., Urban, M., Palmgren, M.G., Vosch, T., Schiller, J., and Günther Pomorski, T. (2015). Lipid-conjugated fluorescent pH sensors for monitoring pH changes in reconstituted membrane systems. Analyst *140*, 6313–6320.

Keppler, A., Gendreizig, S., Gronemeyer, T., Pick, H., Vogel, H., and Johnsson, K. (2003). A general method for the covalent labeling of fusion proteins with small molecules in vivo. Nat. Biotechnol. *21*, 86–89.

Kirchhausen, T. (2000). Tomas Kirchhausen. Blood 699–727.

Van der Kloot, W. (1991). The regulation of quantal size. Prog. Neurobiol. *36*, 93–130.

Krapf, R., Berry, C.A., and Verkman, A.S. (1988). Estimation of intracellular chloride activity in isolated perfused rabbit proximal convoluted tubules using a fluorescent indicator. Biophys. J. *53*, 955–962.

Kraszewski, K., Mundigl, O., Daniell, L., Verderio, C., Matteoli, M., and De Camilli, P. (1995). Synaptic vesicle dynamics in living cultured hippocampal neurons visualized with CY3-conjugated antibodies directed against the lumenal domain of synaptotagmin. J. Neurosci. *15*, 4328–4342.

Kuner, T., and Augustine, G.J. (2000). A genetically encoded ratiometric indicator for chloride: Capturing chloride transients in cultured hippocampal neurons. Neuron *27*, 447–459.

Kuromi, H., and Kidokoro, Y. (1998). Two Distinct Pools of Synaptic Vesicles in Single Presynaptic Boutons in a Temperature-Sensitive Drosophila Mutant, shibire. Neuron *20*, 917–925.

Kuromi, H., and Kidokoro, Y. (1999). The Optically Determined Size of Exo/Endo Cycling Vesicle Pool Correlates with the Quantal Content at the Neuromuscular Junction of Drosophila Larvae. J. Neurosci. *19*, 1557–1565.

Kuromi, H., and Kidokoro, Y. (2000). Tetanic Stimulation Recruits Vesicles from Reserve Pool via a cAMP-Mediated Process in Drosophila Synapses. Neuron *27*, 133–143.

Kwon, S.E., and Chapman, E.R. (2011). Synaptophysin Regulates the Kinetics of Synaptic Vesicle Endocytosis in Central Neurons. Neuron *70*, 847–854.

Lakowicz, J.R. (2013). Principles of fluorescence spectroscopy (Springer Science & Business Media).

de Lange, R.P.J., de Roos, A.D.G., and Borst, J.G.G. (2003). Two Modes of Vesicle Recycling in the Rat Calyx of Held. J. Neurosci. *23*, 10164–10173.

Lau, A., and Tymianski, M. (2010). Glutamate receptors, neurotoxicity and neurodegeneration. Pflügers Arch. - Eur. J. Physiol. *460*, 525–542.

Li, F., Eriksen, J., Finer-Moore, J., Chang, R., Nguyen, P., Bowen, A., Myasnikov, A., Yu, Z., Bulkley, D., Cheng, Y., et al. (2020). Ion transport and regulation in a synaptic vesicle glutamate transporter. Science (80-.). *368*, 893–897.

Liu, G. (2003). Presynaptic control of quantal size: Kinetic mechanisms and implications for synaptic transmission and plasticity. Curr. Opin. Neurobiol. *13*, 324–331.

Los, G. V, Encell, L.P., McDougall, M.G., Hartzell, D.D., Karassina, N., Zimprich, C., Wood, M.G., Learish, R., Ohana, R.F., Urh, M., et al. (2008). HaloTag: A Novel Protein Labeling Technology for Cell Imaging and Protein Analysis. ACS Chem. Biol. *3*, 373–382.

Lou, X., Scheuss, V., and Schneggenburger, R. (2005). Allosteric modulation of the presynaptic Ca2+ sensor for vesicle fusion. Nature *435*, 497–501.

Ma, C., Su, L., Seven, A.B., Xu, Y., and Rizo, J. (2013). Reconstitution of the Vital Functions of Munc18 and Munc13 in Neurotransmitter Release. Science (80-.). *339*, 421–425.

Mackenzie, B., Illing, A.C., Morris, M.E.K., Varoqui, H., and Erickson, J.D. (2008). Analysis of a vesicular glutamate transporter (VGLUT2) supports a cell-leakage mode in addition to vesicular packaging. Neurochem. Res. *33*, 238–247.

Markova, O., Mukhtarov, M., Real, E., Jacob, Y., and Bregestovski, P. (2008). Genetically encoded chloride indicator with improved sensitivity. J. Neurosci. Methods *170*, 67–76.

Martens, H., Weston, M.C., Boulland, J.L., Grønborg, M., Grosche, J., Kacza, J., Hoffmann, A., Matteoli, M., Takamori, S., Harkany, T., et al. (2008). Unique luminal localization of VGAT-C terminus allows for selective labeling of active cortical GABAergic synapses. J. Neurosci. *28*, 13125–13131.

Martineau, M., Guzman, R.E., Fahlke, C., and Klingauf, J. (2017). VGLUT1 functions as a glutamate/proton exchanger with chloride channel activity in hippocampal glutamatergic synapses. Nat. Commun. *8*, 2279.

Matteoli, M., and Takei, K. (1992). Exo-endocytotic Recycling of Synaptic Vesicles in Developing Processes of Cultured Hippocampal Neurons. *117*, 849–861.

Matthew, W.D., Tsavaler, L., and Reichardt, L.F. (1981). Identification of a synaptic vesicle-specific membrane protein with a wide distribution in neuronal and neurosecretory tissue. J. Cell Biol. *91*, 257–269.

Maycox, P.R., Deckwerth, T., Hell, J.W., and Jahn, R. (1988). Glutamate uptake by brain synaptic vesicles. Energy dependence of transport and functional reconstitution in proteoliposomes. J. Biol. Chem. *263*, 15423–15428.

Merrifield, C.J., Moss, S.E., Ballestrem, C., Imhof, B.A., Giese, G., Wunderlich, I., and Almers, W. (1999). Endocytic vesicles move at the tips of actin tails in cultured mast cells. Nat. Cell Biol. *1*, 72–74.

Miesenböck, G., De Angelis, D.A., and Rothman, J.E. (1998). Visualizing secretion and synaptic transmission with pH-sensitive green fluorescent proteins. Nature *394*, 192–195.

Miksa, M., Komura, H., Wu, R., Shah, K.G., and Wang, P. (2009). A novel method to determine the engulfment of apoptotic cells by macrophages using pHrodo succinimidyl ester. J. Immunol. Methods

342, 71–77.

Milosavljevic, N., Monet, M., Léna, I., Brau, F., Lacas-Gervais, S., Feliciangeli, S., Counillon, L., and Poët, M. (2014). The Intracellular Na+/H+ Exchanger NHE7 Effects a Na+-Coupled, but Not K+-Coupled Proton-Loading Mechanism in Endocytosis. Cell Rep. *7*, 689–696.

Mindell, J.A. (2012). Lysosomal Acidification Mechanisms. Annu. Rev. Physiol. *74*, 69–86.

Moriyama, Y., and Futai, M. (1990). H+-ATPase, a primary pump for accumulation of neurotransmitters, is a major constituent of brain synaptic vesicles. Biochem. Biophys. Res. Commun. *173*, 443–448.

Murthy, V.N., and Stevens, C.F. (1999). Reversal of synaptic vesicle docking at central synapses. Nat. Neurosci. *2*, 503–507.

Muyldermans, S. (2013). Nanobodies: Natural single-domain antibodies. Annu. Rev. Biochem. *82*, 775–797.

Neild, T.O., and Thomas, R.C. (1974). Intracellular chloride activity and the effects of acetylcholine in snail neurones. J. Physiol. *242*, 453–470.

Novarino, G., Weinert, S., Rickheit, G., and Jentsch, T.J. (2010). Endosomal Chloride-Proton Exchange Rather Than Chloride Conductance Is Crucial for Renal Endocytosis. Science (80-.). *328*, 1398–1401.

Omote, H., Miyaji, T., Juge, N., and Moriyama, Y. (2011). Vesicular Neurotransmitter Transporter: Bioenergetics and Regulation of Glutamate Transport. Biochemistry *50*, 5558–5565.

Opazo, F., Punge, A., B??ckers, J., Hoopmann, P., Kastrup, L., Hell, S.W., and Rizzoli, S.O. (2010). Limited Intermixing of Synaptic Vesicle Components upon Vesicle Recycling. Traffic *11*, 800–812.

Orthaus-Müller, S., Krämer, B., Dowler, R., Devaux, A., Tannert, A., Roehlicke, T., Wahl, M., Rahn, H.-J., and Erdmann, R. (2016). rapidFLIM : The New and Innovative Method for Ultra fast FLIM Imaging. PicoQuant Appl. Note 1–8.

Osei-Owusu, J., Yang, J., Leung, K.H., Ruan, Z., Lü, W., Krishnan, Y., and Qiu, Z. (2021). Proton-activated chloride channel PAC regulates endosomal acidification and transferrin receptor-mediated endocytosis. Cell Rep. *34*.

Ozawa, T., Saito, Y., and Nishiyama, A. (1988). Mechanism of uphill chloride transport of the mouse lacrimal acinar cells: Studies with Cl−-sensitive microelectrode. Pflügers Arch. - Eur. J. Physiol. *412*, 509–515.

Parsons, S.M. (2000). Transport mechanisms in acetylcholine and monoamine storage. FASEB J. *14*, 2423–2434.

Parthier, D., Kuner, T., and Körber, C. (2018). The presynaptic scaffolding protein Piccolo organizes the

readily releasable pool at the calyx of Held. J. Physiol. *596*, 1485–1499.

Pearse, B.M. (1976). Clathrin: a unique protein associated with intracellular transfer of membrane by coated vesicles. Proc. Natl. Acad. Sci. *73*, 1255–1259.

Perin, M.S., Brose, N., Jahn, R., and Sudhof, T.C. (1991). Domain structure of synaptotagmin (p65). J. Biol. Chem. *266*, 623–629.

Ponnalagu, D., Gururaja Rao, S., Farber, J., Xin, W., Hussain, A.T., Shah, K., Tanda, S., Berryman, M., Edwards, J.C., and Singh, H. (2016). Molecular identity of cardiac mitochondrial chloride intracellular channel proteins. Mitochondrion *27*, 6–14.

Prakash, V., Saha, S., Chakraborty, K., and Krishnan, Y. (2016a). Rational design of a quantitative, pH-insensitive, nucleic acid based fluorescent chloride reporter. Chem. Sci. *7*, 1946–1953.

Prakash, V., Saha, S., Chakraborty, K., and Krishnan, Y. (2016b). Rational design of a quantitative, pH-insensitive, nucleic acid based fluorescent chloride reporter. Chem. Sci. *7*, 1946–1953.

Preobraschenski, J., Zander, J., Suzuki, T., Ahnert-hilger, G., and Jahn, R. (2014). Vesicular Glutamate Transporters Use Flexible Anion and Cation Binding Sites for Efficient Accumulation of Neurotransmitter. Neuron *84*, 1287–1301.

Purves, D. (2006). Neuroscience:Third Edition.

Reimer, R.J. (2013). SLC17: A functionally diverse family of organic anion transporters. Mol. Aspects Med. *34*, 350–359.

Reimer, R.J., and Edwards, R.H. (2004). Organic anion transport is the primary function of the SLC17/type I phosphate transporter family. Pflugers Arch. Eur. J. Physiol. Arch. Eur. J. Physiol. *447*, 629–635.

Renger, J.J., Egles, C., and Liu, G. (2001). A Developmental Switch in Neurotransmitter Flux Enhances Synaptic Efficacy by Affecting AMPA Receptor Activation. Neuron *29*, 469–484.

Ries, J., Kaplan, C., Platonova, E., Eghlidi, H., and Ewers, H. (2012). A simple, versatile method for GFP-based super-resolution microscopy via nanobodies. Nat. Methods *9*, 582–584.

Riveros, N., Fiedler, J., Lagos, N., Muñoz, C., and Orrego, F. (1986). Glutamate in rat brain cortex synaptic vesicles: influence of the vesicle isolation procedure. Brain Res. *386*, 405–408.

Rizo, J., and Xu, J. (2015). The Synaptic Vesicle Release Machinery. Annu. Rev. Biophys. *44*, 339–367.

Rizzoli, S.O. (2014). Synaptic vesicle recycling: Steps and principles. EMBO J. *33*, 788–822.

Rizzoli, S.O., and Betz, W.J. (2005). Synaptic vesicle pools. Nat. Rev. Neurosci. *6*, 57–69.

Rizzoli, S.O., and Jahn, R. (2007). Kiss-and-run, collapse and "readily retrievable" vesicles. Traffic *8*, 1137–1144.

Rost, B.R., Schneider, F., Grauel, M.K., Wozny, C., G Bentz, C., Blessing, A., Rosenmund, T., Jentsch, T.J., Schmitz, D., Hegemann, P., et al. (2015). Optogenetic acidification of synaptic vesicles and lysosomes. Nat. Neurosci. *18*, 1845–1852.

Saha, S. (2015). A pH-independent DNA nanodevice for quantifying chloride transport in organelles of living cells. Nat. Nanotechnol. *10*.

Saha, S., Prakash, V., Halder, S., Chakraborty, K., and Krishnan, Y. (2015). A pH-independent DNA nanodevice for quantifying chloride transport in organelles of living cells. Nat. Nanotechnol. *10*, 645–651.

Saheki, Y., and De Camilli, P. (2012). Synaptic vesicle endocytosis. Cold Spring Harb. Perspect. Biol. *4*.

Saint-Criq, V., and Gray, M.A. (2017). Role of CFTR in epithelial physiology. Cell. Mol. Life Sci. *74*, 93–115.

Salem, N., Faúndez, V., Horng, J.-T., and Kelly, R.B. (1998). A v-SNARE participates in synaptic vesicle formation mediated by the AP3 adaptor complex. Nat. Neurosci. *1*, 551–556.

Sätzler, K., Söhl, L.F., Bollmann, J.H., Borst, J.G.G., Frotscher, M., Sakmann, B., and Lübke, J.H.R. (2002). Three-Dimensional Reconstruction of a Calyx of Held and Its Postsynaptic Principal Neuron in the Medial Nucleus of the Trapezoid Body. J. Neurosci. *22*, 10567–10579.

Schäfer, M.K.H., Varoqui, H., Defamie, N., Weihe, E., and Erickson, J.D. (2002). Molecular cloning and functional identification of mouse vesicular glutamate transporter 3 and its expression in subsets of novel excitatory neurons. J. Biol. Chem. *277*, 50734–50748.

Schägger, H. (2006). Tricine–SDS-PAGE. Nat. Protoc. *1*, 16–22.

Schapiro, F.B., and Grinstein, S. (2000). Determinants of the pH of the Golgi complex. J. Biol. Chem. *275*, 21025–21032.

Scheel, O., Zdebik, A.A., Lourdel, S., and Jentsch, T.J. (2005). Voltage-dependent electrogenic chloride/proton exchange by endosomal CLC proteins. Nature *436*, 424–427.

Schenck, S., Wojcik, S.M., Brose, N., and Takamori, S. (2009). A chloride conductance in VGLUT1 underlies maximal glutamate loading into synaptic vesicles. Nat. Neurosci. *12*, 156–162.

Schenck, S., Kunz, L., Sahlender, D., Pardon, E., Geertsma, E.R., Savtchouk, I., Suzuki, T., Neldner, Y., Štefanić, S., Steyaert, J., et al. (2017). Generation and Characterization of Anti-VGLUT Nanobodies Acting as Inhibitors of Transport. Biochemistry *56*, 3962–3971.

Schikorski, T., and Stevens, C.F. (1997). Quantitative Ultrastructural Analysis of Hippocampal. J.

Neurosci. *17*, 5858–5867.

Schikorski, T., and Stevens, C.F. (2001). Morphological correlates of functionally defined synaptic vesicle populations. Nat. Neurosci. *4*, 391–395.

Schwartz, R.D., and Yu, X. (1995). Optical imaging of intracellular chloride in living brain slices. J. Neurosci. Methods *62*, 185–192.

Schwartz, R.D., Jackson, J.A., Weigert, D., Skolnick, P., and Paul, S.M. (1985). Characterization of barbiturate-stimulated chloride efflux from rat brain synaptoneurosomes. J. Neurosci. *5*, 2963–2970.

Sheng, M. (2002). Postsynaptic Signaling and Plasticity Mechanisms. Science (80-.). *298*, 776–780.

Singh, A., Marcoline, F. V., Veshaguri, S., Kao, A.W., Bruchez, M., Mindell, J.A., Stamou, D., and Grabe, M. (2019). Protons in small spaces: Discrete simulations of vesicle acidification. PLoS Comput. Biol. *15*, 1–21.

Smith, A.J., and Lippiat, J.D. (2010). Direct endosomal acidification by the outwardly rectifying CLC-5 Cl − /H + exchanger. J. Physiol. *588*, 2033–2045.

Smith, P.K., Krohn, R.I., Hermanson, G.T., Mallia, A.K., Gartner, F.H., Provenzano, M.D., Fujimoto, E.K., Goeke, N.M., Olson, B.J., and Klenk, D.C. (1985). Measurement of protein using bicinchoninic acid. Anal. Biochem. *150*, 76–85.

Sonawane, N.D., and Verkman, A.S. (2003). Determinants of [Cl ⧖] in recycling and late endosomes and Golgi complex measured using fluorescent ligands. J. Cell Biol. *160*, 1129–1138.

Stobrawa, S.M., Breiderhoff, T., Takamori, S., Engel, D., Schweizer, M., Zdebik, A.A., Bösl, M.R., Ruether, K., Jahn, H., Draguhn, A., et al. (2001). Disruption of ClC-3, a Chloride Channel Expressed on Synaptic Vesicles, Leads to a Loss of the Hippocampus. Neuron *29*, 185–196.

Stokes, G.G. (1869). XI.—On a certain reaction of quinine. J. Chem. Soc. *22*, 174–181.

Südhof, T.C. (2012). The Presynaptic Active Zone. Neuron *75*, 11–25.

Südhof, T.C., and Rizo, J. (2011). Synaptic vesicle exocytosis. Cold Spring Harb. Perspect. Biol. *3*.

Tabares, L., Ruiz, R., Linares-Clemente, P., Gaffield, M.A., Alvarez de Toledo, G., Fernandez-Chacon, R., and Betz, W.J. (2007). Monitoring Synaptic Function at the Neuromuscular Junction of a Mouse Expressing SynaptopHluorin. J. Neurosci. *27*, 5422–5430.

Takamori, S. (2016). Presynaptic Molecular Determinants of Quantal Size. Front. Synaptic Neurosci. *8*, 1–9.

Takamori, S., Holt, M., Stenius, K., Lemke, E.A., Grønborg, M., Riedel, D., Urlaub, H., Schenck, S., Brügger, B., Ringler, P., et al. (2006). Molecular Anatomy of a Trafficking Organelle. Cell *127*, 831–846.

Takei, K., Mundigl, O., Daniell, L., and De Camilli, P. (1996). The synaptic vesicle cycle: a single vesicle budding step involving clathrin and dynamin. J. Cell Biol. *133*, 1237–1250.

Taoufiq, Z., Ninov, M., Villar-Briones, A., Wang, H.-Y., Sasaki, T., Roy, M.C., Beauchain, F., Mori, Y., Yoshida, T., Takamori, S., et al. (2020). Hidden proteome of synaptic vesicles in the mammalian brain. Proc. Natl. Acad. Sci. *117*, 33586–33596.

Teorell, T. (1935). An Attempt to Formulate a Quantitative Theory of Membrane Permeability. Exp. Biol. Med. *33*, 282–285.

Thomas, R.C. (Roger C. (1978). Ion-sensitive intracellular microelectrodes : how to make and use them / R. C. Thomas. (London).

Truckenbrodt, S., Viplav, A., Jähne, S., Vogts, A., Denker, A., Wildhagen, H., Fornasiero, E.F., and Rizzoli, S.O. (2018). Newly produced synaptic vesicle proteins are preferentially used in synaptic transmission. EMBO J. *37*, 1–24.

Upmanyu, N., Jin, J., Ganzella, M., Bösche, L., Malviya, V.N., Zhuleku, E., Politi, A., Ninov, M., Silbern, I., Urlaub, H., et al. (2021). Co-localization of different Neurotransmitter Transporters on the same Synaptic Vesicle is Bona-fide yet Sparse. BioRxiv 2021.06.30.449903.

Voglmaier, S.M., Kam, K., Yang, H., Fortin, D.L., Hua, Z., Nicoll, R.A., and Edwards, R.H. (2006). Distinct Endocytic Pathways Control the Rate and Extent of Synaptic Vesicle Protein Recycling. Neuron *51*, 71–84.

Vyleta, N.P., and Smith, S.M. (2011). Spontaneous Glutamate Release Is Independent of Calcium Influx and Tonically Activated by the Calcium-Sensing Receptor. J. Neurosci. *31*, 4593–4606.

Wachter, R.M., and Remington, S.J. (1999). Sensitivity of the yellow variant of green fluorescent protein to halides and nitrate [2]. Curr. Biol. *9*, 628–629.

Wachter, R.M., Yarbrough, D., Kallio, K., and Remington, S.J. (2000). Crystallographic and energetic analysis of binding of selected anions to the yellow variants of green fluorescent protein. J. Mol. Biol. *301*, 157–171.

Wan, F.-Y., Wang, Y.-N., and Zhang, G.-J. (2002). Influence of the physical states of membrane surface area and center area on lysosomal proton permeability. Arch. Biochem. Biophys. *404*, 285–292.

Wang, G., and Xu, X.S. (2004). Peptide nucleic acid (PNA) binding-mediated gene regulation. Cell Res. *14*, 111–116.

Watanabe, S., Rost, B.R., Camacho-Pérez, M., Davis, M.W., Söhl-Kielczynski, B., Rosenmund, C., and Jorgensen, E.M. (2013). Ultrafast endocytosis at mouse hippocampal synapses. Nature *504*, 242–247.

Weilinger, N.L., and LeDue, J.M. (2020). Quantitative fluorescence lifetime imaging uncovers a novel role

for KCC2 chloride transport in dendritic microdomains. BioRxiv Prepr. 1–40.

Weinert, S., Jabs, S., Supanchart, C., Schweizer, M., Gimber, N., Richter, M., Rademann, J., Stauber, T., Kornak, U., and Jentsch, T.J. (2010). Lysosomal pathology and osteopetrosis upon loss of H+-driven lysosomal Cl- accumulation. Science (80-.). *328*, 1401–1403.

White, M.M., and Miller, C. (1981). Chloride permeability of membrane vesicles isolated from Torpedo californica electroplax. Biophys. J. *35*, 455–462.

Wienisch, M., and Klingauf, J. (2006). Vesicular proteins exocytosed and subsequently retrieved by compensatory endocytosis are nonidentical. Nat. Neurosci. *9*, 1019–1027.

Willig, K.I., Rizzoli, S.O., Westphal, V., Jahn, R., and Hell, S.W. (2006). STED microscopy reveals that synaptotagmin remains clustered after synaptic vesicle exocytosis. Nature *440*, 935–939.

Wolosker, H., de Souza, D.O., and de Meis, L. (1996). Regulation of Glutamate Transport into Synaptic Vesicles by Chloride and Proton Gradient. J. Biol. Chem. *271*, 11726–11731.

Wu, L.-G., Hamid, E., Shin, W., and Chiang, H.-C. (2014). Exocytosis and Endocytosis: Modes, Functions, and Coupling Mechanisms. Annu. Rev. Physiol. *76*, 301–331.

Wu, M.M., Llopis, J., Adams, S., McCaffery, J.M., Kulomaa, M.S., Machen, T.E., Moore, H.P.H., and Tsien, R.Y. (2000). Organelle pH studies using targeted avidin and fluorescein-biotin. Chem. Biol. *7*, 197–209.

Yagensky, O., Kohansal-Nodehi, M., Gunaseelan, S., Rabe, T., Zafar, S., Zerr, I., Härtig, W., Urlaub, H., and Chua, J.J. (2019). Increased expression of heme-binding protein 1 early in Alzheimer's disease is linked to neurotoxicity. Elife *8*.

Yamashita, T., Ishikawa, T., and Takahashi, T. (2003). Developmental increase in vesicular glutamate content does not cause saturation of AMPA receptors at the calyx of Held synapse. J. Neurosci. *23*, 3633–3638.

Yang, P.-C., and Mahmood, T. (2012). Western blot: Technique, theory, and trouble shooting. N. Am. J. Med. Sci. *4*, 429.

Zajac, M., Chakraborty, K., Saha, S., Mahadevan, V., Infield, D.T., Accardi, A., Qiu, Z., and Krishnan, Y. (2020). What biologists want from their chloride reporters - A conversation between chemists and biologists. J. Cell Sci. *133*.

Zhang, G.-J., Liu, H.-W., Yang, L., Zhong, Y.-G., and Zheng, Y.-Z. (2000). Influence of Membrane Physical State on the Lysosomal Proton Permeability. J. Membr. Biol. *175*, 53–62.

(2006). Terrific Broth. Cold Spring Harb. Protoc. *2006*, pdb.rec8620.